CHARACTERIZATION OF ROCK-MAGNETIC SIGNATURE DURING SUBAERIAL EXPOSURE IN PLATFORM CARBONATES FROM NEW PROVIDENCE, BAHAMAS

A Senior Honors Thesis
Presented in Partial Fulfillment of the Requirements for graduation with distinction in Geological Sciences in the undergraduate colleges of The Ohio State University

by

Debra Leann Carlo

The Ohio State University
May 1996

Project Adviser: Professor Hallan C. Noltimier, Department of Geological Sciences

Approved by

Dr. Hallan C. Noltimier, Adviser
Department of Geological Sciences

ABSTRACT

The marine carbonate Bahamian bank bore hole core BH-5 from New Providence Island was subsampled for paleomagnetic study at The University of Miami, Rosenstiel School of Marine and Atmospheric Science. Susceptibility, magnetic remanence of Natural Remanent Magnetism and Alternating Field intensities, Saturation Isothermal Remanent Magnetism, and coercivity spectral analysis experiments on sixty-four subsamples were conducted. A study of magnetic mineralogy identified conclusive results for a sea level lowstand and a subaerial exposure surface horizon at a depth of 14.7 meters below core top within the Early to Late Pleistocene Epoch following the Matuyama-Brunhes geomagnetic reversal. This interpretation is based upon one subsample (sample #41) containing the magnetic minerals hematite and coarse-grained magnetite identified by coercivity spectral analysis. This Bahamian bank marine carbonate lowstand, the result of a eustatic fall in sea level during a global glacial event is of Pleistocene age and may correspond either to the Early Pleistocene pre-Illinoian G Glaciation or the Middle Pleistocene Illinoian Glaciation.

ACKNOWLEDGMENTS

I wish to thank Dr. Hallan C. Noltimier, my faculty adviser for assistance in analysis and writing this thesis. His support and guidance was greatly appreciated throughout this project. I also thank Dr. Noltimier for participating on the panel for my defense.

A very special thanks goes to Dr. Donald F. McNeill for the opportunity to begin this project with him at the University of Miami, RSMAS. Without his knowledge, generosity, and the use of his laboratory facilities, this project would not have been possible.

Thanks also goes to Dr. Terry J. Wilson and Dr. Loren E. Babcock for representing the department by participating on the panel for my defense.

I want to thank Laura Guertin, a Ph.D. candidate at the University of Miami, RSMAS for explaining the use of the equipment in the lab and helping me to drill my samples.

Thanks also to Bryan Canterbury for assistance with data entry and software.

Financial support for laboratory work and three months stay on Key Biscayne, Florida, was provided by grant money from Dr. McNeill. Financial support in Ohio was provided by an Undergraduate Research Scholarship from the Honors Program of the College of Arts and Sciences.

TABLE OF CONTENTS

INTRODUCTION

The recognition of subaerial disconformities in carbonate platforms is critical in the reconstruction of depositional history and changes in relative (local) and eustatic (global) sea level. Recognition and confirmation of periods of subaerial exposure is especially important in studies using core borings with limited coverage. In addition, this information helps identify platform emergence (or subsidence) and sequential development.

Samples removed from a shallow bore hole core are used in this study to differentiate the magnetic mineralization formed during periods of non-deposition from that formed during normal marine carbonate deposition. Analysis of carbonate sediments and subaerial exposure horizons with selected rock-magnetic techniques delineate the effect of subaerial exposure on the host carbonates with respect to magnetization and/or remagnetization. Significant differences in magnetization result from subaerial exposure. Using these distinct physical characteristics, disconformable surfaces can be identified with more confidence.

Processes that influence magnetization in carbonates include the primary magnetization (often ultrafine-grained magnetite), the subsequent dissolution and/or oxidation of magnetite to maghemite, the intense oxidation processes found at subaerial exposures (i.e., oxidation of maghemite to goethite, hematite), and the external input of magnetic material (multidomain magnetite) in relatively pure carbonate systems (i.e., Fe-rich aerosols). Often we can recognize these subaerial exposure surfaces through color and textural changes within the core. Reddish limestones owe their color to secondary oxidation of magnetite and maghemite as well as other iron-bearing minerals. In bore hole cores, subsequent marine flooding of carbonate exposure surfaces may often erode or

remove prominent subaerial characteristics, and the need to rely on other physical properties such as magnetization becomes more important. Furthermore, the proposed occurrence of penetrative calcretes (those forming well below the near surface exposure profile) makes identifying distinguishing physical characteristics even more necessary.

The development of highly sensitive superconducting magnetometers during the nineteen seventies allows the reliable measurement of weakly magnetized platform carbonates. This project was designed to differentiate the rock-magnetic features of known subaerial carbonate exposure horizons from those of normal marine carbonate facies. Facies- and diagenetic-specific rock-magnetic properties assist recognition and confirmation of exposure disconformities in pure carbonate platform facies.

GEOGRAPHIC SETTING

The Bahamas are located in the North Atlantic Ocean between the longitudes of 72° 42' W and 80° 45' W and the latitudes 20° 45' N and 28° N. The 1400 km-long Bahama Archipelago is an arc-shaped system of shallow-water carbonate platforms topped by low-lying islands located to the east and south of the subsiding eastern continental margin of North America. The archipelago (Figures 1a and 1b) extends from Little Bahama Bank to the north off the coast of Florida, south to the Turks and Caicos Islands, Silver Bank and Navidad Bank, off the island of Hispaniola. Present water depths on these banks are typically less than 10 meters; and much of the region must have been subaerial during numerous Pliocene and Pleistocene sea level lowstands. However, the banks themselves are separated by inter- or intra-platform, deep-water basins and troughs with depths of up to 4 km (as found in the Northeast Providence Channel).

A geographic layout of the Bahamas depicts the islands surrounded by extensive areas of shallow-water and submerged plateaus called the Great Bahama Bank and Little Bahama Bank (Figure 2). Extending directly upward from the Great Bahama Bank are the islands of Andros, Eleuthera, New Providence (the location of the bore hole core in this project), and the Exuma chain. Little Bahama Bank borders the northern shores of Grand Bahama Island and surrounds the islands of Abaco chain. On the west are the Straits of Florida and to the north, separating Grand Bahama and Andros, is the Northwest Providence Channel. The Northeast Providence Channel separates the Abacos from Eleuthera, the Berry Islands, and New Providence. The Tongue of the Ocean (TOTO) is a deep submarine canyon that divides the Great Bahama Bank.

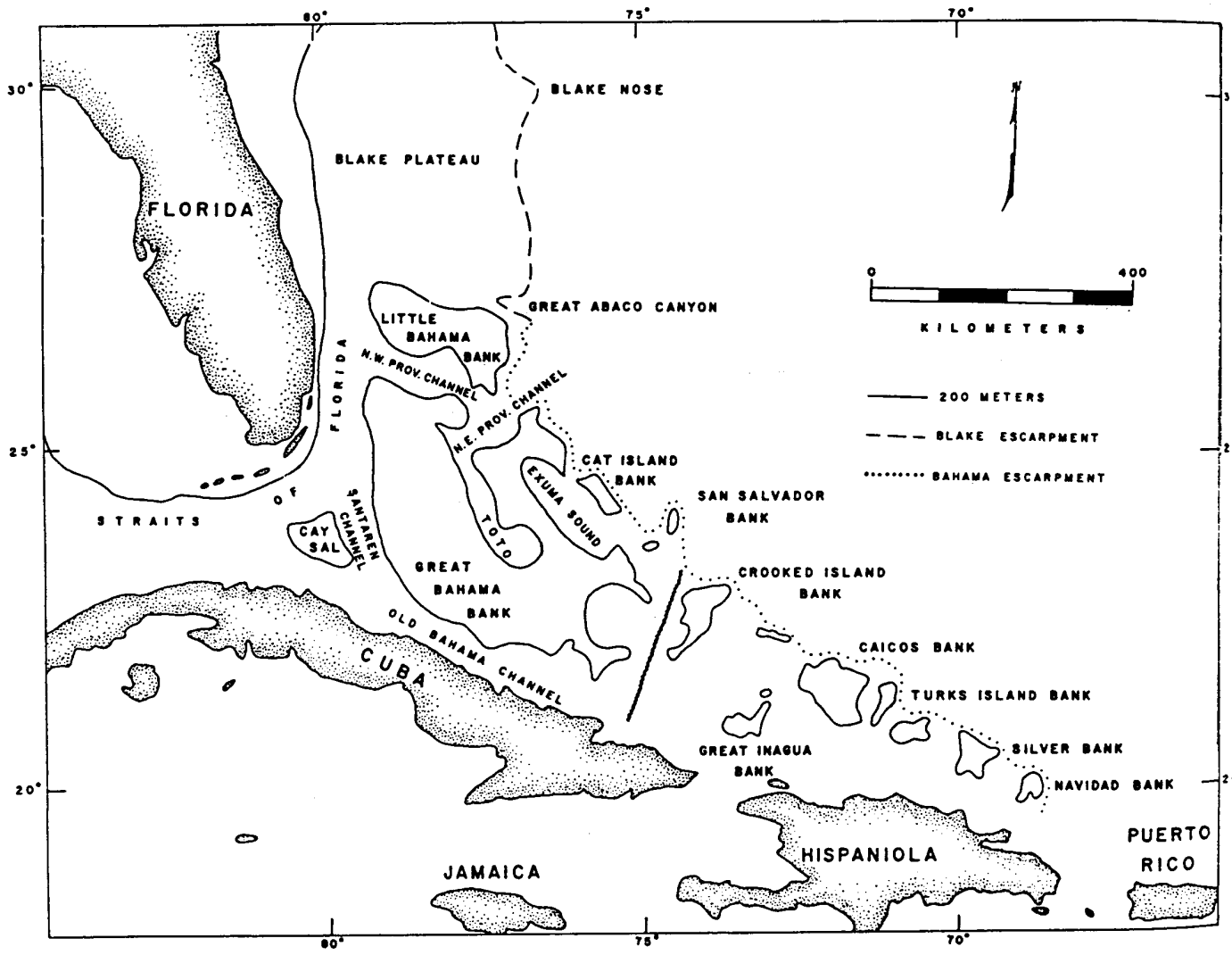

Figure 1a. Map of the Bahama Platform. The heavy dark line in the center divides the platform into the northwestern and southeastern sections. (Mullins and Lynts, 1977)

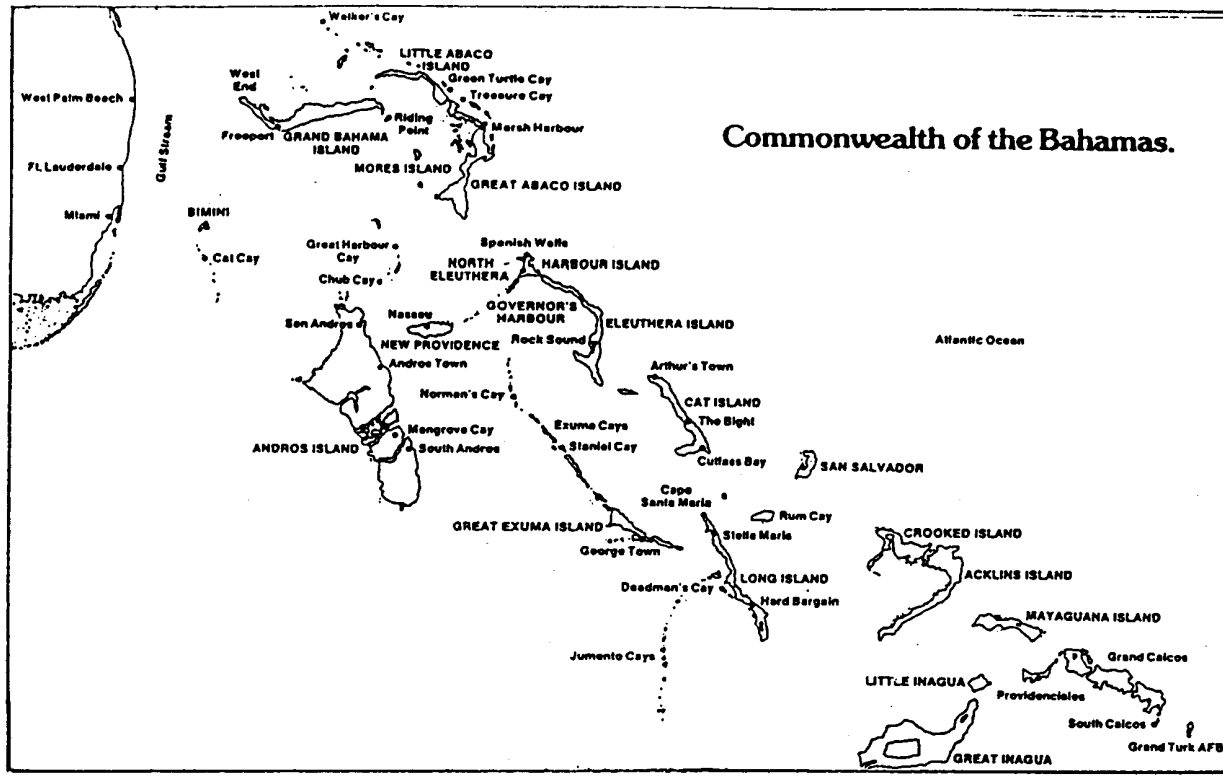

Figure 1b. A view of the Commonwealth of the Bahamas, Islands and Towns. (Curran, 1985)

Figure 2. Map of the Bahama Islands with bathymetry. (Curran, 1985)

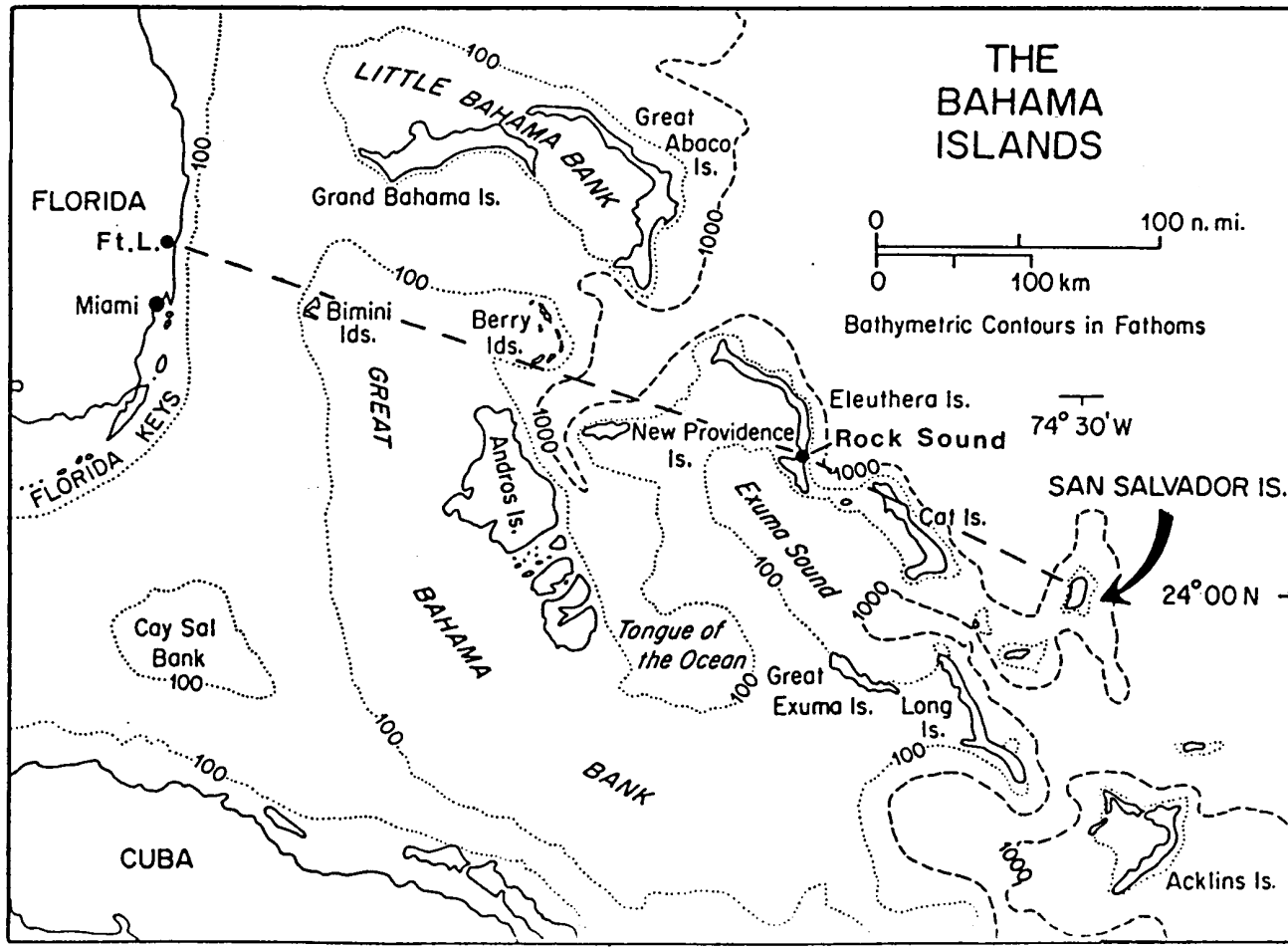

The geologic setting demonstrates that the present islands of the Bahamas rise just above the shallow areas of the Bahama banks. The islands are low-lying, generally only 6-15 meters high. The shallow-water banks are underlain by thick successions of carbonate rock and accumulation has kept pace with the isostatic subsidence of the Bahamian continental margin platform since Early Jurassic time (Curran, 1985). The low amplitude of marine magnetic anomalies over the Bahamas indicates that the total shallow-water carbonate section beneath the Bahama banks may be up to 10 km thick. Bore hole data reveals that it is at least 5.4 km thick (Mullins and Lynts, 1977). On the southwest, the Bahama Platform is bounded tectonically by the Cuban orogen and to the south by the Caribbean lithospheric plate. On the east the platform drops to the abyssal depths of the Atlantic Ocean along slopes that are as steep as 28° to 40° (Mullins and Lynts, 1977). On the north and northwest the Bahama Platform is contiguous with the Blake Plateau and the South Florida Platform, forming one of the largest carbonate provinces in the world (Mullins and Lynts, 1977).

THE BAHAMIAN PLATFORM BASEMENT

The geologic origin of the Bahama Archipelago is hotly debated. One concern is whether or not the Bahamian Platforms are underlain by oceanic or continental crust (Curran, 1985). Many have documented that the Bahamas are a terrain whose basement either has formed in place or has drifted in elsewhere during the opening of the North Atlantic in the Jurassic to Early Cretaceous. This implies that, in the Late Cretaceous and Tertiary the shallow banks of the Bahama platform have been the source of sediment that has been deposited in the surrounding deep intra-platform channels and basins (Ladd and Sheridan, 1987).

Mullins and Lynts (1977) proposed an interpretation of a basement of originally pre-Triassic continental material that was thoroughly intruded by mafic and ultramafic rock during rifting of North America from Africa and South America in Late Triassic time (Figure 3). When reconstructed into a pre-drift juxtaposition with North Africa, shown in Figure 4, the Bahama Platform appears to overlap the African continent by approximately 1,500 km (Mullins and Lynts, 1977), which suggests the Bahamas are a post-rift feature less than 175 my old (Smith and Noltimier, 1979).

Ladd and Sheridan (1987) state that detrital shallow-water carbonates shed from nearby carbonate banks into deep intra-bank basins that were established in the Late Cretaceous (Figure 5). The Lower Cretaceous units are shallow-water carbonate banks that were drowned in the Middle Cretaceous, but which during Early Cretaceous extended from Florida throughout the Bahamas region. Marine seismic reflection profiles reveal a sharp angular unconformity in northwest Tongue of the Ocean, suggesting a rift-drift unconformity and deposition on thinned continental crust. No such unconformity is seen in central

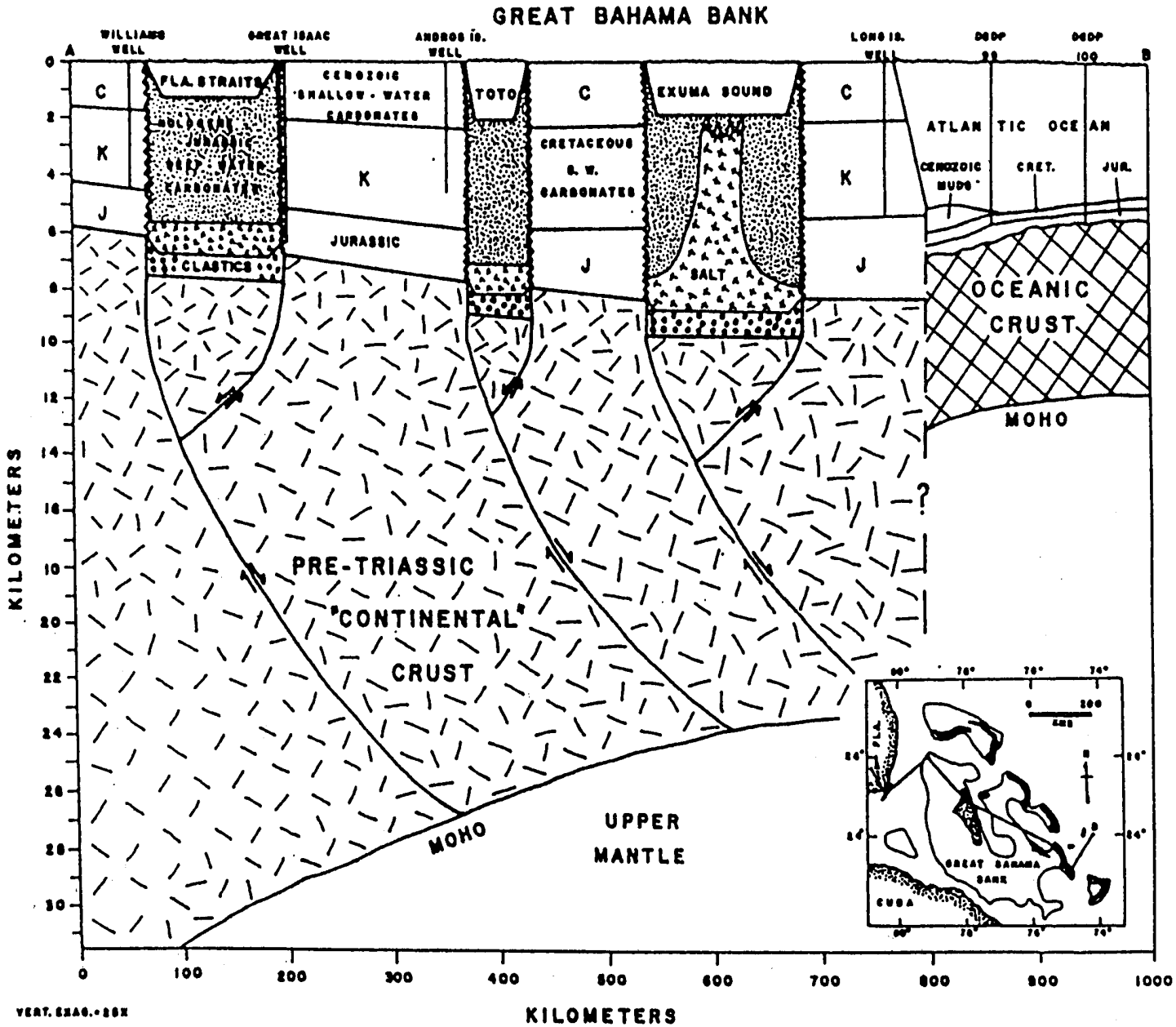

Figure 3. Schematic cross section of the crust beneath the northwestern Bahama Platform.
C = Cenozoic shallow-water carbonates;
K = Cretaceous shallow-water carbonates;
J = Jurassic shallow-water carbonates;
$o^{o}o^{o}$ = Late Triassic continental arkosic arenites and rudites;
$x^{x}x^{x}$ = Jurassic salt and organic-rich shales.
(Mullins and Lynts, 1977)

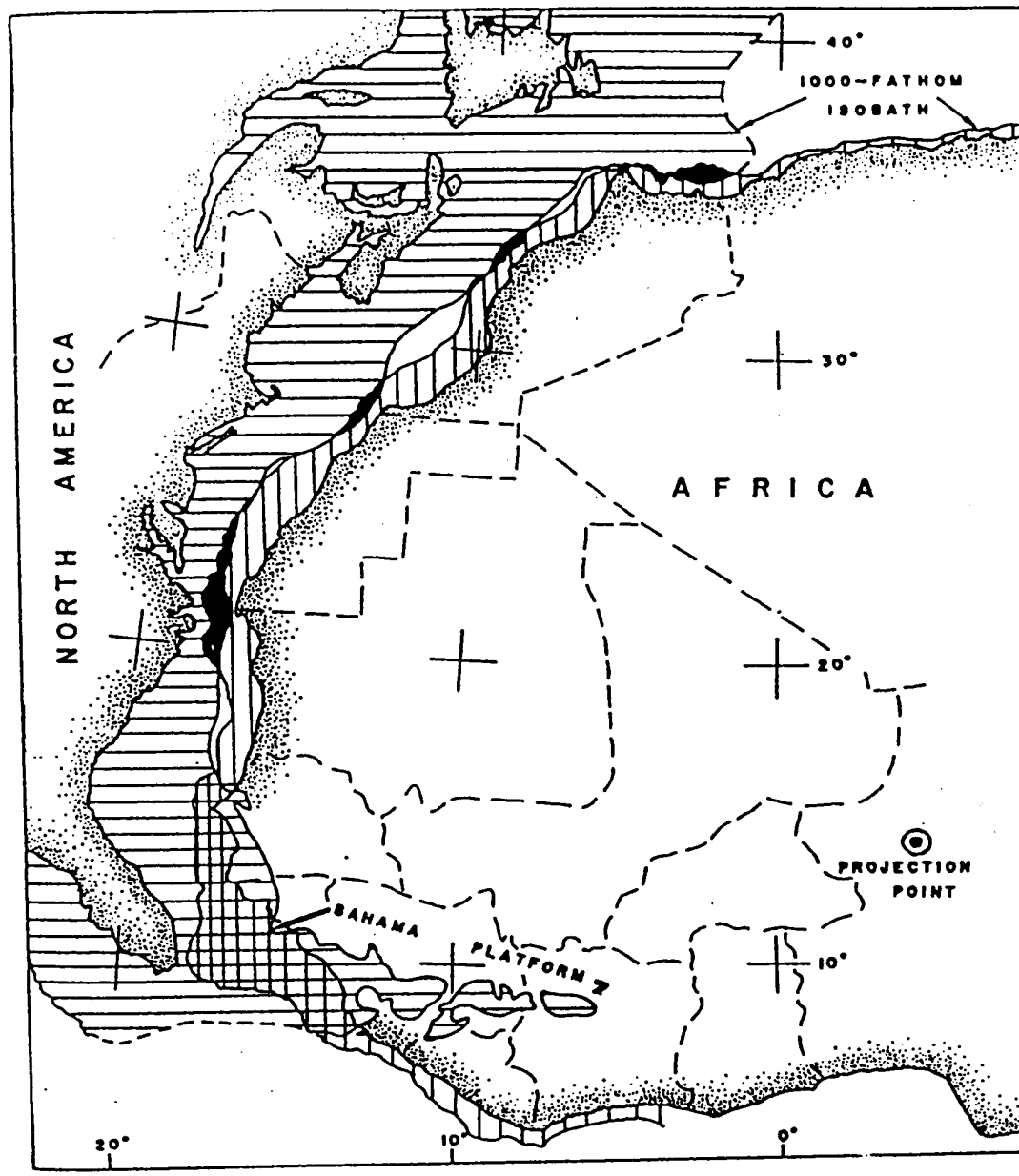

Figure 4. A reconstruction of the North American and African continents, showing the overlap of the Bahama Platform onto Africa. (Mullins and Lynts, 1977)

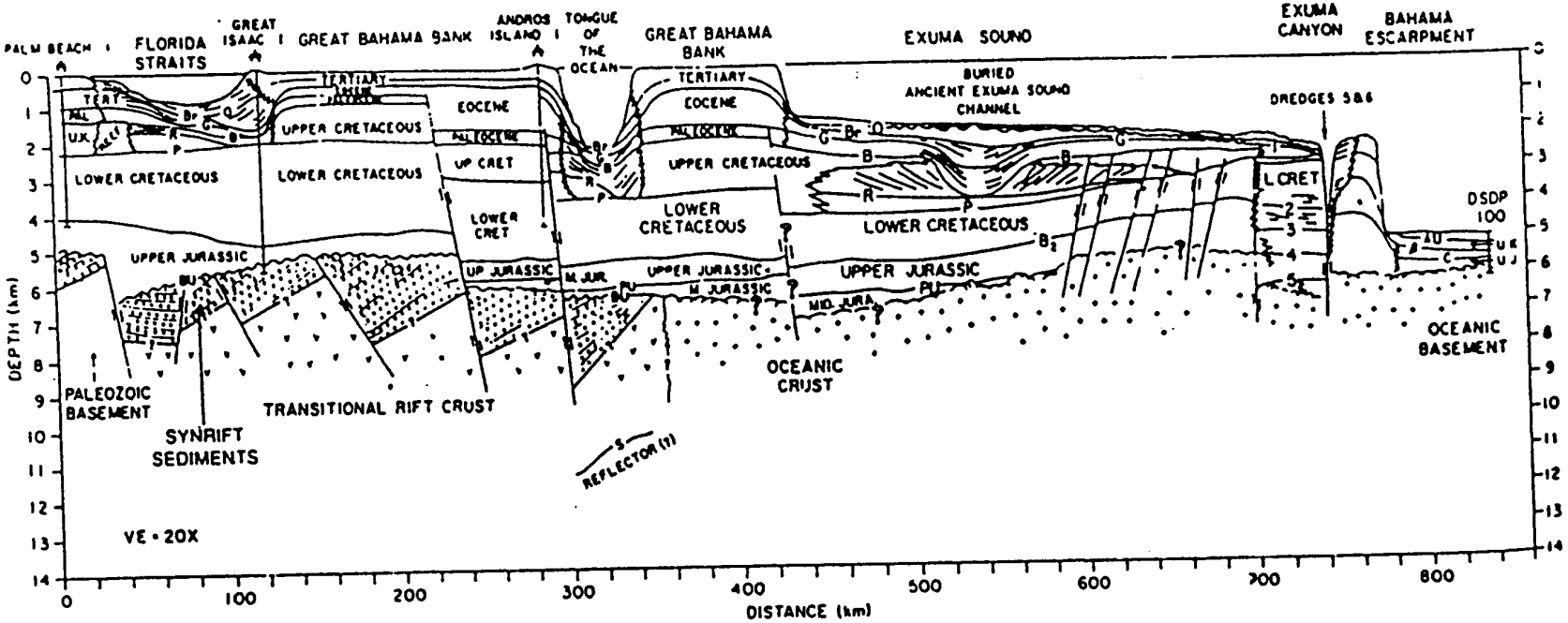

Figure 5. Schematic cross section of the Bahama Platform illustrating interpreted correlations and structural features. (Ladd and Sheridan, 1987)

and southeast Tongue of the Ocean or in Exuma Sound, suggesting that these areas are built on oceanic crust.

THE ORIGIN OF THE BAHAMIAN BANKS AND BASINS

There are several hypotheses proposed for the origin of the Bahamian banks and basins. I believe that the most reasonable hypotheses are those of Mullins and Lynts (1977), Ladd and Sheridan (1987), and Eberli and Ginsburg (1987). These three hypotheses are quite different, and any one could reasonably explain the origin of the Bahamian banks and basins.

The "graben" hypothesis of Mullins and Lynts (1977) proposes strong fault control on the bank-basin pattern, with the basins originating from grabens during the rifting stage of the North Atlantic Ocean opening (Figure 3). Mullins and Lynts (1977) stated that the orientations of the deep-water channels that surround and dissect the northwestern Bahama Platform demonstrate a radial pattern superimposed on a northwest/southeast structural trend. Upon further examination, Mullins and Lynts (1977) determined that the northern and southern Straits of Florida, Old Bahama Channel, and the projection of Northeast Providence Channel converge radially near Cay Sal Bank, whereas the eastern half of the Northwest Providence Channel, Tongue of the Ocean, Exuma Sound, and the Bahama Escarpment strike northwest/southeast, subparallel to the magnetic anomaly trends across the northwestern Bahama Platform.

The pattern of channels is consistent with the major fault pattern along the eastern continental margin of North America that was produced by the rifting of North America and Africa 180-200 million years ago. However, they noted that the Bahama Platform is unusual in that all four major tectonic patterns are spatially coincident. If the deep channels of the northwestern Bahamas are structurally controlled by basement faults, and if they are temporally coincident,

then the pattern of faults can be explained only by mechanical reasoning. The stress system would produce radial normal faults because of the induced tension, as is commonly found over anticlinal or domed structures. Mullins and Lynts (1977) concluded that if such a stress system was superimposed on a pre-existing structural trend strongly lineated northwest to southeast, the result should be the development of radial grabens subordinate to grabens paralleling the antecedent structural trend, which agrees with the data for the deep-water channels that surround and dissect the northwestern Bahama Platform.

Ladd and Sheridan (1987) presented a different interpretation of the geologic history of the Bahamas (Figure 5). During the breakup related to the origin of the Blake Spur magnetic anomaly at the Callovian/Bathonian boundary in the Middle Jurassic, the transitional rifted and volcanic crust under the western Bahamas was accreted by oceanic crust on its southeast margin. This created a major crustal boundary projecting through the northwest corner of Tongue of the Ocean. After this breakup, thermal subsidence led to marine transgressions across the northwest Bahamas. Meanwhile, the Bahama basement of oceanic nature to the southeast under Exuma Sound remained shallow, yet oceanic in nature. An oceanic volcanic ridge followed the location of the Bahamas transform fracture zone (Figure 6) with a southeasterly trend. As spreading continued, the oceanic crust along the ridge became younger in age to the southeast, where it is of Late Jurassic age southeast of Exuma Canyon. On this shallow oceanic crust, reefs and carbonate platforms formed with continued subsidence in the Late Jurassic and Early Cretaceous.

Ladd and Sheridan (1987) proposed that some reentrants and deep-water channels formed in the southeast during the Early Cretaceous, as near Exuma Canyon. Elsewhere a broad megabank of carbonates and evaporites developed

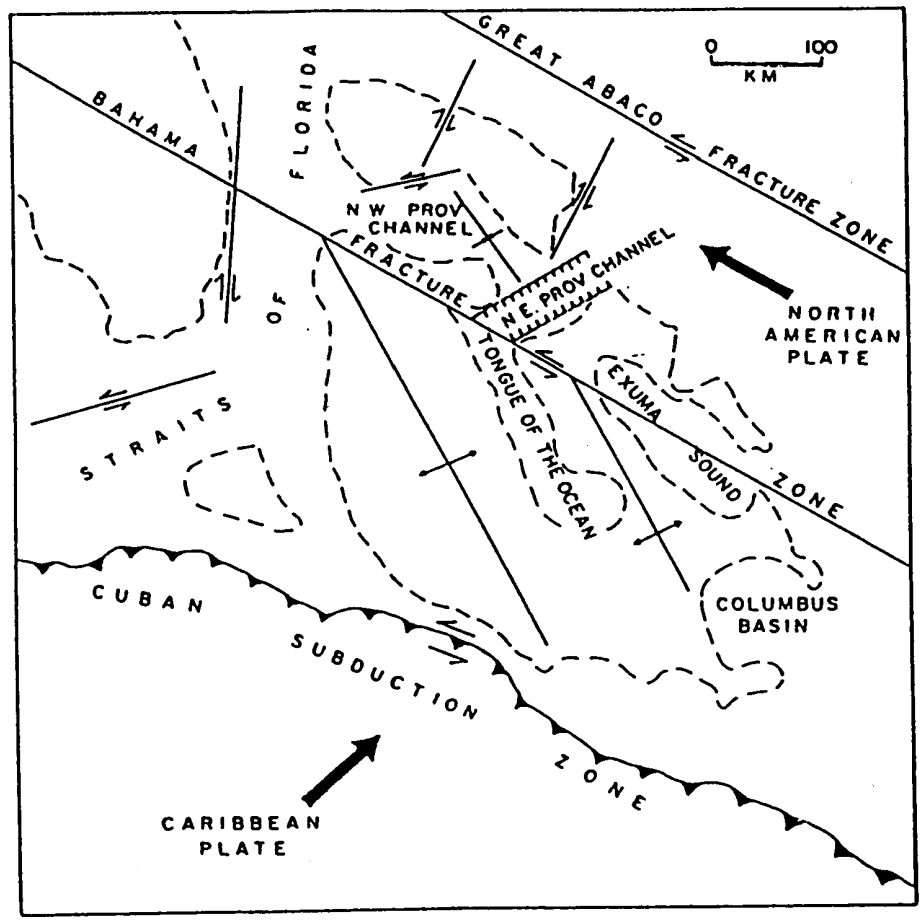

Figure 6. A view of the Bahama Fracture Zone in a hypothetical tectonic model for the Bahama Platform. (Sheridan et al., 1988)

over nearly all the Bahamas, Florida and the Blake Plateau until the end of the Early Cretaceous. After this time, deep channels and basins formed in the Bahamas, separating isolated banks. Extensive progradation from the reorganized banks occurred in the Late Cretaceous through Holocene. The progradation caused the migration of banks and channels in the past, and some channels have become extinct and buried, such as under the Exuma Sound.

In the Early Tertiary, active faulting caused great vertical displacement and tilting of the previously flat-lying geology of the megabank. The faults occur close to the boundary of the transitional rift crust under Northwest Providence Channel, Northeast Providence Channel, and Tongue of the Ocean, and near the position of the Bahama transform fracture zone. Sheridan (1981) suggested that the relatively young, post-Cretaceous faulting in the Bahamas was caused by the tectonic interactions of the Antilles and North American plates, which created the Cuban orogeny; the stresses from these plate collisions reactivated the older Jurassic basement faults and transform fracture zones (Ladd and Sheridan, 1987). Headward erosion by submarine density currents cut deep canyons, such as Exuma Canyon, that connect from the deep Atlantic into the channels of Exuma Sound, Tongue of the Ocean, Northwest Providence Channel, and Northeast Providence Channel. The combination of upward platform growth and deep-water depositional and erosional processes formed and perpetuated the unique deep-water channel geomorphology throughout the Cenozoic.

Eberli and Ginsburg (1987) have an interpretation based upon a detailed seismic study of the history of the Great Bahama Bank (Figure 7). Most of the earlier researchers in the Bahamas assumed that once the platforms were established they grew upward with little lateral migration of the margins.

However, recent Ocean Drilling Project (ODP) results indicate that certain bank margins have retreated and prograded tens of kilometers in the past 100 million years (Eberli and Ginsburg, 1987). Seismic profiles from the top of the Great Bahama Bank demonstrate that bank migration is even more extensive, that Great Bahama Bank is the result of coalescence of three smaller banks combined with significant lateral progradation. Two major features are recognized in the seismic data of northwestern Great Bahama Bank that give evidence to support this proposal. Beginning in Late Cretaceous to Early Tertiary time (Figure 7a) a north-south-trending depression, the Straits of Andros, separated an eastern platform, Andros bank, from a western platform, Bimini bank. Initially, the Straits of Andros had dimensions similar to the modern Tongue of the Ocean but was progressively filled from east to west. In Early to Middle Tertiary time (Figure 7b) a second depression, the Bimini embayment, formed within Bimini bank by folding, having a maximum depth of about 470 m. This depression was also filled from east to west. Subsequently (Figure 7c), lateral prograding systems built the western margin of Bimini bank more than 25 km westward into the Straits of Florida.

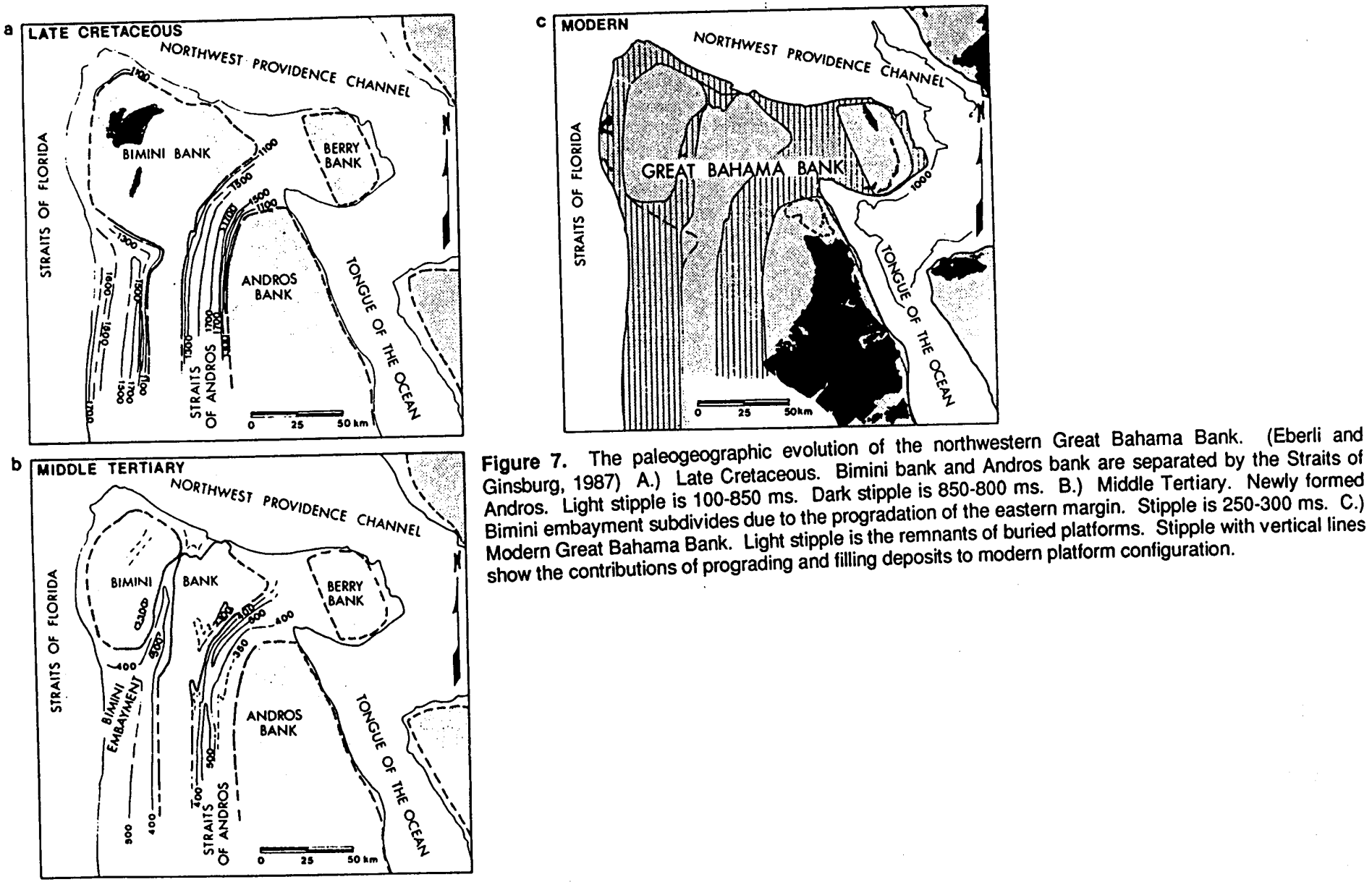

Figure 7. The paleogeographic evolution of the northwestern Great Bahama Bank. (Eberli and Ginsburg, 1987) A.) Late Cretaceous. Bimini bank and Andros bank are separated by the Straits of Andros. Light stipple is 100-850 ms. Dark stipple is 850-800 ms. B.) Middle Tertiary. Newly formed Bimini embayment subdivides due to the progradation of the eastern margin. Stipple is 250-300 ms. C.) Modern Great Bahama Bank. Light stipple is the remnants of buried platforms. Stipple with vertical lines show the contributions of prograding and filling deposits to modern platform configuration.

PREVIOUS WORK

New Providence Island is in the westernmost part of the Northeast Providence Channel, northwest of Yellow Bank and is in the eastern part of the Great Bahama Bank (Figure 8). New Providence has a high-energy coast type located in the cliffed northern and western coasts and a low-energy coastal type located in the southern and eastern coasts which slope off gently into the Yellow Bank. Bore hole core BH-5 was recovered during the construction of the Clifton Pier Power Station by the Bahamian Government, located in the westernmost part of the island seen in Figure 8, (Aurell et al., 1995).

Carbonate mineralogy was determined by x-ray diffraction (Aurell et al., 1995), stable isotope data (C-13 and O-18 measured in per mil PDB, see Appendix B-1 and B-2), and oriented subcores were removed to determine the location of the Middle Pleistocene Brunhes/Matuyama reversal boundary. Each subcore or sample was subjected to a variety of paleomagnetic techniques (i.e., an alternating field and thermal demagnetization) to determine inclination and polarity. Figure 9 is taken from Aurell et al. (1995) as an example of paleomagnetic and mineralogical work previously accomplished on bore hole core BH-5. Units were dated by radiometric dating. Stratigraphy and a core description (Figure 10) are from Aurell et al., (1995). Along with this previous work, location of my subsamples are shown at the same scales in Figures 9 and 10.

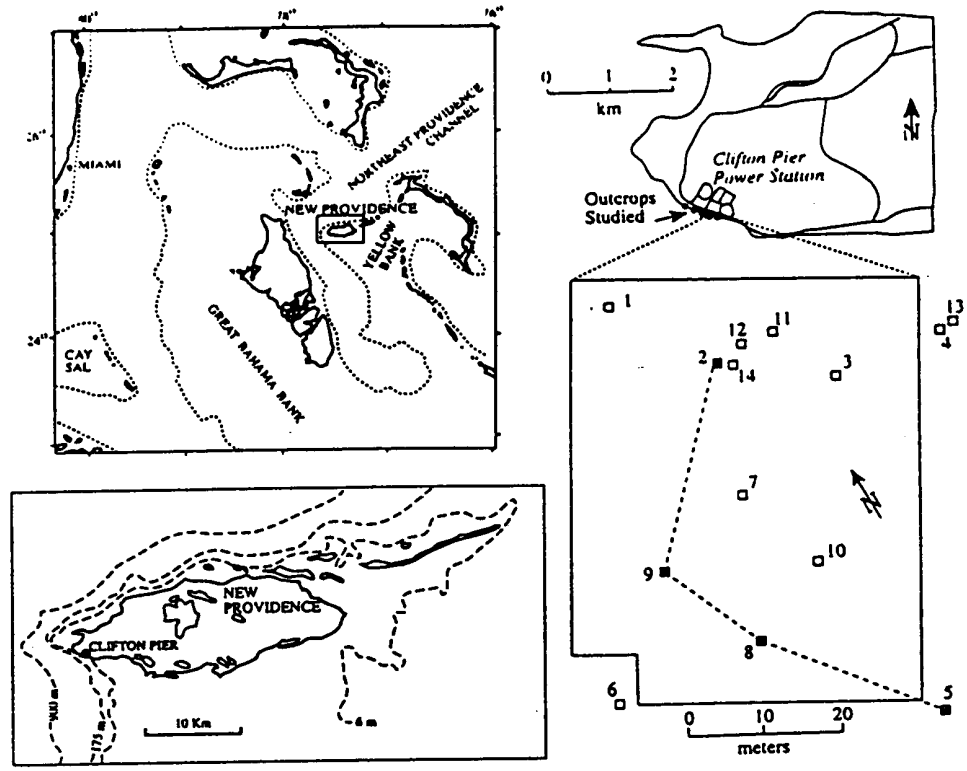

Figure 8. Location of New Providence Island and core BH-5. (Aurell et al., 1995)

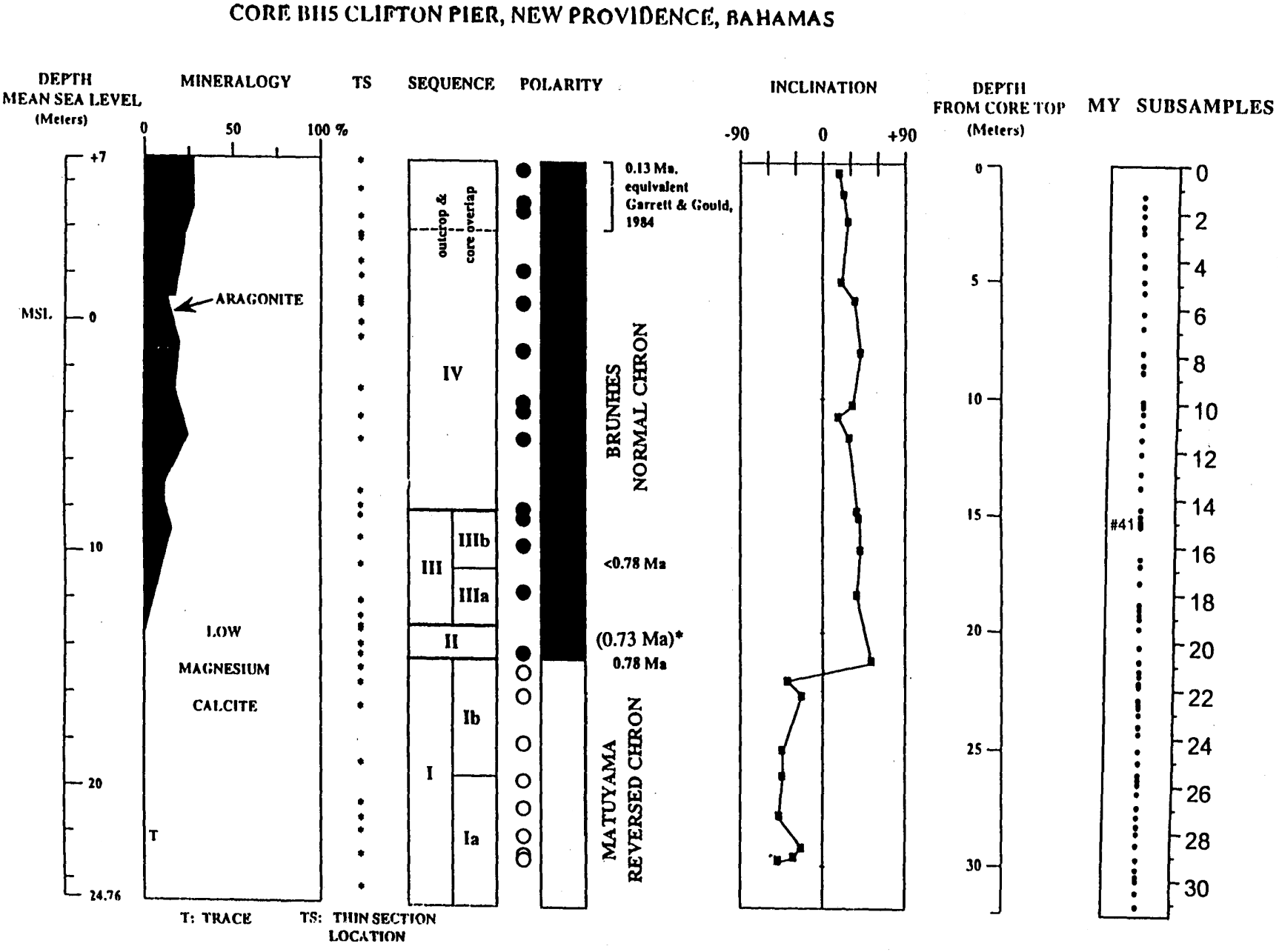

Figure 9. Paleomagnetism and mineralogy of bore hole core BH-5 (Aurell et al., 1995). Location of my paleomagnetic subsamples of core BH-5 has been plotted on the right. *Disputed age for Matuyama-Brunhes magnetostratigraphic boundary (Harland et al., 1982; Butler, 1992).

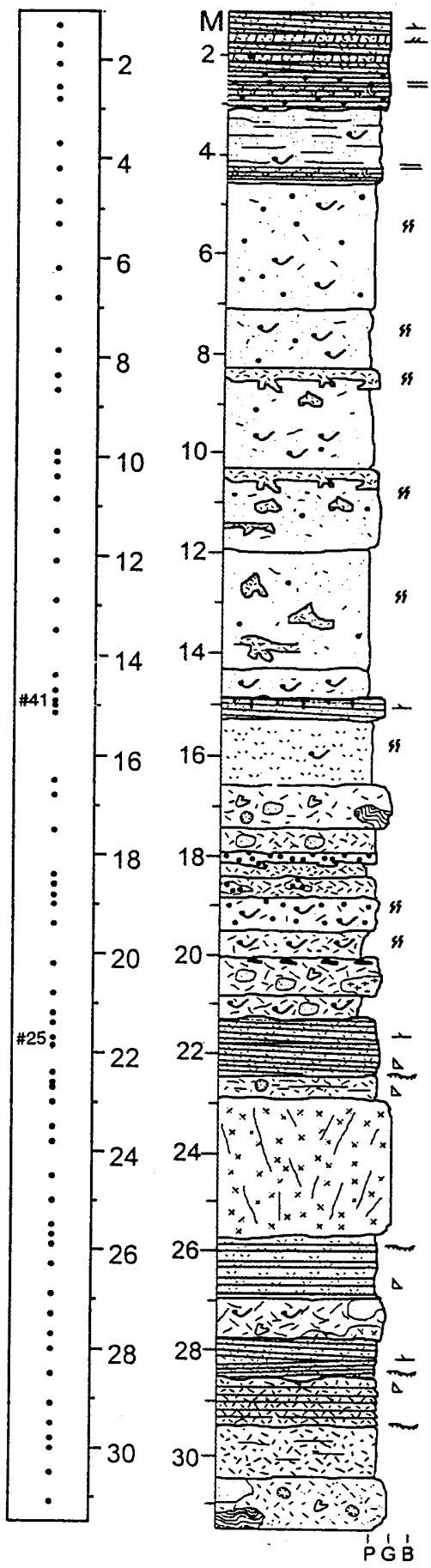

Core BH-5

- fine skeletal grains
- coarse skeletal grains
- peloids
- ooids
- large molluscs
- graded skeletal layers (tempestites)
- high-angle cross-lamination
- parallel lamination
- low-angle cross-lamination
- bioturbation
- branching *Porites* sp.
- *Agaricia* sp.
- massive Porites
- *Diploria* sp.
- *Siderastrea* sp.
- *Montastrea* sp.
- *Callianassa* burrows
- micritic crust
- subaerial exposure/disconformity surface
- P packstone
- G grainstone
- B boundstone

Figure 10. Stratigraphy and brief description of bore hole core BH-5 modified after (Aurell et al., 1995). The scale on the left gives depth in meters from the core top as indicated in Figure 9. The location of my subsamples is indicated by "o".

OBJECTIVES

The primary objective of this project is to distinguish the magnetic characteristics of marine carbonates developed during subaerial exposure from the characteristics of unexposed platform carbonates for the purpose of identifying past disconformities in subsurface bore hole cores. Recognition of disconformities is essential to proper interpretation of the depositional record and associated change in sea level. I have documented these features in a continuous core where zones of subaerial exposure and normal marine deposition are well documented using lithologies (Appendix A-2) and stable isotopes (Appendix B-1).

The core chosen for this study was drilled in 1988 as part of a power plant geotechnical study and is currently reposited at the University of Miami. The core is 32 meters in length and has a diameter of 10 cm. Core recovery was excellent and approached 100 percent. Detailed core description, magnetostratigraphy, and depositional interpretation can be found in Aurell et al. (1995). Isotopic data presented in this study was collected in 1992 at the Stable Isotope Laboratory, University of Miami.

Carbonate Rock Magnetization

Carbonate paleomagnetism is relatively new in geological research due to earlier limitations in rock magnetometers (mainly the inability to have low enough background sensitivity). However, development of superconducting rock magnetometers during the nineteen seventies has opened many new techniques in pure carbonate rocks and sediments, especially those formed in the shallow platform, periplatform, and deep-water environments. Along with this new technology, an understanding developed for the origin of magnetism in

carbonates. This includes studies on the nature of carbonate magnetic remanence, the source of magnetic grains, post-depositional factors that affect directional data and alignment of grains, and the sensitivity of remanence to diagenetic changes and remagnetization. The nature of remanence is important for interpreting primary versus secondary remanence and resultant directional changes. Thus, studying carbonate magnetism involves an important comparison between primary and secondary origins of magnetic remanence. The first studies of carbonate paleomagnetism using a cryogenic magnetometer were on Paleozoic marine limestones from Sweden, the Appalachian Plateau, and the Michigan Basin (Noltimier and Bergstrom, 1976; Bartman et al., 1978; Bergstrom et al., 1980; Stupp and Noltimier, 1980; Patzwahl and Noltimier, 1981; Bergstrom and Noltimier, 1982; Noltimier and Patzwahl, 1982; Noltimier and Patzwahl, 1982).

Generally, magnetic grains found in shallow-water carbonates are often subjected to several sedimentary processes (deposition, initial dewatering, compaction, cementation, mineralogic alteration and recrystallization). However, in most cases these do not affect polarity but may slightly modify remanence directions (McNeill et al., 1991). Due to their presence near sea level, shallow-water limestones are susceptible to many diagenetic environments ranging from marine fluid burial to meteoric fluid exposure to a complicated, (often repetitive) mixed fluid, past depositional history. In many carbonate environments, both oxidation and reduction play a major role in sediment diagenesis with progressive burial or periodic subaerial exposure (McNeill, 1990).

The Presence of Biogenic Magnetite in Carbonate Facies

Stolz et al. (1989) documented the presence of abundant biogenic magnetite by observing one specific species of abundant living magnetotactic

bacteria in an intertidal carbonate marsh in south Florida. The presence of fine-grained single-domain living magnetotactic bacteria has significant importance for the formation and preservation of the paleomagnetic record, especially in those areas isolated from detrital magnetic material. Successful application of paleomagnetism in shallow-water carbonates and the recent reports on the presence of biogenic magnetite in modern carbonate environments have provided the impetus to utilize this ubiquitous source of magnetization in the paleomagnetic study of Cenozoic carbonates (McNeill, 1990).

Whether biogenic or authigenic, fine-grained single-domain magnetite in pure carbonate environments can acquire and preserve a stable remanent magnetization. Remanence preservation and confirmation of depositional remanence is of utmost importance for magnetostratigraphic dating of carbonate rocks.

Formation of Maghemite

Maghemite is formed by the low temperature oxidation of magnetite (maghemitization) in both subaerial and submarine environments. Maghemitization of single-domain magnetite grains produces a decrease in coercivity and an increase in the ratio of induced to remanent magnetizations. Nevertheless, rocks with these higher ratios tend to be magnetically stable and they are good recorders of the ancient geomagnetic field. Maghemite has the same composition as hematite but possesses a cubic inverse spinel crystal structure. The crystal structure that maghemite possesses is very similar to magnetite which leads these two minerals to have comparable magnetic properties and the saturation magnetizations are nearly equal. Maghemite has a slight lattice defect structure, but is stabilized by impurities in small amounts which control the temperatures at which maghemite subsequently converts to

hematite. This conversion of maghemite to hematite at temperatures above 300°C can identify the presence of maghemite in limestones (Lowrie and Heller, 1982).

Subaerial Exposure Surface Horizons

Carbonate subaerial exposure surfaces produce distinctive features that can be recognized in the lithologic, mineralogic, and isotopic record. In addition, the depositional formation of magnetic minerals and their successive alteration through diagenesis can provide a distinct rock magnetic signal. Subaerial exposure tends to concentrate fine-grained eolian particles (aerosols) (Glaccum and Prospero, 1980) and can provide additional iron-rich minerals that are also subject to oxidation. The minerals goethite and hematite are good indicators of subaerial oxidation, and have been identified in many subaerial disconformity surfaces in Bahamian limestones. Goethite carries a remanent magnetization and is metastable in the presence of water and oxygen in the diagenetic environment. Hematite is formed as an early diagenetic product from goethite through a dehydration reaction. This dehydration reaction is non-reversible and may result in limestones with the characteristic red and pink coloration.

Magnetization in or at subaerial disconformity surfaces may also be due to a combination of fine-grained hematite and maghemite as well as from detrital eolian magnetite grains. As mentioned above, one likely detrital source of magnetite grains is the deposition of atmospheric dust (Saharan aerosols) transported westward across the Atlantic Ocean. Multidomain magnetite particles may occur in dominantly single-domain carbonate sediments due to these eolian sources, although these grains are concentrated on subaerial exposure surfaces.

Penetrative Calcretes

The concept of penetrative calcretes as proposed by Rossinsky et al. (1992) for those calcretes formed below the actual exposure surface suggests that these types of calcretes can easily be misinterpreted as individual subaerial exposure events. Individual exposure events can produce true surficial calcretes plus many associated, underlying, penetrative calcretes separated from the true surficial exposure. Failure to identify penetrative calcretes may lead to misinterpretation of the number of disconformity events. For example, one may predict an erroneously high number of sea level lowstands interrupting marine sedimentation when they are in actuality a continuous series of penetrative calcretes.

Penetrative calcretes are those calcretes formed (up to 5 meters) below the surficial exposure zone. In comparison to surficial calcretes, penetrative calcretes have distinctly lower elemental concentrations of Fe and Al, perhaps due to leaching from the surficial zone of highest concentration. Therefore, it is advantageous to magnetically distinguish between these two substantially different calcretes by distinguishing between the lower net magnetic moment, greater goethite/hematite content, lower isothermal remanent magnetization, and greater resistance to acquisition of saturation magnetization in surficial versus penetrative calcretes.

In the Bahamas-Florida region, marine units are correlated with eustatic sea level changes particularly with highstands, and discontinuity surfaces during subaerial exposure with lowstands of sea level in Pleistocene units (Aurell et al., 1995). However, these recorded lowstands which, are thought to be subaerial exposure disconformities, may in fact be a series of calcrete discontinuity surfaces. Correlation of the subaerial exposure and calcrete events one-to-one is highly unlikely (Rossinsky, 1990). Calcretes marking true subaerial exposure

disconformities are commonly associated with facies changes, upward truncations of various structures (also marine hardgrounds), and the tops of shallowing-upward sequences (Rossinsky, 1990).

RESEARCH DESCRIPTION AND METHODOLOGY

Core description and analysis have identified vertically restricted zones of obvious diagenesis, usually associated with subaerial exposure, including void filling calcite and secondary iron-oxides associated with ancient soil horizons. See core description in Appendix A-2, consistent with Dunham's (1962) classification of carbonate rocks (Appendix A-1). I drilled 64 samples from core BH-5 from New Providence Island out of the 32 meter core and cleaned, trimmed, and labeled each one.

Susceptibility

Each sample was weighed on a scientific balance to the nearest gram, and magnetic susceptibility was measured. Magnetic susceptibility measurements help to estimate the occurrence and distribution of any strong, high-susceptibility magnetic phases. Measurements were done on individual samples using a Bartington magnetic susceptibility bridge. See Appendix C-1 for data and C-2 for a plot in depth (meters) vs. susceptibility (cgs).

Magnetic Remanence

Natural remanent magnetism (NRM) was measured with the superconducting magnetometer along with a few low alternating field (AF) steps to assess NRM intensity. All paleomagnetic measurements were performed using a 2G Enterprises 755 magnetometer at the University of Miami, Rosenstiel School of Marine and Atmospheric Science. After measurement of NRM (Natural Remanent Magnetism) and susceptibility, samples were demagnetized in progressively higher alternating fields, usually at 5 to 10 mT steps. The alternating field (AF) subjects the sample to a peak alternating magnetic field

that is then smoothly reduced to zero. As the field decreases, the sample is cycled through hysteresis loops of decreasing amplitude, so that domains with progressively lower coercive force are left stranded along their easy axes of magnetization. The peak field is incremented in stages (5, 10, 15 mT) so that the lower part of the coercive force spectrum is selectively removed to leave a progressively narrower portion of the higher part of the spectrum. See Appendix C-1 for data and C-2 for a plot in depth (meters) vs. AF 15 (Am^2/Kg).

Saturation Isothermal Remanent Magnetism (SIRM)

Saturation isothermal remanent magnetization (SIRM) measurements proceeded along with coercivity spectral analysis. The samples were subjected to a steady direct current (DC) magnetic field where it acquired a magnetization by the hysteresis behavior in which most reached maximum (saturation) remanence. Maximum DC field used was 1000 mT at 287.37 Volts. A coercivity spectrum is given by the shape of the SIRM acquisition curve and the field where saturation is reached (Lowrie and Heller, 1982). These diagnostic coercivities show the evidence of specific magnetic mineral content by comparison with other mineral spectra. SIRM is simply the residual magnetization left after an external field is applied to saturation and removed from a magnetic material. The nature of SIRM acquisition is often characteristic of the magnetic mineralogy (magnetite, goethite, hematite, and maghemite in limestones), grain-size, grain-packing, and possibly the influence of oxidation. See Appendix D-1 for data and D-2 for individual plots in normalized percent acquired SIRM versus AF demagnetization in all 64 samples drilled.

Coercivity Spectral Analysis

Coercivity spectra for each sample was determined using saturation isothermal remanent magnetization (SIRM) and alternating field (AF) demagnetization. Coercivity is a measure of resistance of the domain structure to change. In single-domain grains, the coercivity is dependent on the anisotropy, or directional control, of the magnetic energy of the particle, as well as the arrangement of crystals in the rock matrix. The magnetic field required to demagnetize a saturation magnetization is often referred to as the coercivity of that magnetization (especially when referring to AF demagnetization). See Appendix D-1 and D-2 for all data and plots.

INTERPRETATION OF DATA AND DISCUSSION

Mineral composition of each core sample was determined by coercivity spectral analysis with saturation isothermal remanent magnetization followed by a demagnetizing alternating field to determine a subaerial exposure horizon. Data also used to identify this evidence for a sea level lowstand are represented in Figure 11 with the comparison between the stable isotope Carbon-13 and AF15 intensity. Negative (or light values) of the carbon isotope and a trend of increasing AF15 intensity may show evidence for an exposure horizon. The data I collected identified a diagnostic subaerial exposure surface horizon (indicating a sea level lowstand) in one sample with hematite and coarse-grained magnetite.

Sample #41 (data in Appendix D-1 and plot in Appendix D-2) has a diagnostic coercivity spectra as compared to the mixed hematite standard and coarse-grained magnetite standard spectra (Figure 12) from Chang et al. (1987). Hematite shows its resistance to saturation as expected from its high-coercivity magnetic properties (Lowrie and Heller, 1982). Presence of hematite leaves strong evidence for subaerial exposure where the sample was collected.

Figure 13, from Chang et al. (1987), illustrates the coarse-grained magnetite standard, ultrafine-grained magnetite standard, and magnetotactic bacteria (single domain) spectra. These figures were used as a basis for my interpretation of the magnetic mineralogy and sea level lowstand of core BH-5. SIRM data were plotted in Figure 14 showing the magnetic mineralogical behavior data from this core, which is mainly due to coarse to fine-grained magnetite. The exception is sample #41 with significant hematite content as seen in yellow to the far right of the plot. Normal marine carbonate rocks do not contain hematite. Hematite in marine carbonates is formed by subaerial exposure during a sea level lowstand. Hematite formed during subaerial

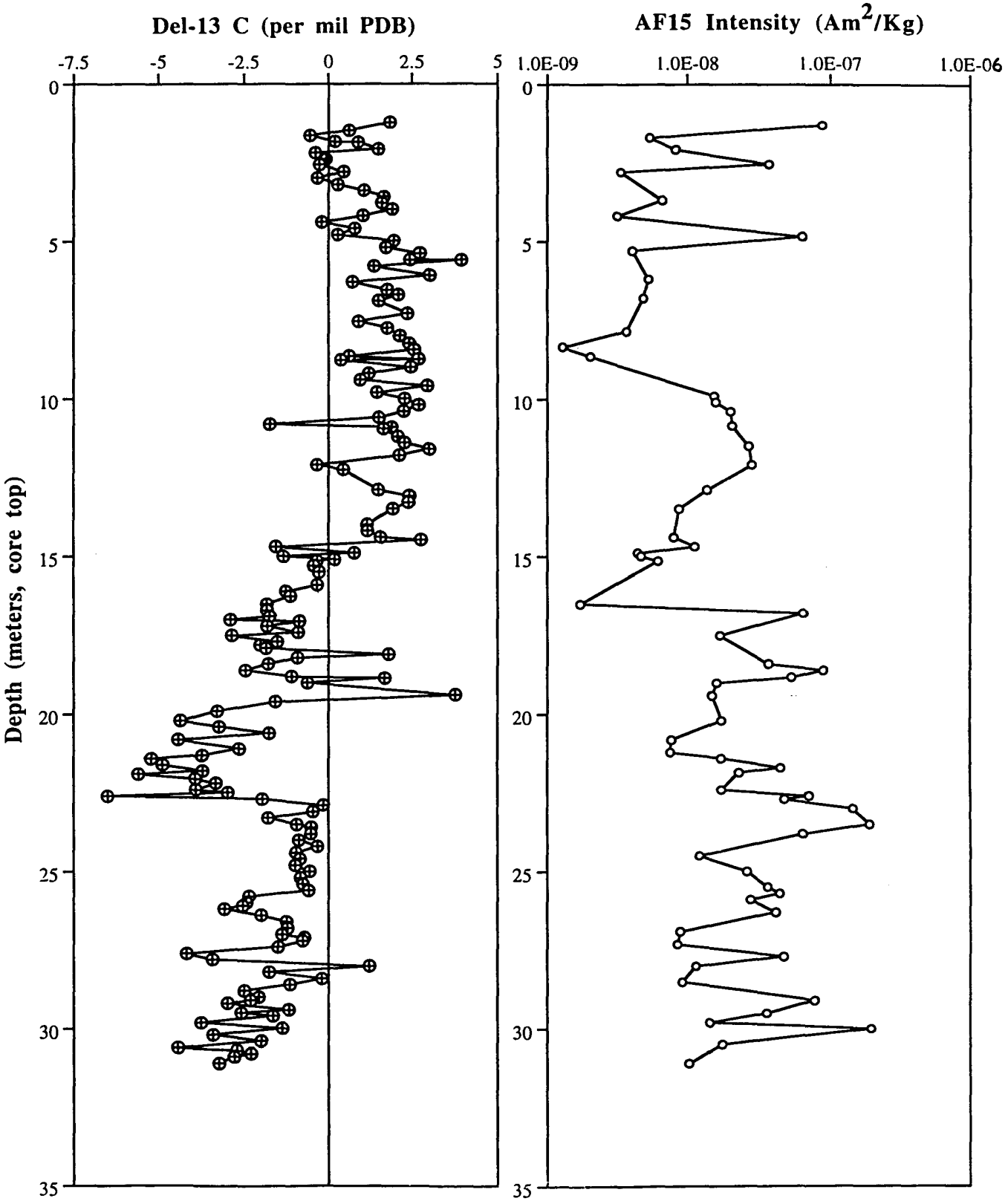

Figure 11. Stable isotope plot of carbon-13 measured in per mil PDB. AF15 intensity plot measured in Am^2/Kg. Comparison of these two plots help identify subaerial exposure surface horizons throughout the core depth (in meters from the core top).

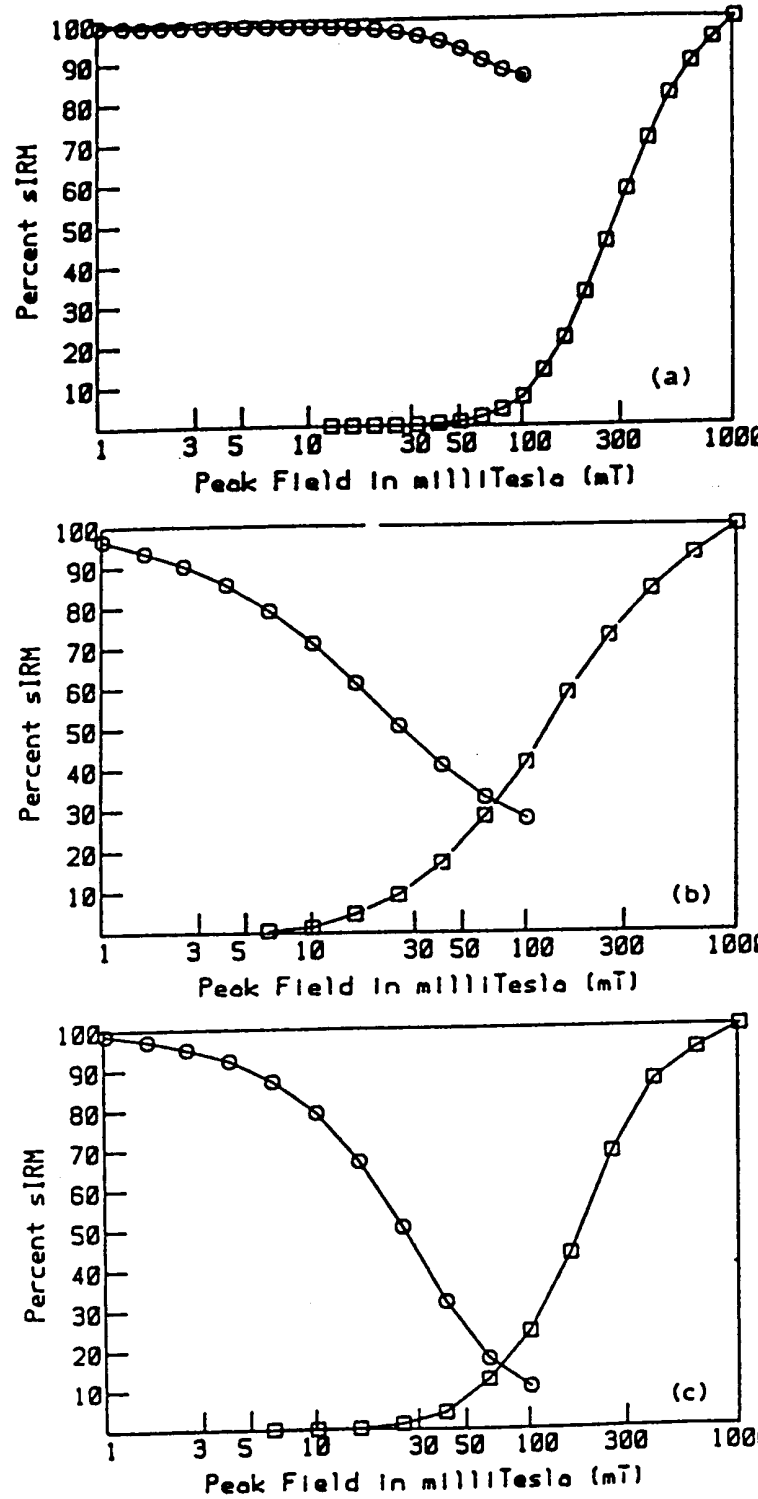

Figure 12. Coercivity spectra of A) hematite standard, B) mixture of hematite standard and coarse-grained magnetite standard, and C) mixture of hematite standard and ultrafine-grained magnetite standard. (Chang et al., 1987)

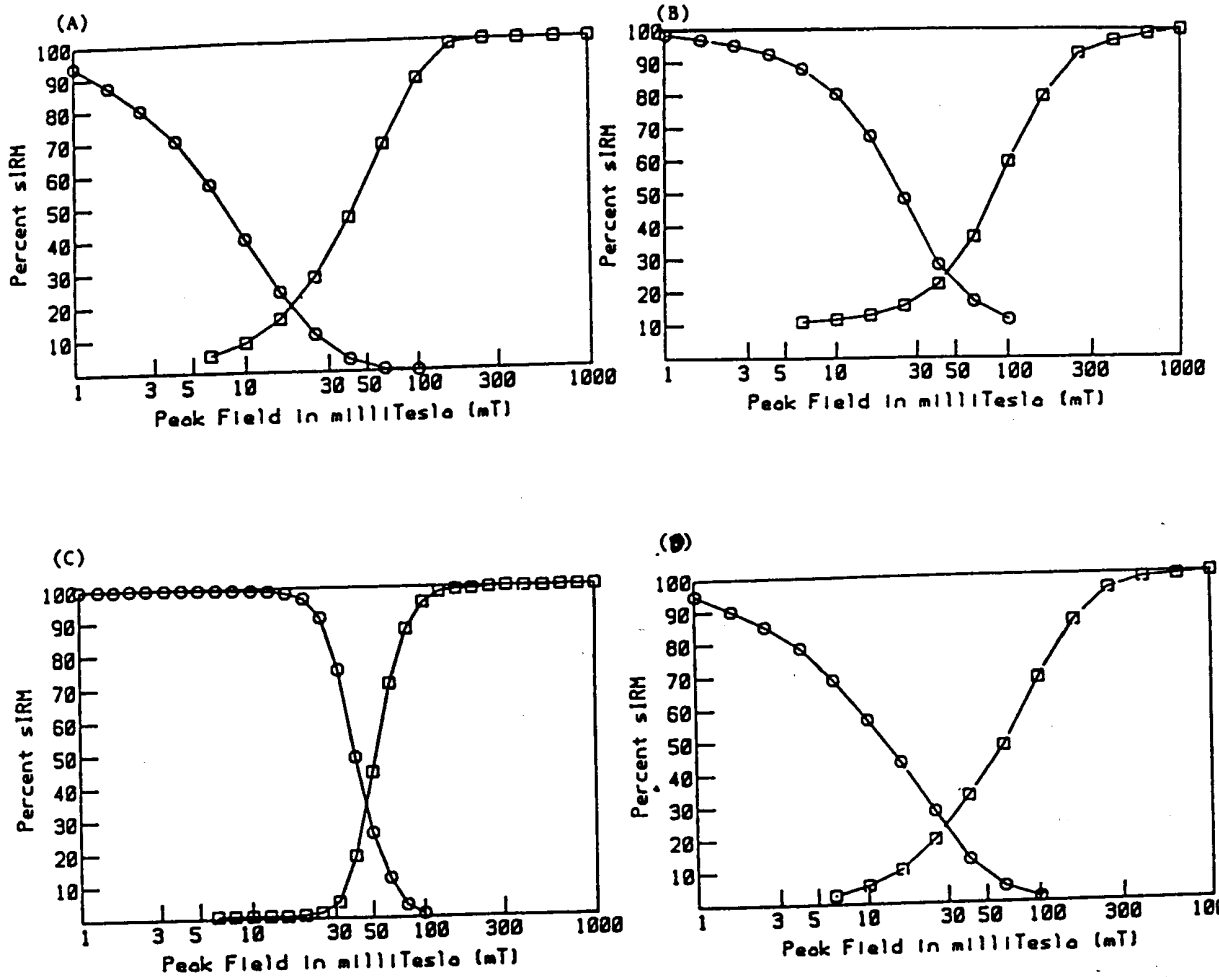

Figure 13. Coercivity spectra of A) coarse-grained magnetite standard, B) ultrafine-grained magnetite standard, C) magnetotactic bacteria, and D) mixture of coarse-grained and ultrafine-grained magnetite standard. (Chang et al., 1987)

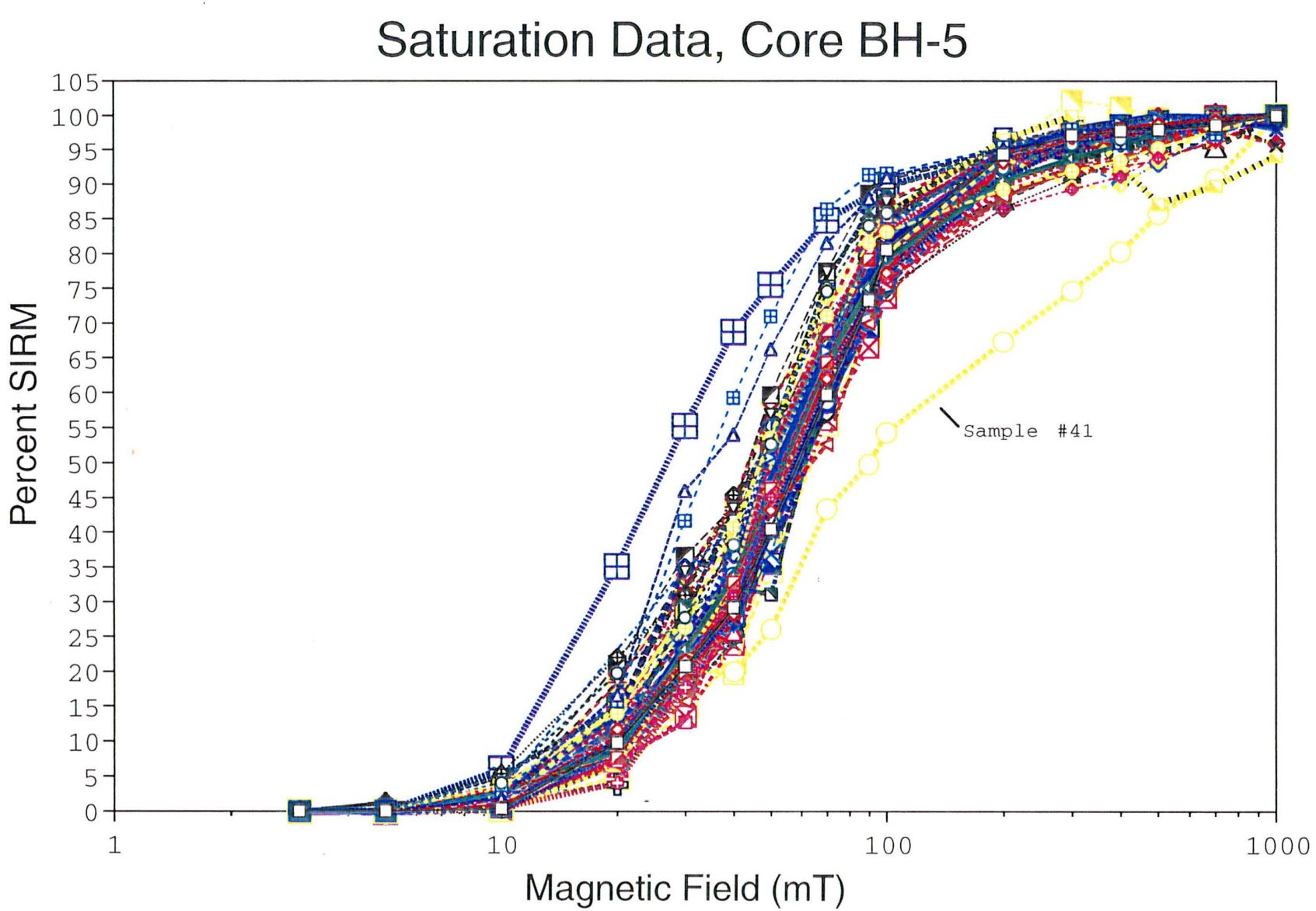

Figure 14. SIRM data shown for all 64 samples in bore hole core BH-5. Sample #41 shown in yellow on the right side of the plot represents a combination of hematite and coarse-grained magnetite mineral composition, which is a diagnostic subaerial exposure surface horizon. All other samples represent a pure marine depositional environment of fine-grained to coarse-grained magnetite.

exposure may be dispersed downward in the section during the formation of penetrative calcrete horizons which occur only during subaerial exposure. The uppermost horizon of carbonate rock containing hematite (sample #41) is the only certain marker horizon indicating subaerial exposure and a sea level lowstand. Hematite (and maghemite) in subjacent penetrative calcretes are not certain indicators. Sample #25 is regarded as representing a penetrative calcrete. Thus, only sample #41 is a certain indicator of subaerial exposure.

AGE OF CORE BH-5; PROBLEMS AND DISCUSSION

The age of the Matuyama Reverse and Brunhes Normal magnetic polarity reversal boundary is in dispute in the current reference literature. This reversal boundary is used as a global stratigraphic polarity reversal record between the Early and Middle Pleistocene. The exact timing of this polarity reversal has not been determined, the age is an estimation based on apparent ages of older (reversed polarity of the Matuyama chron), and younger (normal polarity of the Brunhes chron) rocks that surround the reversal horizon (Richmond and Fullerton, 1986).

Potassium-argon dates acquired by several researchers show the inconsistencies of the actual age of the Matuyama-Brunhes boundary. Mankinen and Dalrymple (1979) found an age of 0.730 Ma BP (Harland et al., 1982, and Butler, 1992, agree to this age). This age is used in recent studies of Quaternary terrestrial stratigraphy in the United States, while a younger age of 0.700 Ma BP found by Shackleton and Opdyke (1973, 1976) is used by some studies in Quaternary marine stratigraphy (Richmond and Fullerton, 1986). The 0.700 Ma BP boundary is thought to be too young and is not adopted in my research. Aurell et al. (1995) and Richmond and Fullerton (1986) have adopted the age of the Matuyama-Brunhes boundary to be 0.78 Ma BP, for consistency in a standard numerical age and for purposes of correlation. The astronomical age 0.788 Ma BP for the Matuyama-Brunhes polarity reversal boundary was adopted by Johnson (1982) and was used by Richmond and Fullerton (1986) for correlation of glacial periods.

"The most basic stratigraphic geology has not heretofore been elucidated for any Bahamian island" (Garret and Gould, 1984). The basic stratigraphy for New Providence Island proposed by Garret and Gould (1984) is based primarily

on a rapidly evolving snail, *Cerion*, and is supported by only one radiometric age result, a C^{14} age of 3680 ± 550 yr. BP age for *Cerion glans*. Although based on considerable field work, their age of 0.125 Ma BP for the most extensively exposed (youngest?) sedimentary deposits on New Providence Island is an estimate. The implication of accepting this age is (that) for the past 125,000 years, deposition and erosion have been occurring at the same rate on New Providence and the island's surface has been undergoing constant reworking by wind, wave, and tidal action, leaving the age of the surface sediments uncertain.

I am left with two options in interpreting the significance and stratigraphic correlation of the single and certain sea level lowstand identified in sample #41. These two options, A and B, are forced by (1) the uncertainty of the age of the youngest sediments on New Providence Island and (2) the uncertainty in current reference literature about the age of the Matuyama Reverse (MR) - Brunhes Normal (BN) magnetostratigraphic boundary which is the only stratigraphic marker horizon in core BH-5. This discrepancy in the literature for the age of the MR-BN magnetic polarity reversal directly affects the correlation between the sea level lowstand found and a single glaciation period represented in bore hole core BH-5 studied in my research.

Interpretation A is consistent with the MR-BN boundary being 0.78 Ma BP used by Aurell et al. (1995), Richmond and Fullerton (1986), and Bonnett et al. (1991). Interpretation B is consistent with the MR-BN boundary being 0.73 Ma BP, followed by Harland et al. (1982) and Butler (1992).

A.) The age of the base of core BH-5 below the MR-BN boundary is clearly greater than 0.78 Ma BP, and the top of core BH-5 may be as old as 0.13 Ma BP, as estimated by Garret and Gould (1994) and used by Aurell et al. (1995). In this case, the lowstand in sample #41 just above the MR-BN boundary approximately correlates with the Lower

Pleistocene Minford Silt Member of the Teays Formation in Ohio and West Virginia. The Minford Silt Member is a lacustrine unit deposited behind an ice dam of the pre-Illinoian G Glaciation in southern Ohio, approximately between 0.79 and 0.88 Ma BP (Bonnett et al., 1991).

B.) The age of the base of BH-5 is no older (and most likely younger) than 0.78 Ma BP while the top must be younger than 0.13 Ma BP. The lowstand in sample #41 will, therefore, be younger than the MR-BN boundary (0.73 Ma BP), and may mark the certain eustatic lowstand of the Illinoian Glaciation from 0.30 to 0.13 Ma BP (Richmond and Fullerton, 1986).

My research cannot resolve this issue until the age of the MR-BN boundary is resolved. I have established that there is a sea level lowstand in core BH-5 during the Early to Middle Pleistocene Epoch. Whether the lowstand is pre-Illinoian or Illinoian must await further study.

CONCLUSIONS

1.) Coercivity spectra data analysis from saturation isothermal remanent magnetization by a DC field followed by a demagnetizing alternating field in sample #41 display evidence of a subaerial exposure surface horizon containing hematite and coarse-grained magnetite. This sea level lowstand during Pleistocene time (following the MR-BN reversal) also matches the second type of data analysis from the stable isotope Carbon-13 measured in per mil PDB and AF15 demagnetization data measured in mT.

2.) Most samples taken from core BH-5 range in age from Early to Late Pleistocene time. These samples display a saturation coercivity spectra ranging from fine- to coarse-grained magnetite. The majority of the samples may contain both single domain and multiple domain magnetite, characteristic of a subaqueous marine depositional environment.

3.) Of the three hypotheses proposed for the origin of the Bahamian banks and basins, my results do not support or conflict with the studies of Mullins and Lynts (1977), (pre-Triassic); Ladd and Sheridan (1987), (Middle Jurassic - Tertiary); or Eberli and Ginsburg (1987), (Cretaceous-Tertiary). Based upon the geomagnetic polarity results of core BH-5 shown in Figure 9 (Aurell et al., 1995), my research concerned Early to Late Pleistocene (Figure 15) marine carbonates. These carbonates formed much later in geologic history than the time frames considered in the three hypotheses.

4.) My research clearly indicates a recorded of one sea level lowstand, presumably of glacial eustatic origin, at a depth of 14.7 meters from the core top

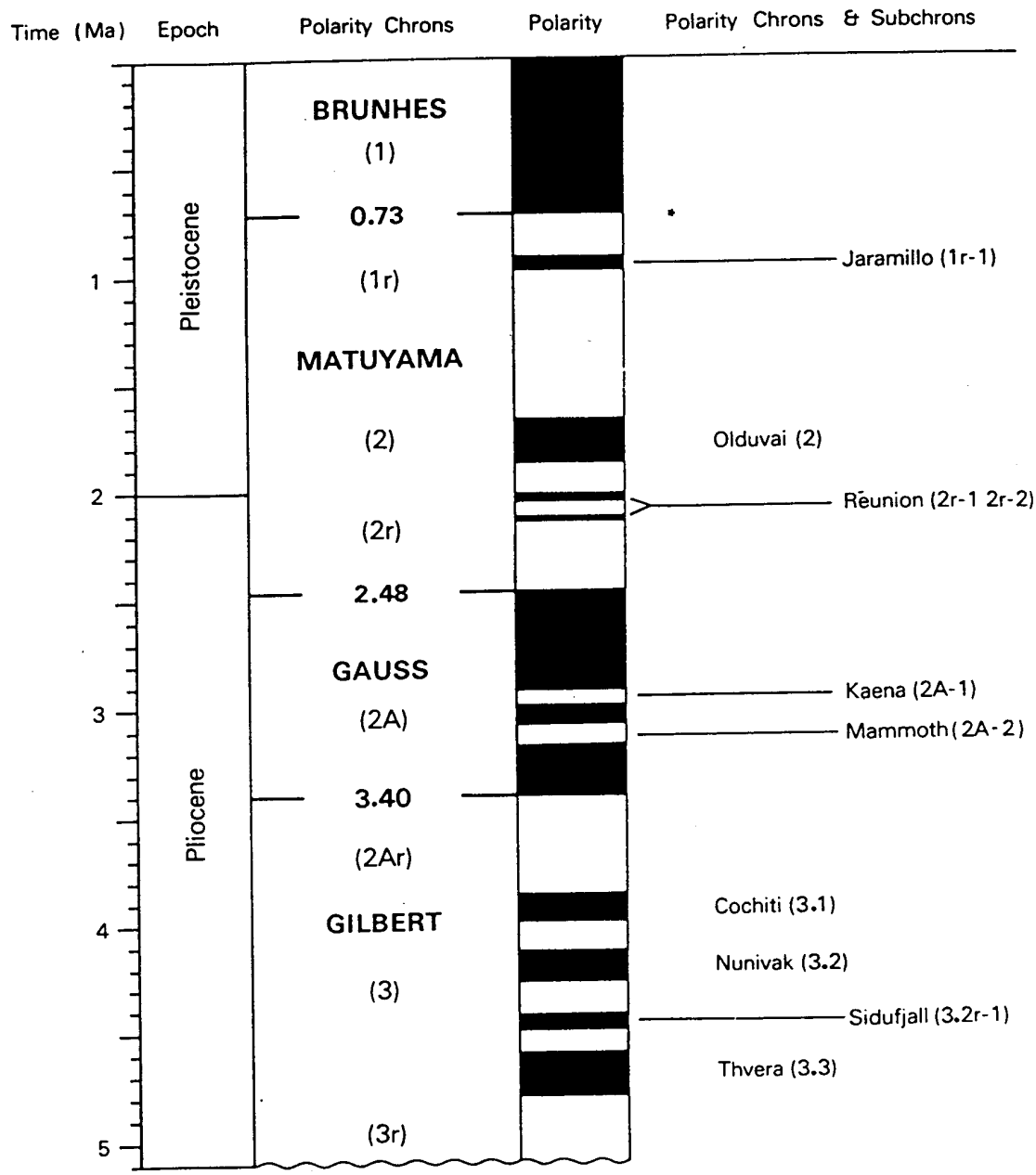

Figure 15. Magnetostratigraphic time scale displaying polarity of the Pleistocene Epoch, the age of core BH-5. The black sections represent normal polarity and reverse polarity is white (Harland et al., 1982). *Disputed age for the Matuyama Reverse - Brunhes Normal magnetostratigraphic boundary discussed in detail in text.

(sample #41). This confirms a global cooling event represented a disconformity and subaerial exposure on New Providence Island, Bahamas. This lowstand (above and younger than the MR-BN boundary because of the normal geomagnetic polarity of sample #41) may correlate with the Early Pleistocene Minford Silt Member, Teays Formation in Ohio and West Virginia (Bonnett et al., 1991) or the onset of the Illinoian Glaciation in the Middle Pleistocene (Richmond and Fullerton, 1986).

REFERENCES

Aurell, M., McNeill, D.F., Guyomard, T., and Kindler, P., 1995, Pleistocene shallowing-upward sequences in New Providence, Bahamas: signature of high-frequency sea-level fluctuations in shallow carbonate platforms: Journal of Sedimentary Research, v. B65, no. 1, p.170-182.

Bartman, R.C., Musser, K.J., and Noltimier, H.C., 1978, Paleomagnetic results from Upper Ordovician limestones in a long bore core from eastern Kentucky: EOS, v. 59, p. 225.

Bergstrom, S.M., Faber, J.A., and Noltimier, H.C., 1980, Geomagnetic reversal stratigraphy and conodont biostratigraphy of the Middle Ordovician Trenton Limestone, Michigan Basin: EOS, v. 61, p. 50.

Bergstrom, S.M., and Noltimier, H.C., 1982, Latitudinal positions of Ordovician plates based on paleomagnetic evidence: IV International Symposium on the Ordovician System, Abstracts for Meetings: Paleontological Conference at the University of Oslo, no. 280, p. 8.

Bonnett, R.B., Noltimier, H.C., and Sanderson, D.D., 1991, A paleomagnetic study of the Early Pleistocene Minford Silt Member, Teays Formation, West Virginia, *in* Melhorn, W.N., and Kempton, J.P., eds., Geology and hydrogeology of the Teays-Mahomet Bedrock Valley System: Boulder, Colorado, Geological Society of America Special Paper 259, p. 9-18.

Bowen, D.Q., Richmond, G.M., Fullerton, D.S., Sibrava, V., Fulton, R.J., Velichko, A.A., 1986, Correlation of Quaternary glaciations in the Northern Hemisphere: Quaternary Science Reviews, v. 5, p. 509-510.

Butler, R.F., 1992, Paleomagnetism: Magnetic Domains to Geologic Terrains: Boston, Massachusettes, Blackwell Scientific Publications, 319 p.

Chang, S-B. R., Kirschvink, J.L., and Stolz, J.F., 1987, Biogenic magnetite as a primary remanence carrier in limestone deposits: Physics of the Earth and Planetary Interiors, v. 46, p. 289-303.

Cisowski, S., 1981, Interacting vs. non-interacting single domain behavior in natural and synthetic samples: Physics of the Earth and Planetary Interiors, v. 26, p. 56-62.

Curran, H.A., 1985, Introduction to the geology of the Bahamas and San Salvador Island, with an overflight guide, *in* Curran, H.A., ed., Pleistocene and Holocene carbonate environments on San Salvador Island: Bahamas Guidebook for Geological Society of America, p. 1-8.

Dunham, J.R., 1962, Classification of carbonate rocks according to depositional texture, in W.E. Ham (ed.), Classification of carbonate rocks: Am. Assoc. Petroleum Geologists Mem. 1. Table 1, p.117.

Eberli, G.P., Ginsburg, R.N., 1987, Segmentation and coalescence of Cenozoic carbonate platforms, Northwestern Great Bahama Bank: Geology, v. 15, p. 75-79.

Garrett, P., and Gould, S.J., 1984, Geology of New Providence Island, Bahamas: Geological Society of America Bulletin, v. 95, p. 209-220.

Glaccum, R.A., and Prospero, J.M., 1980, Saharan aerosols over the tropical North Atlantic-mineralogy: Marine Geology, v. 37, p. 295-321.

Harland, W.B., Cox, A.V., Llewellyn, P.G., Pickton, G.A.G., Smith, A.G., Walters, R., 1982, A Geological Time Scale: Cambridge, Cambridge University Press, 131 p.

Johnson, R.G., 1982, Matuyama-Brunhes polarity reversal dated at 790,000 yr B.P. by marine-astronomical correlations: Quaternary Research, v. 17, p. 135-147.

Ladd, J.W., and Sheridan, R.E., 1987, Seismic stratigraphy of the Bahamas: AAPG Bulletin, v. 71, no. 6, p. 710-736.

Lins de Barros, H.G.P., and Esquivel, M.S., 1985, Magnetic microorganisms found in muds from Rio de Janeiro, *in* Kirschvink, J.L., Jones, D.S., and MacFadden, B.J., eds., Magnetite biomineralization and magnetoreception in organisms: Plenum, New York, p. 289-309.

Lovley, D.R., Stolz, J.F., Nord, F.L., Jr., and Phillips, E.J.P., 1987, Anaerobic production of magnetite by a dissimilatory iron-reducing microorganism: Nature, v. 330, p. 252-254.

Lowrie, W., and Fuller, M., 1971, On the alternating field demagnetization characteristics of multidomain thermoremanent magnetization in magnetite: Journal of Geophysical Research, v. 76, p. 6339-6349.

Lowrie, W., and Heller, F., 1982, Magnetic properties of marine limestones: Reviews of Geophysics and Space Physics, v. 20, no. 2, p. 171-192.

Mankinen, E.A., and Dalrymple, G.B., 1979, Revised geomagnetic polarity time scale for the interval 0-5 m.y. BP: Journal of Geophysical Research, v. 17, p. 135-147.

McNeill, D.F., Ginsburg, R.N., Chang, S.-B.R., and Kirschvink, J.L., 1988, Magnetostratigraphic dating of shallow-water carbonates from San Salvador, the Bahamas: Geology, v. 16, p. 8-12.

McNeill, D.F., 1990, Biogenic magnetite from surface Holocene carbonate sediments, Great Bahama Bank: Journal of Geophysical Research, v. 95, p. 4353-4371.

McNeill, D.F., Guyomard, T.S., and Hawthorne, T.B., 1993, Magnetostratigraphy and the nature of magnetic remanence in platform/periplatform carbonates, Queensland Plateau, Australia: Proceedings of the Ocean Drilling Program, Scientific Results, v. 133, p. 573-614.

McNeill, D.F., 1993, A review and comparison of carbonate rock magnetization: Leg 133, Queensland Plateau, Australia: Proceedings of the Ocean Drilling Program, Scientific Results, v. 133, p. 749-753.

McNeill, D.F., and Kirschvink, J.L., 1993, Early dolomitization of platform carbonates and the preservation of magnetic polarity: Journal of Geophysical Research, v. 98, p. 7977-7986.

Mullins, H.T., and Lynts, G.W., 1977, Origin of the Northwestern Bahama Platform: review and reinterpretation: Geological Society of America Bulletin, v. 88, p. 1447-1461.

Noltimier, H.C., and Bergstrom, S.M., 1976, Paleomagnetic studies in Early and Middle Ordovician limestones from the Baltic Shield: Geological Society of America Abstracts with Programs, North-Central Meeting, v. 8, p. 501.

Noltimier, H.C. and Patzwahl, D.W., 1982, Comparison of paleomagnetic records in two Middle Ordovician borehole cores correlated biostratigraphically: EOS, v. 63, p. 615.

Noltimier, H.C., and Patzwahl, D.W., 1982, Review of paleomagnetic results from 600 continuous feet of Middle and Upper Ordovician limestone borehole core: EOS, v. 63, p. 616.

Patzwahl, D.W., and Noltimier, H.C., 1981, Paleomagnetic study of the Middle Ordovician Lexington Limestone in reference core CA-38, Minerva, Kentucky: EOS, v. 62, p. 271.

Piper, J.D.A., 1987. Paleomagnetism and the Continental Crust: Milton Keynes, England, Open University Press, 434 p.

Richmond, G.M., and Fullerton, D.S., 1986, Introduction to Quaternry glaciations in the United States of America: Quaternary Science Reviews, v. 5, p. 3-10.

Rossinsky, V., Jr., Wanless, H.R., and Swart, P.K., 1992, Penetrative calcretes and their stratigraphic implications: Geology, v. 20, p. 331-334.

Rossinsky, V., Jr., 1990, Topographic, vegetative, and climatic controls on the petrography and geochemistry of calcretes in the Bahamas and south Florida [Ph.D. thesis]: Miami, Florida, University of Miami, 228 p.

Shackleton, N.J., and Opdyke, N.D., 1973, Oxygen isotope and paleomagnetic stratigraphy of equatorial Pacific core V28-238: Oxygen isotope temperatures and ice volumes on a 10^5 year and 10^6 year scale: Quaternary Research, v. 3, p. 39-55.

Shackleton, N.J., and Opdyke, N.D., 1976, Oxygen-isotope and paleomagnetic stratigraphy of Pacific core V28-239, late Pliocene to latest Pleistocene, *in* Cline, R.M., and Hays, J.D., eds., Investigation of late Quaternary paleoceanography and paleoclimatology: Geological Society of America Memoir, v. 145, p. 449-464.

Sheridan, R.E., Mullins, H.T., Austin, J.A., Jr., Ball, M.M., and Ladd, J.W., 1988, Geology and geophysics of the Bahamas, *in* Sheridan, R.E., Grow, J.A., eds., The Atlantic continental margin: U.S.: Geological Society of America, v. I-2, p. 329-364.

Smith, T.E., and Noltimier, H.C., 1979, Paleomagnetism of the Newark trend igneous rocks of the north central Appalachians and the opening of the central Atlantic Ocean: American Journal of Science, v. 279, p. 778-807.

Stoltz, J.F., Chang, S.-B.R., and Kirschvink, J.L., 1989, The effect of magnetotactic bacteria on the magnetic properties of marine sediments, *in* Crick, R.E., ed., Origin, evolution and modern aspects of biomineralization in plants and animals: Plenum, New York, p. 497-506.

Stupp, B.J., and Noltimier, H.C., 1980, Paleomagnetic study of the Middle and Upper Ordovician reference standard core CA-38, Minerva, Kentucky: EOS, v. 62, p. 217.

Thompson, R., and Oldfield, F., 1986, Environmental Magnetism: London, England, Allen and Unwin, 227 p.

Towe, K.M., and Moench, T.T., 1981, Electro-optical characterization of bacterial magnetite: Earth and Planetary Science Letters, v. 52, p. 213-220.

APPENDIX A-1

DUNHAM'S (1962) CLASSIFICATION OF CARBONATE ROCKS

Dunham's (1962) Classification for Carbonate Rocks

<table>
<tr><th colspan="5">DEPOSITIONAL TEXTURE RECOGNIZABLE</th><th>DEPOSITIONAL TEXTURE NOT RECOGNIZABLE</th></tr>
<tr><td colspan="4">Original components not bound together during deposition</td><td rowspan="3">Original componenets were bound together during deposition... as shown by inter-grown skeletal matter, lamination contrary to gravity, or sediment-floored cavities are roofed over by organic or questionably organic matter and are too large to be interstices.</td><td rowspan="3">CRYSTALLINE CARBONATE

(Subdivide according to classifications designed to bear on physical texture or diagenesis.)</td></tr>
<tr><td colspan="3">Contains mud (particles of clay and fine silt size)</td><td rowspan="2">Lacks mud and is grain-supported</td></tr>
<tr><td colspan="2">Mud-supported</td><td rowspan="2">Grain-supported</td></tr>
<tr><td>Less than 10% grains</td><td>More than 10% grains</td><td></td><td></td><td></td></tr>
<tr><td>MUDSTONE</td><td>WACKESTONE</td><td>PACKSTONE</td><td>GRAINSTONE</td><td>BOUNDSTONE</td><td></td></tr>
</table>

APPENDIX A-2

CORE DESCRIPTION

Core BH-5

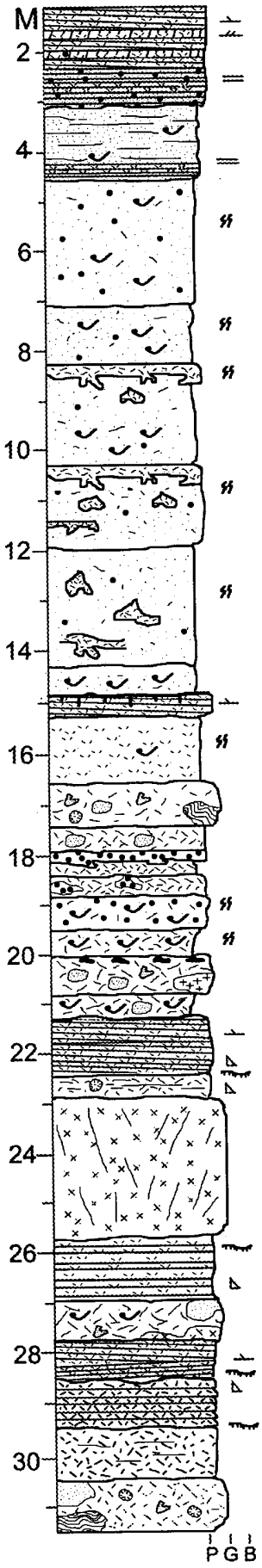

- fine skeletal grains
- coarse skeletal grains
- peloids
- ooids
- large mollusks
- graded skeletal layers (tempestites)
- high-angle cross-lamination
- parallel lamination
- low-angle cross-lamination
- bioturbation
- branching *Porites* sp.
- *Agaricia* sp.
- massive Porites
- *Diploria* sp.
- *Siderastrea* sp.
- *Montastrea* sp.
- *Callianassa* burrows
- micritic crust
- subaerial exposure/disconformity surface
- P packstone
- G grainstone
- B boundstone

CORE DESCRIPTION

Specimen Number (drilled)	Depth Estimate (meters)	Description (using Dunham's (1962)Classification, Appendix A-1)
1	31.1	dense, indurated grainstone, freshwater flow features present 2" above, some orange-brown staining, vuggy
2	30.5	dense, indurated grainstone, fresh water flow features present, some orange-brown staining, vugs present
3	30.0	dense, well indurated wackestone, brown color
4	29.8	dense indurated grainstone, well sorted
5	29.5	dense indurated grainstone, orange stained, vugs present
6	29.1	coarse-grained skeletal grainstone, well indurated, well sorted
7	28.5	coarse-grained skeletal grainstone, well indurated, well sorted
8	28.0	coarse-grained skeletal grainstone, very well indurated, well sorted, brown-tan color
9	27.7	well indurated, coral-rich grainstone/packstone
10	27.3	well indurated, coral-rich grainstone/packstone, less dense, vugs following corals
11	26.9	coarse-grained grainstone, well cemented, medium sorting
12	26.3	very coarse-grained grainstone, slight orange staining, skeletal
13	25.9	very coarse-grained grainstone, slight orange staining, skeletal, just below a brown/tan calcrete (?) layer
14	25.7	coarse-grained grainstone, well indurated, skeletal 1" below dense tan interval from sample 15
15	25.5	dense, packstone, very well indurated, perhaps a recrystallized coral present (?)
16	25.0	very dense, packstone, very well indurated, recrystallized coral (?), brown/tan staining
17	24.5	packstone, recrystallized coral
18	23.8	packstone, recrystallized coral
19	23.5	very dense, well indurated brown-tan packstone, some vugs
20	23.0	very dense, well indurated brown-tan packstone, some vugs, recrystallized coral
21	22.7	coarse grainstone, moderately well indurated, skeletal
22	22.6	dark brown, exposure horizon, dense, well indurated
23	22.4	coarse grained grainstone, skeletal, moderately well indurated

24	21.85	partial subaerial exposure/calcrete horizon, dark brown
25	21.7	dark brown, calcrete, penetrative calcrete (?), trellis structure
26	21.4	dark brown, calcrete, penetrative calcrete (?), trellis structure
27	21.2	moderately indurated packstone/grainstone, chalky
28	20.8	moderately indurated packstone/grainstone, chalky
29	20.2	coarse-grained grainstone, molds of bivalves, moderately well indurated
30	19.4	tan matrix of ooid-rich burrow infills, matrix also contains ooids
31	19.0	tan matrix of ooid-rich burrow infills, matrix also contains ooids, ooid filled vugs, matrix more indurated, dense, tan
32	18.82	
33	18.6	dense, very well indurated grainstone, white
34	18.4	dense, tan, very well indurated packstone, wackestone, more dense than specimen 33
35	17.5	dense, tan, very well indurated packstone/wackestone
36	16.8	coarse grainstone, skeletal, white
37	16.5	friable, poorly indurated, orange-tan stained grainstone
38	15.15	dense, tan, very well indurated packstone/wackestone
39	15.0	well indurated grainstone, white
40	14.9	coarse-fine laminated grainstone
41	14.7	
42	14.4	
43	13.5	
44	12.9	
45	12.1	
46	11.5	
47	10.85	
48	10.4	
49	10.1	well-sorted, fine grainstone, burrowed-partially burrowed
50	9.9	

51	8.65	
52	8.35	well-sorted, fine grainstone, burrowed-partially burrowed
53	7.85	well-sorted, fine grainstone, burrowed-partially burrowed
54	6.8	well-sorted, fine grainstone, burrowed-partially burrowed
55	6.2	well-sorted, fine grainstone, burrowed-partially burrowed
56	5.3	well-sorted, fine grainstone, burrowed-partially burrowed
57	4.85	well-sorted, fine grainstone, burrowed-partially burrowed, finer grained
58	4.2	finer grained, well-sorted, fine grainstone, burrowed-partially burrowed
59	3.7	finer grained, well-sorted, fine grainstone, burrowed-partially burrowed
60	2.8	cross-bedded, finer grained, well-sorted, fine grainstone, burrowed-partially burrowed
61	2.55	finer grained, well-sorted, fine grainstone, burrowed-partially burrowed
62	2.08	cross-bedded, coarse grainstone, moderately well indurated
63	1.7	cross-bedded, coarse grainstone, moderately well indurated
64	1.3	cross-bedded, coarse grainstone, moderately well indurated, iron-stained orange

APPENDIX B-1

STABLE ISOTOPE DATA

Depth (m)	Del-13 C	Del-18 O
1.23	1.85	-1.82
1.48	0.63	-2.67
1.64	-0.55	-3.33
1.84	0.2	-2.9
1.86	0.9	-2.84
2.08	1.51	-1.75
2.2	-0.38	-2.64
2.4	-0.06	-2.7
2.58	-0.26	-2.86
2.8	0.47	-2.75
3	-0.33	-3.2
3.2	0.29	-3.03
3.4	1.08	-2.78
3.6	1.68	-2.58
3.8	1.62	-2.11
4	1.93	-3.3
4.2	1.05	-3.28
4.4	-0.19	-3.95
4.6	0.8	-3.03
4.8	0.29	-3.82
5	1.97	-3.31
5.2	1.74	-3.33
5.4	2.73	-3.22
5.6	2.45	-2.42
5.61	3.94	-1.74
5.8	1.38	-3.59
6.1	3	-2.71
6.3	0.73	-3.49
6.55	1.77	-3.49
6.7	2.11	-1.5
6.9	1.52	-3.28
7.3	2.37	-3.3
7.55	0.91	-3.15
7.75	1.77	-2.98
8	2.15	-3.51
8.25	2.43	-5.26
8.45	2.56	-2.68
8.65	0.63	-2.72
8.75	2.69	-3.23
8.77	0.38	-3.78
9	2.46	-3.2
9.2	1.22	-2.78
9.4	0.96	-3.03
9.6	2.94	-3.14
9.8	1.47	-2.79
10	2.29	-2.96
10.2	2.69	-2.72
10.4	2.26	-3.1
10.6	1.52	-3.06
19.4	3.75	0.01
19.6	-1.58	-2.81
19.9	-3.29	-2.62
20.2	-4.36	-2.33
10.8	-1.74	-3.25
10.9	1.9	-2.78
10.95	1.66	-3.06
11.2	2.09	-2.6
11.4	2.29	-2.83
11.6	2.99	-2.79
11.8	2.13	-2.55
12.1	-0.34	-3.4
12.25	0.45	-3.03
12.9	1.51	-2.6
13.1	2.43	-2.48
13.3	2.4	-2.41
13.5	1.94	-3.04
14	1.17	-2.71
14.2	1.19	-3.17
14.4	1.58	-3.6
14.5	2.75	-3.81
14.7	-1.56	-2.92
14.9	0.79	-2.93
15	-1.34	-2.89
15.1	0.19	-3.4
15.15	-0.34	-2.91
15.3	-0.44	-2.36
15.5	-0.27	-2.17
15.9	-0.33	-2.76
16.1	-1.26	-2.61
16.25	-1.13	-2.8
16.5	-1.83	-3.19
16.7	-1.83	-2.77
16.9	-1.75	-2.92
17	-2.89	-2.85
17.05	-0.86	-3.79
17.2	-1.81	-2.81
17.4	-0.89	-2.59
17.5	-2.86	-2.89
17.7	-1.52	-2.31
17.8	-2.02	-2.34
17.9	-1.85	-2.67
18.1	1.81	-0.87
18.2	-0.92	-2.51
18.4	-1.78	-2.52
18.6	-2.45	-2.81
18.8	-1.09	-2.3
18.85	1.7	-0.37
19	-0.62	-2.53

Depth (m)	Del-13 C	Del-18 O
22.5	-2.98	-2.49
22.6	-6.49	-2
22.7	-1.96	-2.4
22.9	-0.14	-3.14
23.1	-0.45	-2.19
23.3	-1.79	-3.05
23.5	-0.94	-2.41
23.6	-0.51	-2.14
23.8	-0.52	-2.24
24	-0.88	-2.09
24.2	-0.32	-3.41
24.4	-0.96	-2.33
24.6	-0.84	-3.03
24.8	-0.98	-2.44
25	-0.55	-2.7
25.2	-0.83	-2.13
25.4	-0.76	-2.63
25.6	-0.59	-2.53
25.8	-2.36	-2.24
26	-2.43	-2.11
26.1	-2.53	-2.09
26.2	-3.07	-2.16
26.4	-1.99	-2.21
26.6	-1.24	-2.37
26.8	-1.22	-2.1
27	-1.38	-2
27.1	-0.72	-1.9
27.2	-0.77	-1.94
27.4	-1.5	-2.06
27.6	-4.18	-2.17
27.8	-3.43	-2.31
28.8	-2.5	-2.25
29	-2.06	-1.81
29.1	-2.3	-2.31
29.2	-2.98	-2.72
29.4	-1.17	-1.23
29.5	-2.58	-2.39
29.6	-1.64	-2.32
29.8	-3.76	-2.29
30	-1.37	-1.04
30.2	-3.41	-2.09
30.4	-1.99	-1.42
30.6	-4.43	-2.55
30.7	-2.7	-2.05
30.8	-2.29	-1.93
30.9	-2.78	-2.22
31.1	-3.23	-2.34

APPENDIX B-2

STABLE ISOTOPE PLOTS
DEPTH (M) VS. DEL-13 C (per mil PDB)
DEPTH (M) VS. DEL-18 O (per mil PDB)

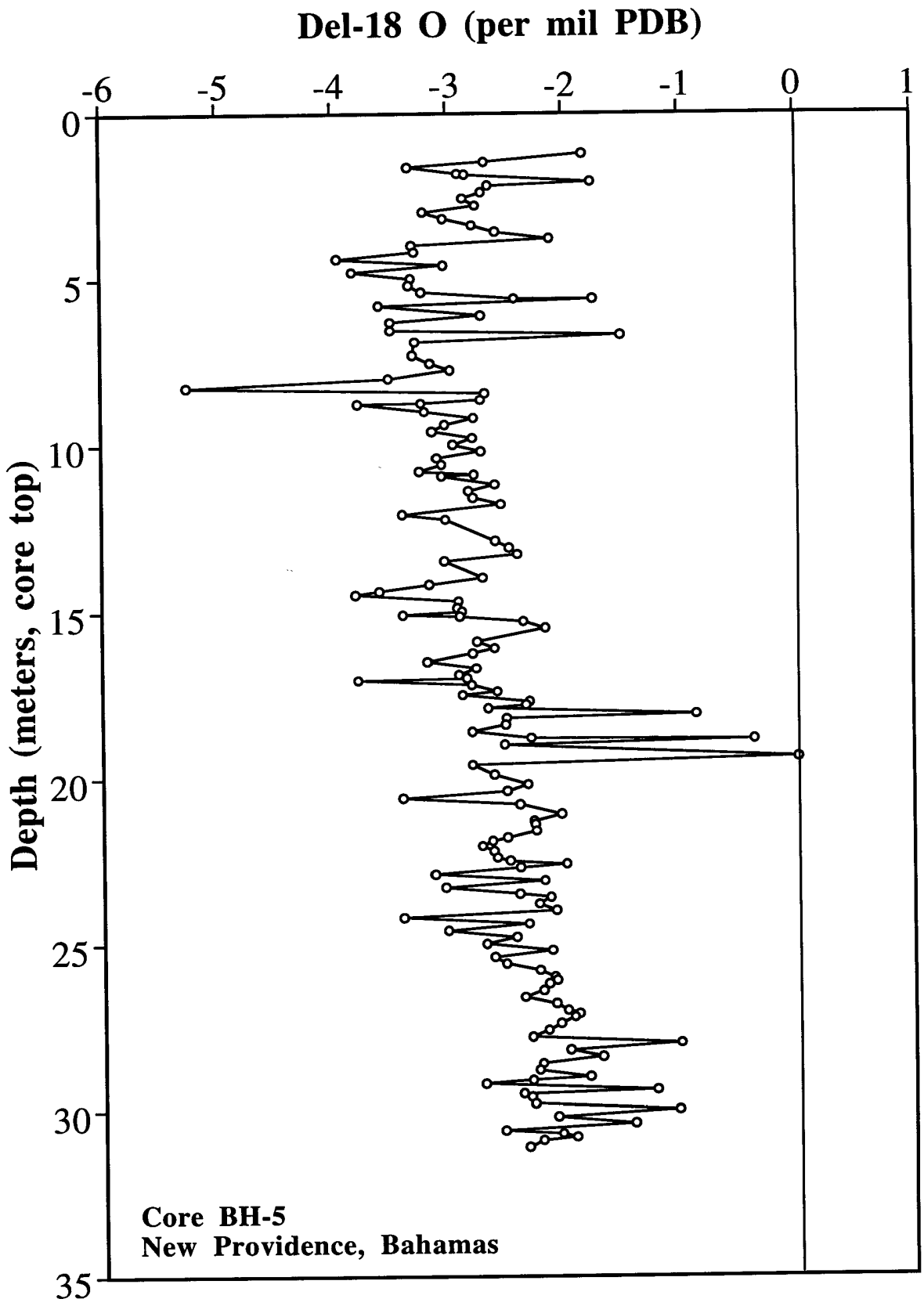
Del-18 O (per mil PDB)
-6
-5
-4
-3
-2
-1
0
1
Depth (meters, core top)
0
5
10
15
20
25
30
35
Core BH-5
New Providence, Bahamas

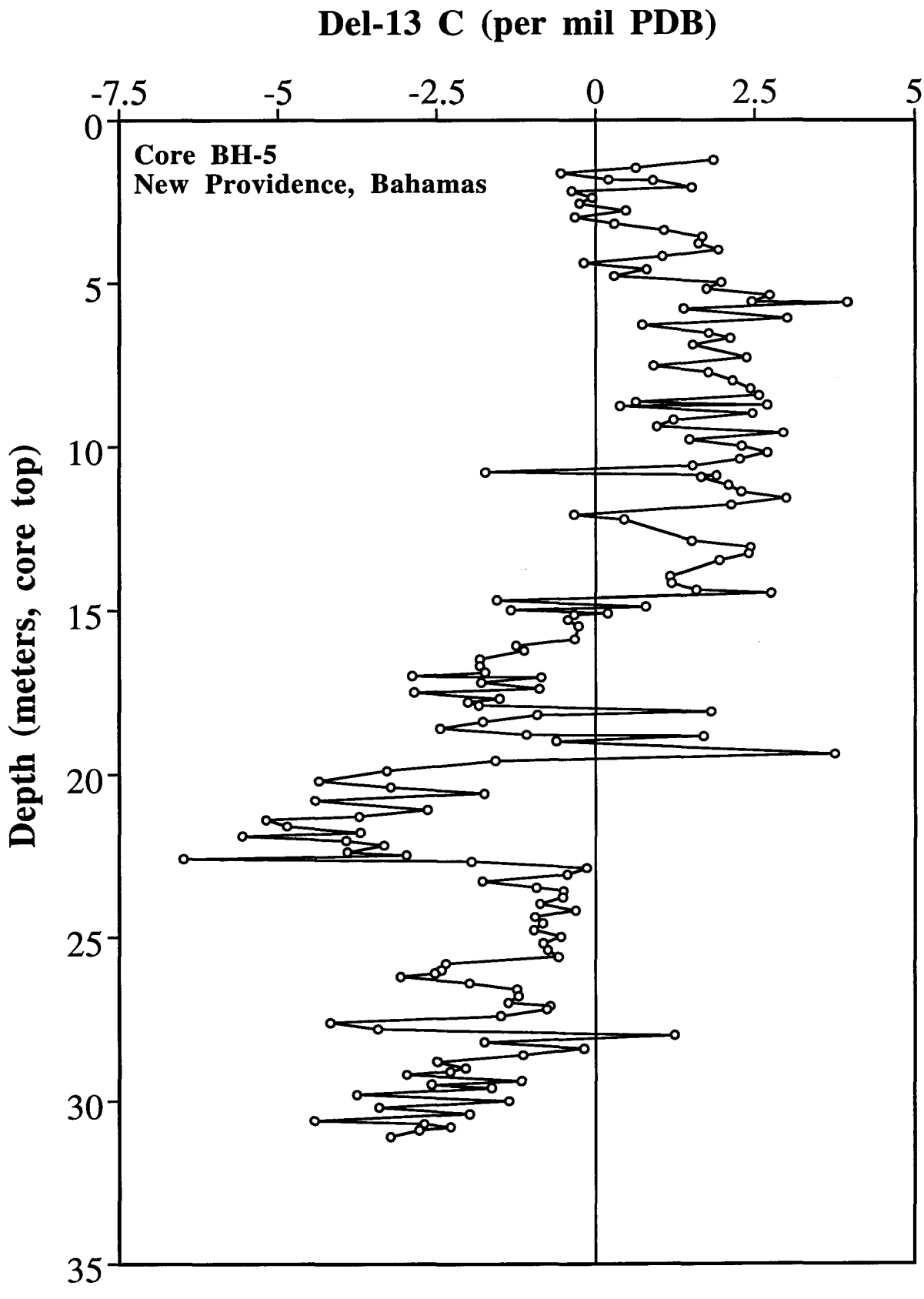
Del-13 C (per mil PDB)
-7.5
-5
-2.5
0
2.5
5
Core BH-5
New Providence, Bahamas
Depth (meters, core top)
0
5
10
15
20
25
30
35

APPENDIX C-1

DATA OF SAMPLE WEIGHT,
SUSCEPTIBILITY, NRM, AND AF 15
(in emu and SI units)

Depth (m)	Weight (Kg)	Susceptibility	NRM (emu)	AF 15 (emu)	NRM (Am^2/Kg)	AF 15 (Am^2/Kg)
31.1	0.0494	-1.3	1.5000E-06	5.1000E-07	3.04000000E-08	1.03000000E-08
30.5	0.0492	-1.2	7.1000E-06	8.7000E-07	1.44000000E-07	1.77000000E-08
30	0.0379	0.6	0.000086	0.000011	2.27000000E-06	2.90000000E-07
29.8	0.0437	0.1	1.5000E-06	6.3000E-07	3.43000000E-08	1.44000000E-08
29.5	0.0415	-1.1	4.4000E-06	1.5000E-06	1.06000000E-07	3.61000000E-08
29.1	0.0399	-1	0.00001	3.1000E-06	2.51000000E-07	7.40000000E-08
28.5	0.0487	-1.3	1.7000E-06	4.5000E-07	3.49000000E-08	9.24000000E-09
28	0.0529	-1.4	2.6000E-06	6.1000E-07	4.91000000E-08	1.15000000E-08
27.7	0.0421	-0.8	4.3000E-06	2.0000E-06	1.02000000E-07	4.75000000E-08
27.3	0.0387	-0.9	7.8000E-07	3.3000E-07	2.02000000E-08	8.53000000E-09
26.9	0.0336	-0.7	1.1000E-06	3.0000E-07	3.27000000E-08	8.93000000E-09
26.3	0.0204	-0.2	1.3000E-06	8.5000E-07	6.37000000E-08	4.17000000E-08
25.9	0.0344	-0.7	1.9000E-06	9.5000E-07	5.52000000E-08	2.76000000E-08
25.7	0.0407	-1.1	4.9000E-06	1.8000E-06	1.20000000E-07	4.42000000E-08
25.5	0.0466	-1	3.9000E-06	1.7000E-06	8.37000000E-08	3.65000000E-08
25	0.0459	-1.1	2.2000E-06	1.2000E-06	4.79000000E-08	2.61000000E-08
24.5	0.0345	-0.7	5.5000E-07	4.2000E-07	1.59000000E-08	1.22000000E-08
23.8	0.0358	-0.7	4.8000E-06	2.3000E-06	1.34000000E-07	6.42000000E-08
23.5	0.048	-0.9	0.000021	9.1000E-06	4.37000000E-07	1.90000000E-07
23	0.0474	-1.2	0.000013	6.8000E-06	2.74000000E-07	1.43000000E-07
22.7	0.0274	-0.6	1.9000E-06	1.3000E-06	6.93000000E-08	4.74000000E-08
22.6	0.0355	1.3	8.8000E-06	2.3000E-06	2.48000000E-07	6.48000000E-08
22.4	0.0249	-0.5	8.4000E-07	4.3000E-07	3.37000000E-08	1.73000000E-08
21.85	0.038	-1	1.4000E-06	8.7000E-07	3.68000000E-08	2.29000000E-08
21.7	0.0313	0.2	5.0000E-06	1.4000E-06	1.60000000E-07	1.72000000E-08
21.4	0.0233	-0.2	1.3000E-06	4.0000E-07	5.58000000E-08	7.56000000E-09
21.2	0.045	-1.1	7.0000E-07	3.4000E-07	1.56000000E-08	7.69000000E-09
20.8	0.0403	-1	5.1000E-07	3.1000E-07	1.27000000E-08	1.73000000E-08
20.2	0.0324	-0.8	1.2000E-06	5.6000E-07	3.70000000E-08	1.48000000E-08
19.4	0.0297	-0.8	1.1000E-06	4.4000E-07	3.70000000E-08	1.60000000E-08
19	0.0369	-1	1.3000E-06	5.9000E-07	3.52000000E-08	5.34000000E-08
18.82	0.0468	-1.1	5.0000E-06	2.5000E-06	1.07000000E-07	8.85000000E-08
18.6	0.0418	-0.9	4.8000E-06	3.7000E-06	1.15000000E-07	3.66000000E-08
18.4	0.0492	-1.2	3.7000E-06	1.8000E-06	7.52000000E-08	1.68000000E-08
17.5	0.0463	-1	1.3000E-06	7.8000E-07	2.81000000E-08	1.68000000E-08
16.8	0.0371	-0.8	9.7000E-07	6.6000E-07	2.53000000E-08	1.78000000E-08
16.5	0.042	-1	1.8000E-07	7.2000E-08	4.29000000E-09	1.71000000E-09
15.15	0.0389	-1.2	2.8000E-07	2.4000E-07	7.20000000E-09	6.17000000E-09
15	0.0384	-0.9	3.2000E-07	1.8000E-07	8.33000000E-09	4.69000000E-09
14.9	0.0361	-1	3.2000E-07	1.6000E-07	8.86000000E-09	4.43000000E-09
14.7	0.0374	-0.7	8.3000E-07	4.2000E-07	2.22000000E-08	1.12000000E-08
14.4	0.0274	-0.8	4.3000E-07	2.2000E-07	1.57000000E-08	8.03000000E-09
13.5	0.023	0.7	3.0000E-07	2.0000E-07	1.30000000E-08	8.70000000E-09
12.9	0.0219	-0.6	4.2000E-07	3.0000E-07	1.92000000E-08	1.37000000E-08
12.1	0.0221	-0.8	7.6000E-07	6.2000E-07	3.44000000E-08	2.81000000E-08

Depth (m)	Weight (Kg)	Susceptibility	NRM (emu)	AF 15 (emu)	NRM (Am^2/Kg)	AF 15 (Am^2/Kg)
11.5	0.0239	-0.8	9.2000E-07	6.4000E-07	3.85000000E-08	2.68000000E-08
10.85	0.021	-0.8	6.6000E-07	4.3000E-07	3.14000000E-08	2.05000000E-08
10.4	0.0185	-0.7	5.9000E-07	3.7000E-07	3.19000000E-08	2.00000000E-08
10.1	0.0298	-0.7	7.9000E-07	4.7000E-07	2.65000000E-08	1.58000000E-08
9.9	0.0208	-0.6	5.4000E-07	3.2000E-07	2.60000000E-08	1.54000000E-08
8.65	0.0222	-0.6	4.1000E-08	4.5000E-08	1.85000000E-09	2.03000000E-09
8.35	0.056	-0.7	9.3000E-08	7.2000E-08	1.66000000E-09	1.29000000E-09
7.85	0.0261	-0.7	1.6000E-07	9.6000E-08	6.13000000E-09	3.68000000E-09
6.8	0.0205	-0.6	2.0000E-07	1.0000E-07	9.76000000E-09	4.88000000E-09
6.2	0.0397	-1	2.9000E-07	2.1000E-07	7.30000000E-09	5.29000000E-09
5.3	0.0343	-0.9	2.2000E-07	1.4000E-07	6.41000000E-09	4.08000000E-09
4.85	0.0369	-1.1	1.8000E-07	1.5000E-07	4.88000000E-09	4.07000000E-09
4.2	0.0347	-0.8	1.7000E-07	1.1000E-07	4.90000000E-09	3.17000000E-09
3.7	0.0361	-0.9	8.1000E-07	2.4000E-07	2.24000000E-08	6.65000000E-09
2.8	0.0358	-0.9	2.0000E-07	1.2000E-07	5.59000000E-09	3.35000000E-09
2.55	0.0377	-1.1	3.3000E-07	2.3000E-07	8.75000000E-09	6.10000000E-09
2.08	0.0302	-0.6	3.1000E-07	2.5000E-07	1.03000000E-08	8.28000000E-09
1.7	0.0315	-0.7	2.3000E-07	1.7000E-07	7.30000000E-09	5.40000000E-09
1.3	0.0253	2	5.3000E-06	2.2000E-06	2.09000000E-07	8.70000000E-08

APPENDIX C-2

PLOTS
DEPTH (M) VS. SUSCEPTIBILITY (CGS)
DEPTH (M) VS. NRM (Am^2/Kg)
DEPTH (M) VS. AF 15 (Am^2/Kg)

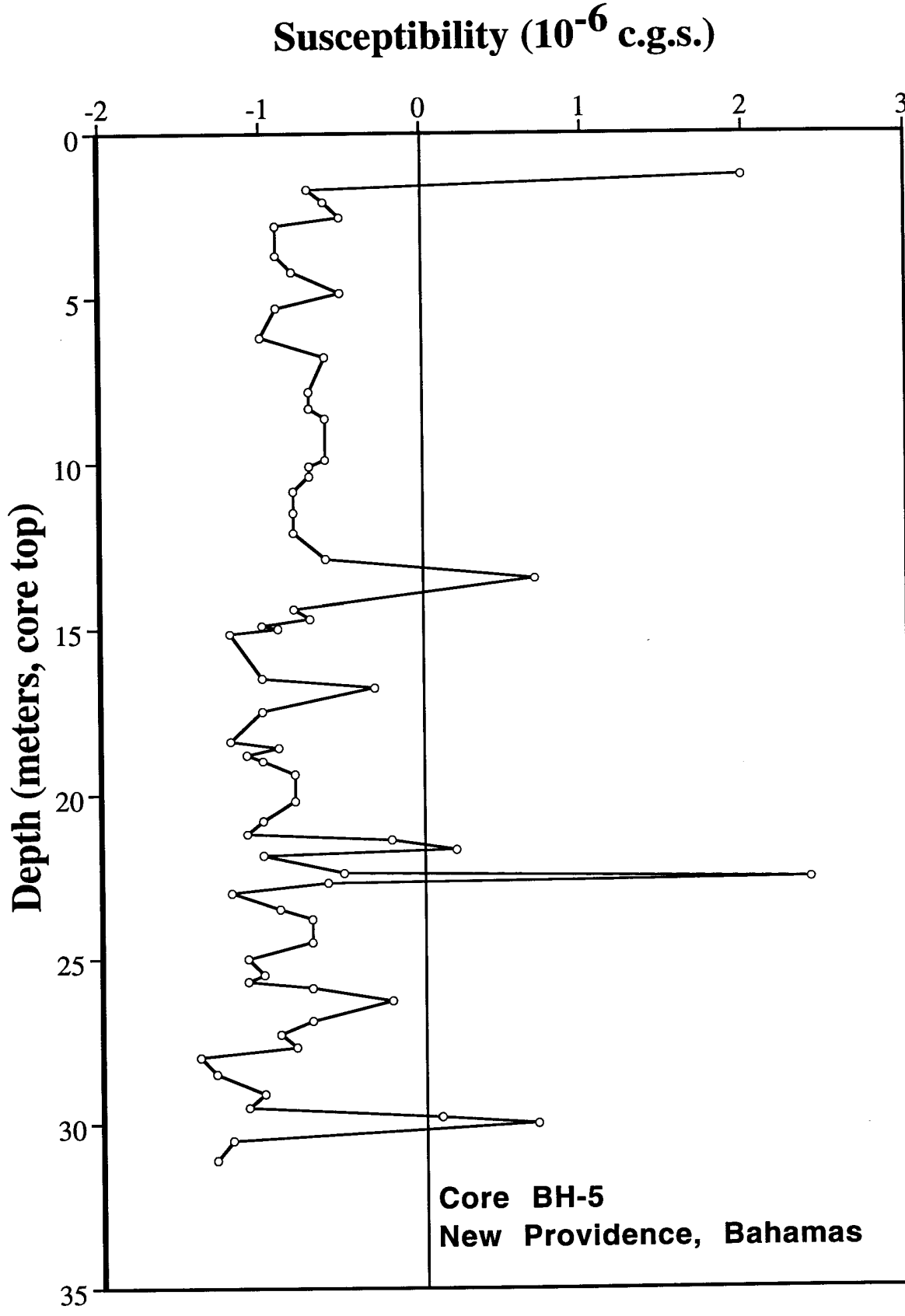
Susceptibility (10^{-6} c.g.s.)
-2
-1
0
1
2
3
0
5
10
15
20
25
30
35
Depth (meters, core top)
Core BH-5
New Providence, Bahamas

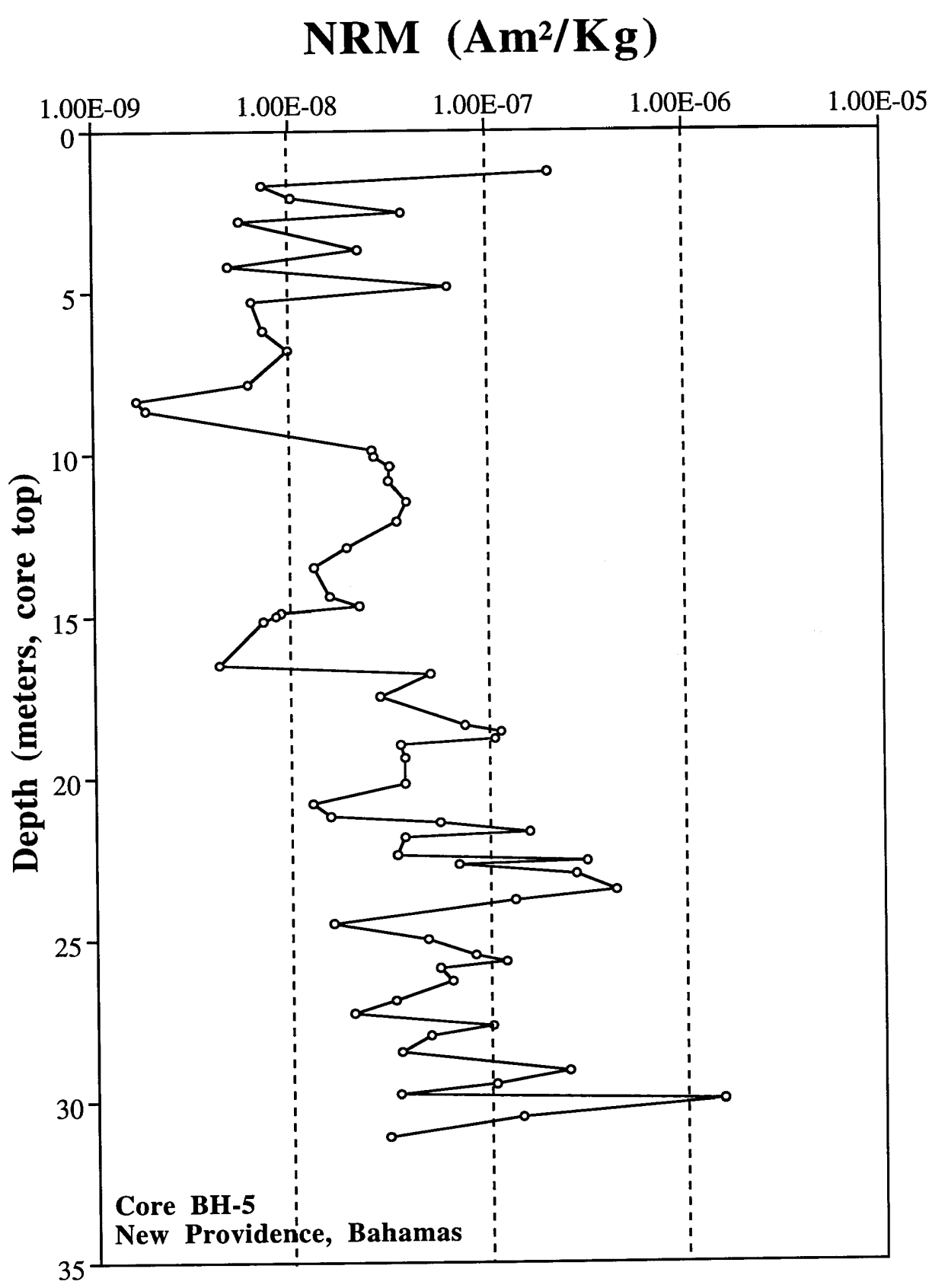
NRM (Am²/Kg)
1.00E-09
1.00E-08
1.00E-07
1.00E-06
1.00E-05
Depth (meters, core top)
0
5
10
15
20
25
30
35
Core BH-5
New Providence, Bahamas

AF15 Intensity (Am^2/Kg)

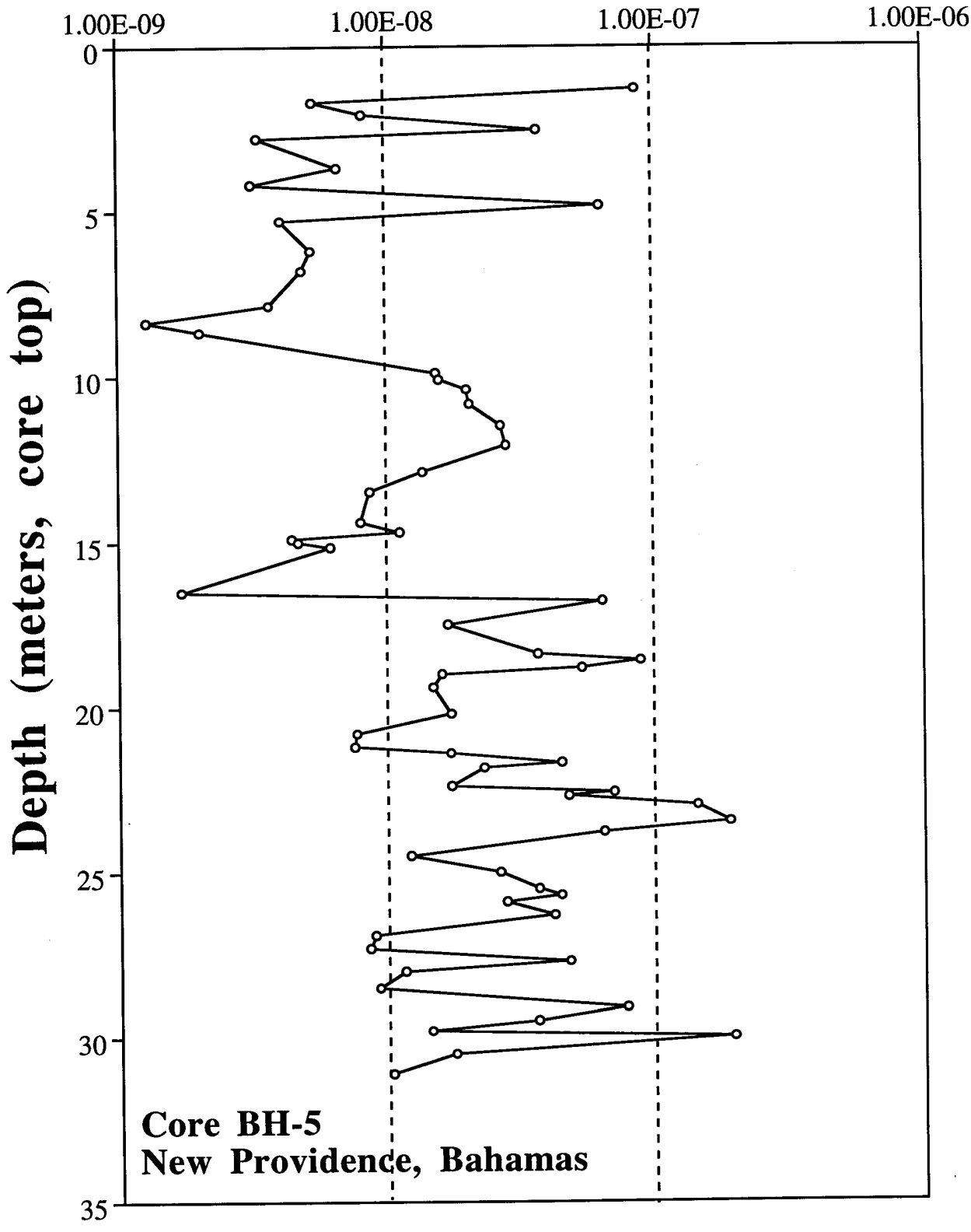

APPENDIX D-1

SIRM AND AF DATA

SIRM #1	Percent IRM	AF Field	Percent AF
3	0	1	95.51
5	0.02	5	88.64
10	4.08	10	76.14
20	19.72	20	53.65
30	27.73	30	33.22
40	38.16	35	26.69
50	52.66	40	22.58
70	74.6	45	17.95
90	84.07	50	14.83
100	85.93	55	12.39
200	92.37	60	11.02
300	95.85	70	8.92
400	96.61	80	7.8
500	97.71	90	6.92
700	99.24	100	6.35
1000	100	110	

SIRM #2	Percent IRM	AF Field	Percent AF
3	0	1	95.97
5	0.03	5	88.57
10	1.91	10	73.16
20	16.6	20	47.72
30	46.03	30	27.92
40	54.06	35	21.34
50	66.27	40	18.59
70	81.62	45	14.96
90	88	50	11.51
100	91.09	55	9.92
200	95.17	60	8.83
300	96.83	70	6.92
400	98.18	80	5.63
500	98.15	90	5.31
700	99.17	100	4.52
1000	100	110	

SIRM #3	Percent IRM	AF Field	Percent AF
3	0	1	100.74
5	0	5	89.51
10	2.85	10	74.02
20	15.71	20	47.89
30	41.69	30	26.67
40	59.33	35	16.38
50	70.99	40	13.57
70	86.48	45	11.42
90	91.44	50	9.19
100	91.66	55	7.59
200	95.46	60	6.41
300	98.1	70	4.99
400	96.06	80	3.96
500	97.85	90	3.31
700	97.29	100	2.97
1000	100	110	2.77

SIRM #4	Percent IRM	AF Field	Percent AF
3	0	1	95.67
5	0.02	5	90.32
10	1.61	10	80.17
20	10.88	20	62.56
30	21.42	30	44
40	30.82	35	37.55
50	45.09	40	32.69
70	62.24	45	27.68
90	72.48	50	23.97
100	76.48	55	13.63
200	86.48	60	19.29
300	89.38	70	16.41
400	91.24	80	14.74
500	93.95	90	13.51
700	96.4	100	12.54
1000	100	110	11.65

SIRM #5	Percent IRM	AF Field	Percent AF
3	0.02	1	96.17
5	0	5	89.19
10	3.98	10	77.89
20	13.92	20	57.08
30	26.27	30	38.1
40	40.83	35	30.72
50	53.53	40	25.45
70	71.15	45	20.74
90	81.72	50	17.24
100	83.24	55	15.06
200	89.31	60	13.45
300	91.98	70	11.26
400	93.5	80	10.06
500	95.38	90	9.32
700	97.87	100	8.77
1000	100	110	8.35
		120	7.96

SIRM #6	Percent IRM	AF Field	Percent AF
3	0.01	1	96.04
5	0	5	88.71
10	1.49	10	75.31
20	18.54	20	52.91
30	34.29	30	33.91
40	43.38	35	26.72
50	56.9	40	22.02
70	77.36	45	17.57
90	84.49	50	13.4
100	87.42	55	11.03
200	94.4	60	9.33
300	96.28	70	6.99
400	98.12	80	5.77
500	98.5	90	4.94
700	99.47	100	4.39
1000	100	110	3.97
		120	3.81

SIRM #7	Percent IRM	AF Field	Percent AF
3	0	1	96
5	0	5	89.64
10	3.19	10	77.2
20	7.71	20	54.85
30	19.77	30	36.18
40	32.82	35	28.68
50	46.33	40	24.26
70	64.39	45	19.36
90	79.25	50	15.81
100	83.29	55	12.81
200	93.94	60	10.47
300	96.52	70	7.22
400	97.5	80	5.59
500	98.53	90	4.59
700	99.74	100	3.93
1000	100	110	3.46
		120	3.12

SIRM #8	Percent IRM	AF Field	Percent AF
3	0	1	96.13
5	0.01	5	90.63
10	2.8	10	79.81
20	8.54	20	59.53
30	23.16	30	40.16
40	33.67	35	33.47
50	45.25	40	28.48
70	64.34	45	23.53
90	74.13	50	19.8
100	79.33	55	17.06
200	90.5	60	15.01
300	93.81	70	12.76
400	95.73	80	11.15
500	97.67	90	9.97
700	99.39	100	9.1
1000	100	110	8.43

SIRM #9	Percent IRM	AF Field	Percent AF
3	0.19	1	92.39
5	0.15	5	85.9
10	0	10	63.7
20	8.14	20	40.18
30	20.8	30	26.35
40	27.97	35	21.88
50	43.04	40	19.29
70	61.7	45	16.55
90	73.88	50	14.78
100	77.27	55	13.21
200	90.92	60	12.06
300	95.66	70	10.23
400	97.74	80	9.06
500	98.57	90	8.06
700	100	100	7.36
1000	98.04	110	6.66

SIRM #10	Percent IRM	AF Field	Percent AF
3	0	1	93.43
5	0.02	5	81.45
10	1.66	10	60.62
20	9.78	20	32.12
30	23.03	30	17.41
40	37.68	35	13.41
50	50.86	40	10.73
70	66.03	45	8.49
90	78.26	50	7.01
100	83.81	55	5.8
200	95.02	60	4.82
300	96.91	70	3.55
400	98.99	80	2.74
500	99.52	90	2.14
700	100	100	1.64
1000	99.42	110	1.28

SIRM #11	Percent IRM	AF Field	Percent AF
3	0	1	94.86
5	0.01	5	82.7
10	1.11	10	59.95
20	7.21	20	27.69
30	12.75	30	11.75
40	30.86	35	8.02
50	51.54	40	6.03
70	69.06	45	4.51
90	80.8	50	3.36
100	85.41	55	2.74
200	94.8	60	2.27
300	96.84	70	1.67
400	98.31	80	1.43
500	98.09	90	1.18
700	98.95	100	1.02
1000	100	110	0.89
500	98.09	90	1.18
700	98.95	100	1.02
1000	100	110	0.89

SIRM #12	Percent IRM	AF Field	Percent AF
3	0	1	95.46
5	0	5	81.94
10	0.41	10	56.17
20	14.97	20	32.03
30	27.59	30	17.04
40	39.87	35	12.93
50	53.56	40	10.37
70	74.89	45	8.2
90	74.74	50	6.31
100	80.16	55	5.19
200	93.87	60	4.38
300	89.77	70	3.12
400	89.8	80	2.39
500	93.34	90	1.87
700	99.07	100	1.42
1000	100	110	1.12
500	93.34	90	1.87
700	99.07	100	1.42
1000	100	110	1.12

SIRM #13	Percent IRM	AF Field	Percent AF
3	0.02	1	90.01
5	0	5	77.71
10	1.31	10	55.67
20	15.17	20	30.2
30	32.17	30	17.13
40	40.15	35	13.33
50	54.07	40	10.78
70	67.99	45	8.59
90	80.86	50	7.15
100	86.01	55	6
200	95.87	60	5.09
300	98.37	70	3.78
400	98.88	80	2.97
500	100	90	2.39
700	99.29	100	1.89
1000	95.7	110	1.54

SIRM #14	Percent IRM	AF Field	Percent AF
3	0	1	94.81
5	0.03	5	87.67
10	1.2	10	75.01
20	6.73	20	49.29
30	15.73	30	37.03
40	27.73	35	31.21
50	43.22	40	27.08
70	52.65	45	23.13
90	70.01	50	19.93
100	76.05	55	17.74
200	88.25	60	16.04
300	92.21	70	13.51
400	93.64	80	11.91
500	95.65	90	10.69
700	97.99	100	9.86
1000	100	110	8.61

SIRM #15	Percent IRM	AF Field	Percent AF
3	0	1	97.06
5	0.05	5	84.49
10	0.44	10	85.9
20	8.92	20	37.91
30	29.27	30	21.96
40	32.02	35	17.19
50	31.08	40	14.19
70	61.31	45	11.48
90	80.37	50	9.35
100	84.88	55	8.04
200	94.13	60	7.03
300	93.87	70	5.7
400	99.04	80	4.88
500	97.37	90	4.23
700	100	100	3.76
1000	99.74	110	3.36
700	100	100	3.76
1000	99.74	110	3.36

SIRM #16	Percent IRM	AF Field	Percent AF
3	0.08	1	96.85
5	0	5	82.77
10	1.32	10	66.02
20	8.57	20	42.79
30	23.7	30	23.38
40	26.5	35	21.95
50	47.59	40	18.04
70	65.97	45	14.68
90	76.73	50	11.48
100	81.3	55	9.8
200	94.02	60	8.4
300	98.04	70	6.33
400	99.13	80	5.05
500	100	90	4.04
700	99.89	100	3.27
1000	98.21	110	2.11
700	99.89	100	3.27
1000	98.21	110	2.11

SIRM #17	Percent IRM	AF Field	Percent AF
3	0	1	95.21
5	0.03	5	83.14
10	0.56	10	63.11
20	4.13	20	32.56
30	17.73	30	16.41
40	31.34	35	12.24
50	48.02	40	9.6
70	64.08	45	7.71
90	78.74	50	6.06
100	83.52	55	4.94
200	92.7	60	4.15
300	95.56	70	2.95
400	97.53	80	2.27
500	97.52	90	1.71
700	99.22	100	1.3
1000	100	110	1

SIRM #18	Percent IRM	AF Field	Percent AF
3	0	1	99.6
5	0.01	5	86.17
10	0.13	10	57.29
20	6.73	20	30.07
30	22.47	30	15.49
40	32.69	35	11.86
50	50.87	40	9.39
70	65.45	45	7.43
90	79.1	50	5.77
100	85.74	55	4.7
200	96.61	60	3.91
300	100	70	2.7
400	92.91	80	2.04
500	87.26	90	1.49
700	89.88	100	1.05
1000	94.2	110	0.8

SIRM #19	Percent IRM	AF Field	Percent AF
3	0.09	1	95.47
5	0	5	88.18
10	0.22	10	74.36
20	10.38	20	51.9
30	20.89	30	35.11
40	30.39	35	28.98
50	43.85	40	24.72
70	63.65	45	20.65
90	75.78	50	17.54
100	77.99	55	15.26
200	88.42	60	13.64
300	92.47	70	11.25
400	91.98	80	9.63
500	96.72	90	8.39
700	98.27	100	7.29
1000	100	110	6.35
700	98.27	100	7.29
1000	100	110	6.35

SIRM #20	Percent IRM	AF Field	Percent AF
3	0.01	1	96.08
5	0	5	88.65
10	1.64	10	76.15
20	9.79	20	53.12
30	19.56	30	34.41
40	31.47	35	27.66
50	52.42	40	22.5
70	67.28	45	17.97
90	78.87	50	14.34
100	82.49	55	11.95
200	90.76	60	10.21
300	93.54	70	7.89
400	95.11	80	6.53
500	96.56	90	5.5
700	98.13	100	4.71
1000	100	110	4.09
700	98.13	100	4.71
1000	100	110	4.09

SIRM #21	Percent IRM	AF Field	Percent AF
3	0	1	96.14
5	0.02	5	87.89
10	2.26	10	71.87
20	13.52	20	48.43
30	35	30	31.57
40	36.79	35	26.23
50	44.79	40	22.11
70	68.01	45	18.15
90	77.35	50	14.91
100	81.8	55	12.65
200	93.1	60	10.79
300	96.09	70	8.14
400	97.88	80	6.66
500	97.45	90	5.86
700	99.73	100	5.02
1000	100	110	4.37

SIRM #22	Percent IRM	AF Field	Percent AF
3	0	1	96.87
5	0	5	88.91
10	2.17	10	80.09
20	11.67	20	53.6
30	26.44	30	37.85
40	33.81	35	32.01
50	41.33	40	28.17
70	58.76	45	24.3
90	70.28	50	20.79
100	75.68	55	18.57
200	91.56	60	16.55
300	95.54	70	13.48
400	96.92	80	11.57
500	97.82	90	9.79
700	98.86	100	8.45
1000	100	110	7.39

SIRM #23	Percent IRM	AF Field	Percent AF
3	0	1	94.96
5	0.11	5	86.31
10	0.57	10	69.74
20	6.74	20	45.67
30	18.21	30	29.51
40	25.63	35	24.05
50	44.34	40	20.36
70	63.65	45	16.77
90	75	50	14
100	79.15	55	11.95
200	93.06	60	10.31
300	96.95	70	7.84
400	98.28	80	6.29
500	98.59	90	5.18
700	98.76	100	4.26
1000	100	110	3.59
1000	100	110	3.59

SIRM #24	Percent IRM	AF Field	Percent AF
3	0.01	1	95.25
5	0	5	88.47
10	3.35	10	75.95
20	14.36	20	55.1
30	28.77	30	38.1
40	31.02	35	31.58
50	43.28	40	27.01
70	63.42	45	22.57
90	76.27	50	18.89
100	81.46	55	15.98
200	93.53	60	13.85
300	97.27	70	10.94
400	97.59	80	9.36
500	98.36	90	7.93
700	99.3	100	6.87
1000	100	110	6.01
1000	100	110	6.01

SIRM #25	Percent IRM	AF Field	Percent AF
3	0	1	94.24
5	0.06	5	86.04
10	5.39	10	70.13
20	22.04	20	49.21
30	31.01	30	36.55
40	45.43	35	32.46
50	50.79	40	29.73
70	63.97	45	27.03
90	71.77	50	24.77
100	74.93	55	22.87
200	86.63	60	21.35
300	90.75	70	18.92
400	93.53	80	17.1
500	95.76	90	15.45
700	98.2	100	14.03
1000	100	110	12.76

SIRM #26	Percent IRM	AF Field	Percent AF
3	0	1	93.9
5	0.05	5	85.33
10	0.66	10	71.07
20	11.83	20	50.02
30	31.09	30	36.09
40	38.63	35	31.25
50	48.72	40	27.79
70	62.01	45	24.74
90	70.66	50	22.1
100	74.4	55	20.11
200	88.14	60	18.33
300	92.6	70	15.84
400	94.35	80	14.01
500	96.26	90	12.17
700	98.01	100	11.86
1000	100	110	10.7

SIRM #27	Percent IRM	AF Field	Percent AF
3	0.02	1	94.97
5	0	5	87.9
10	0.06	10	74.88
20	7.97	20	52.77
30	23.32	30	34.6
40	27.96	35	27.85
50	39.21	40	22.82
70	60.11	45	18.25
90	72.9	50	14.72
100	78.28	55	12.21
200	93.69	60	10.14
300	96.52	70	7.34
400	98.01	80	6.06
500	98.6	90	4.67
700	99.34	100	3.49
1000	100	110	2.77

SIRM #28	Percent IRM	AF Field	Percent AF
3	0	1	95.94
5	0.01	5	87.65
10	0.38	10	74.61
20	12.01	20	52.1
30	16.25	30	34.02
40	24.59	35	27.42
50	242.92	40	22.85
70	61.21	45	18.37
90	73.23	50	15.02
100	79.58	55	12.4
200	95.03	60	10.4
300	98.02	70	8.16
400	98.38	80	6.3
500	99.3	90	4.82
700	100	100	3.67
1000	99.99	110	2.84

SIRM #29	Percent IRM	AF Field	Percent AF
3	0	1	95.88
5	0.02	5	88.27
10	0.36	10	74.94
20	9.26	20	51.35
30	17.98	30	32.5
40	25.39	35	25.82
50	41.34	40	21.33
70	58.46	45	16.89
90	0	50	13.51
100	77.22	55	11.15
200	97.04	60	9.73
300	96.33	70	6.87
400	97.62	80	5.07
500	97.53	90	3.86
700	99.54	100	2.85
1000	100	110	2.16

SIRM #30	Percent IRM	AF Field	Percent AF
3	0	1	97.19
5	0	5	87.13
10	3.11	10	71.64
20	1.34	20	49.6
30	34.74	30	33.16
40	40.45	35	27.27
50	55.26	40	23.49
70	71.12	45	19.93
90	78.44	50	16.93
100	80.92	55	14.94
200	90.72	60	13.52
300	93.47	70	11.17
400	90.2	80	9.57
500	93.07	90	8.62
700	97.32	100	7.61
1000	100	110	7.06

SIRM #31	Percent IRM	AF Field	Percent AF
3	0.08	1	95.01
5	0	5	86.29
10	0.57	10	71.48
20	18.43	20	48.84
30	32.12	30	31.86
40	43.69	35	26.1
50	53.18	40	22.11
70	69.94	45	18.58
90	77.9	50	15.76
100	90.62	55	14.01
200	89.51	60	12.65
300	91.54	70	10.82
400	92.64	80	9.73
500	93.65	90	8.86
700	96.45	100	8.16
1000	100	110	7.67

SIRM #32	Percent IRM	AF Field	Percent AF
3	0.02	1	95.76
5	0	5	87.09
10	1.26	10	74.36
20	21.03	20	52.42
30	36.7	30	33.23
40	43.69	35	26.57
50	59.71	40	1.19
70	77.46	45	17.17
90	88.73	50	14.15
100	90.67	55	11.8
200	94.83	60	9.66
300	96.2	70	6.82
400	96.92	80	5.28
500	96.86	90	4.43
700	97.94	100	3.96
1000	100	110	3.66

SIRM #33	Percent IRM	AF Field	Percent AF
3	0	1	96.02
5	0.05	5	88.26
10	0.86	10	74.47
20	7.39	20	49.22
30	22.62	30	29.74
40	30.97	35	22.84
50	43.1	40	18.34
70	62.88	45	14.26
90	76.61	50	10.86
100	80.72	55	8.45
200	91.96	60	6.58
300	95.13	70	3.91
400	96.26	80	2.51
500	98.27	90	1.75
700	99.21	100	1.36
1000	100	110	1.12

SIRM #34	Percent IRM	AF Field	Percent AF
3	0	1	96.85
5	0.06	5	90.2
10	5.05	10	7.87
20	14.88	20	56.46
30	27.86	30	36.42
40	43.78	35	27.3
50	53.53	40	22.88
70	76.1	45	17.93
90	86.17	50	14.2
100	89.4	55	11.5
200	95.03	60	9.54
300	96.9	70	6.73
400	97.78	80	5.14
500	98.18	90	4.21
700	98.94	100	3.93
1000	100	110	3.55

SIRM #35	Percent IRM	AF Field	Percent AF
3	0	1	97.07
5	0.01	5	89.71
10	1.72	10	74.51
20	8.88	20	51.34
30	23.11	30	33.48
40	35.84	35	26.97
50	50.22	40	22.51
70	67.11	45	18.2
90	79.68	50	14.79
100	82.59	55	12.21
200	93.06	60	10.39
300	95.73	70	7.64
400	97.07	80	6.04
500	97.66	90	4.94
700	98.75	100	4.55
1000	100	110	3.94

SIRM #36	Percent IRM	AF Field	Percent AF
3	0	1	97.99
5	0.01	5	87.42
10	0.3	10	64.43
20	9.62	20	34.45
30	33.92	30	19.2
40	44.12	35	11.1
50	58.64	40	7.99
70	71.22	45	8.97
90	84.26	50	7.17
100	87.58	55	5.89
200	95.5	60	4.92
300	95.36	70	3.69
400	97.04	80	2.97
500	100	90	2.41
700	98.01	100	2.06
1000	96	110	1.78

SIRM #37	Percent IRM	AF Field	Percent AF
3	0	1	94.75
5	0	5	86.56
10	0.71	10	71.38
20	7.57	20	47.49
30	22.14	30	30.91
40	33.57	35	25.17
50	43.09	40	21.41
70	64.67	45	17.41
90	78.05	50	14.72
100	86.44	55	12.57
200	93.28	60	10.86
300	96.48	70	8.38
400	98.2	80	6.83
500	98.85	90	5.76
700	100	100	5.21
1000	99.84	110	4.59

SIRM #38	Percent IRM	AF Field	Percent AF
3	0.01	1	96.91
5	0	5	87.49
10	0.35	10	72.36
20	9.76	20	49.59
30	20.75	30	33.25
40	29.21	35	27.21
50	40.5	40	23.58
70	59.73	45	20.25
90	73.31	50	16.97
100	80.66	55	14.49
200	94.34	60	12.6
300	97.17	70	9.6
400	97.78	80	7.82
500	97.97	90	6.43
700	98.59	100	5.31
1000	100	110	4.43

SIRM #39	Percent IRM	AF Field	Percent AF
3	0	1	97.21
5	0.02	5	90.14
10	0.64	10	78.15
20	11.72	20	58.28
30	21.65	30	40.66
40	28.23	35	33.58
50	43.21	40	29.05
70	62.03	45	24.62
90	73.27	50	21.2
100	77.33	55	18.69
200	93.19	60	15.92
300	96.8	70	12.37
400	98.16	80	10.02
500	98.87	90	8.36
700	99.32	100	5.15
1000	100	110	6.16

SIRM #40	Percent IRM	AF Field	Percent AF
3	0	1	96.76
5	0.04	5	88.98
10	3.77	10	76.92
20	12.39	20	56.99
30	22.16	30	40.29
40	31.96	35	34.05
50	42.01	40	28.89
70	60.66	45	24.94
90	71.01	50	21.31
100	76.47	55	18.67
200	89.99	60	16.37
300	93.54	70	13.05
400	96.11	80	10.98
500	97.35	90	9.4
700	98.33	100	8.3
1000	100	110	7.48

SIRM #41	Percent IRM	AF Field	Percent AF
3	0	1	99.06
5	0.01	5	94.19
10	2.13	10	85.06
20	9.14	20	71.18
30	20.2	30	60.94
40	19.95	35	57.24
50	26.08	40	54.45
70	43.43	45	51.8
90	49.87	50	49.34
100	54.38	55	47.23
200	67.42	60	45.38
300	74.77	70	42.39
400	80.42	80	39.92
500	85.84	90	37.47
700	90.93	100	35.44
1000	100	110	33.43

SIRM #42	Percent IRM	AF Field	Percent AF
3	0.03	1	98.02
5	0	5	89.95
10	0.54	10	76.61
20	14.33	20	53.56
30	24.33	30	37.09
40	34.61	35	30.94
50	48.87	40	29.55
70	61.04	45	14.55
90	72.95	50	20.03
100	79.34	55	17.51
200	87.86	60	15.58
300	92.76	70	12.8
400	95.13	80	10.96
500	95.8	90	9.66
700	95.53	100	8.65
1000	100	110	7.84

SIRM #43	Percent IRM	AF Field	Percent AF
3	0	1	97.51
5	0.01	5	92.83
10	1.11	10	81.22
20	11.04	20	57.78
30	20.27	30	38.71
40	30.85	35	31.92
50	44.61	40	27.25
70	60.1	45	23.04
90	72.88	50	19.34
100	78.58	55	16.92
200	91.83	60	14.59
300	95.19	70	11.87
400	96.75	80	10.05
500	97.08	90	8.54
700	99.86	100	7.63
1000	100	110	6.72

SIRM #44	Percent IRM	AF Field	Percent AF
3	0	1	98.22
5	0.01	5	90.16
10	0.65	10	76.29
20	12.03	20	63.32
30	22.81	30	34.58
40	32.35	35	28.07
50	46.83	40	23.74
70	65.09	45	19.49
90	77.02	50	15.97
100	81.18	55	13.44
200	92.8	60	11.47
300	97.64	70	8.55
400	98.35	80	6.73
500	99.08	90	5.29
700	99.8	100	4.24
1000	100	110	3.46

SIRM #45	Percent IRM	AF Field	Percent AF
3	0	1	97.5
5	0	5	90.28
10	2.15	10	77.15
20	7.42	20	53.82
30	23.85	30	34.38
40	33.58	35	27.67
50	49.23	40	23.19
70	65.48	45	18.87
90	76.38	50	15.37
100	80.44	55	12.82
200	93.68	60	10.84
300	97.77	70	7.96
400	98.66	80	6.22
500	99.25	90	4.67
700	99.64	100	3.65
1000	100	110	2.94

SIRM #46	Percent IRM	AF Field	Percent AF
3	0	1	97.86
5	0	5	88.33
10	2.48	10	75.29
20	13.63	20	52.08
30	24.85	30	33.27
40	35.15	35	26.35
50	51.59	40	22.1
70	68.03	45	18.11
90	76.51	50	14.68
100	81.58	55	10.19
200	93.9	60	9.24
300	97.31	70	7.75
400	98.12	80	6.02
500	0	90	4.58
700	0	100	3.57
1000	100	110	2.85

SIRM #47	Percent IRM	AF Field	Percent AF
3	0.03	1	98.46
5	0	5	90.34
10	1.81	10	75.68
20	18.21	20	48.73
30	33.6	30	29.48
40	39.64	35	22.68
50	58.72	40	18.63
70	74.17	45	15.06
90	82.98	50	8.13
100	84.5	55	7.18
200	94.66	60	6.29
300	97.34	70	6.46
400	97.89	80	5
500	98.29	90	3.94
700	98.31	100	3.09
1000	100	110	2.48

SIRM #48	Percent IRM	AF Field	Percent AF
3	0.05	1	98.44
5	0	5	90.43
10	1.53	10	76.35
20	14.9	20	51.4
30	25.11	30	31.81
40	39.08	35	25.02
50	54.08	40	20.73
70	68.94	45	16.74
90	79.45	50	13.66
100	83.64	55	11.41
200	96.1	60	9.46
300	97.72	70	7.19
400	98.59	80	5.45
500	99.2	90	4.01
700	100	100	3.02
1000	99.82	110	2.31

SIRM #49	Percent IRM	AF Field	Percent AF
3	0	1	97.51
5	0.05	5	89.47
10	1.34	10	74.44
20	13.21	20	44.86
30	30.06	30	25.43
40	36.15	35	19.27
50	50.44	40	15.1
70	65.24	45	12.15
90	74.17	50	9.46
100	80.54	55	8.64
200	93.14	60	7.19
300	97.26	70	5.05
400	97.51	80	3.8
500	98.93	90	2.9
700	99.44	100	2.18
1000	100	110	1.61

SIRM #50	Percent IRM	AF Field	Percent AF
3	0	1	97.52
5	0.02	5	90.63
10	2.65	10	76.39
20	15.38	20	51.73
30	27.21	30	31.6
40	28.89	35	25.06
50	52.41	40	20.72
70	68.93	45	16.75
90	79.66	50	13.61
100	83.87	55	11.33
200	95.89	60	9.65
300	97.78	70	6.89
400	98.15	80	5.33
500	99.18	90	3.86
700	99.58	100	2.97
1000	100	110	2.34

SIRM #51	Percent IRM	AF Field	Percent AF
3	0	1	97.51
5	0.04	5	90.2
10	1.68	10	79.49
20	10.59	20	58.45
30	22.01	30	39.89
40	28.38	35	33.53
50	40.57	40	28.74
70	58.62	45	24.06
90	70.78	50	20.07
100	77.43	55	16.96
200	92.93	60	15.1
300	96.27	70	11.48
400	96.91	80	9.42
500	97.62	90	7.43
700	97.94	100	6.25
1000	100	110	5.1

SIRM #52	Percent IRM	AF Field	Percent AF
3	0	1	98.28
5	0	5	91.19
10	1.51	10	78.43
20	7.1	20	56.29
30	17.84	30	28.2
40	26.51	35	31.29
50	36.89	40	26.58
70	61.72	45	22.08
90	73.89	50	18.46
100	79.28	55	15.64
200	91.65	60	13.35
300	95.51	70	10.73
400	97.12	80	8.41
500	96.69	90	6.7
700	99.2	100	5.44
1000	100	110	4.59

SIRM #53	Percent IRM	AF Field	Percent AF
3	0.02	1	97.54
5	0	5	90.26
10	0.35	10	76.56
20	10.17	20	53.32
30	24.28	30	34.59
40	30.49	35	27.94
50	44.4	40	23.35
70	63.06	45	18.94
90	75.67	50	15.69
100	80.24	55	13.03
200	94.99	60	11.13
300	97.86	70	8.05
400	98.41	80	6.19
500	99.41	90	4.73
700	99.52	100	3.6
1000	100	110	2.81

SIRM #54	Percent IRM	AF Field	Percent AF
3	0.02	1	99.65
5	0	5	90.8
10	1.83	10	78.81
20	9.13	20	55.3
30	20.3	30	37.16
40	19.63	35	30.13
50	39.1	40	24.76
70	59.48	45	20.75
90	73.73	50	16.62
100	76.95	55	13.9
200	95.36	60	11.83
300	102.32	70	8.48
400	101.34	80	6.54
500	99.8	90	4.84
700	99.77	100	3.65
1000	100	110	2.65

SIRM #55	Percent IRM	AF Field	Percent AF
3	0	1	101.48
5	1.2	5	93.27
10	1.27	10	78.7
20	7.56	20	53.99
30	19.26	30	35.49
40	25.56	35	29.63
50	40.38	40	23.22
70	57.26	45	18.52
90	72.2	50	15.38
100	78.21	55	12.68
200	92.83	60	11.38
300	96.91	70	8.24
400	96.35	80	6.18
500	98.83	90	4.68
700	99.08	100	3.38
1000	100	110	2.51
1000	100	110	2.51

SIRM #56	Percent IRM	AF Field	Percent AF
3	0	1	98.21
5	0.058	5	91.09
10	1.2	10	78.77
20	7.78	20	55.17
30	19.81	30	38.07
40	27.13	35	31.47
50	41.28	40	26.26
70	58.99	45	0
90	72.08	50	17.64
100	78.63	55	14.67
200	94.79	60	12.57
300	97.75	70	8.94
400	98.15	80	6.89
500	98.69	90	5.06
700	98.95	100	3.84
1000	100	110	2.88
1000	100	110	2.88

SIRM #57	Percent IRM	AF Field	Percent AF
3	0	1	97.73
5	0	5	93.02
10	1.58	10	78.16
20	3.79	20	52.77
30	19.85	30	33.75
40	29.83	35	26.64
50	45.56	40	21.72
70	61.41	45	17.46
90	75.31	50	14.57
100	81.7	55	12.75
200	95.32	60	10.88
300	98.34	70	7.84
400	99.02	80	6.06
500	99.23	90	4.54
700	99.65	100	0
1000	100	110	2.71

SIRM #58	Percent IRM	AF Field	Percent AF
3	0	1	97.1
5	0.01	5	94.03
10	1.02	10	79.25
20	7.44	20	53.96
30	19	30	34.48
40	28.55	35	27.45
50	35.55	40	22.95
70	59.87	45	18.64
90	6949	50	14.82
100	76.84	55	12.61
200	93.69	60	10.58
300	96.62	70	7.76
400	98.49	80	6.34
500	99.13	90	4.71
700	99.66	100	3.66
1000	100	110	2.78

SIRM #59	Percent IRM	AF Field	Percent AF
3	0	1	98.25
5	0.04	5	89.21
10	0.87	10	73.52
20	6.4	20	50.21
30	13.56	30	33.73
40	23.85	35	27.46
50	36.56	40	23.29
70	56.19	45	19.11
90	66.62	50	16.14
100	73.77	55	13.36
200	92.9	60	11.37
300	97.43	70	8.27
400	98.48	80	6.99
500	99.39	90	5.36
700	100	100	4.17
1000	99.9	110	3.19

SIRM #60	Percent IRM	AF Field	Percent AF
3	0	1	99.07
5	0.02	5	92.53
10	0.3	10	79.69
20	4.97	20	58.45
30	15	30	40.18
40	21.4	35	33.33
50	34.59	40	28.13
70	55.7	45	23.17
90	68.7	50	19.08
100	75.66	55	16.19
200	94.21	60	13.7
300	98.12	70	10.01
400	99.21	80	8.29
500	99.01	90	6.28
700	99.42	100	4.88
1000	100	110	3.87

SIRM #61	Percent IRM	AF Field	Percent AF
3	0	1	101.19
5	0.01	5	91.86
10	2.44	10	78.78
20	10.94	20	57.8
30	2.26	30	40.3
40	29.74	35	34.13
50	40.43	40	29.6
70	57.61	45	25.38
90	70.75	50	21.55
100	76.56	55	18.63
200	91.44	60	16.21
300	96.64	70	12.53
400	96.89	80	10.38
500	97.97	90	8.31
700	100	100	6.94
1000	99.9	110	5.99

SIRM #62	Percent IRM	AF Field	Percent AF
3	0	1	98.12
5	0	5	92.61
10	2.1	10	78.56
20	8.67	20	56.45
30	18.71	30	38.8
40	22.88	35	32.17
50	39.19	40	26.92
70	57.76	45	22.94
90	70.92	50	19.25
100	76.92	55	16.31
200	93.88	60	13.9
300	97.03	70	10.23
400	99.52	80	7.93
500	98.36	90	6.07
700	99.58	100	4.62
1000	100	110	3.83

SIRM #63	Percent IRM	AF Field	Percent AF
3	0	1	100.84
5	0.03	5	93.3
10	0.34	10	79.95
20	8.6	20	58.22
30	17.24	30	39.68
40	28.18	35	32.91
50	40.05	40	27.74
70	49.47	45	22.57
90	70.23	50	19
100	77.92	55	16.01
200	93.33	60	13.55
300	98.24	70	9.85
400	97.75	80	8.05
500	99.32	90	6.18
700	99.13	100	4.66
1000	100	110	3.67

SIRM #64	Percent IRM	AF Field	Percent AF
3	0	1	92.98
5	0	5	79.95
10	6.03	10	53.5
20	35.1	20	26.2
30	55.28	30	14.92
40	68.77	35	12.45
50	75.57	40	10.86
70	84.85	45	10.17
90	82.28	50	8.91
100	89.97	55	8.09
200	93.86	60	7.4
300	94.84	70	6.35
400	96.41	80	5.67
500	96.26	90	5.06
700	98.47	100	4.59
1000	100	110	4.3

APPENDIX D-2

PLOTS
NORMALIZED PERCENT ACQUIRED SIRM
VS. AF DEMAGNETIZATION

SAMPLE #1

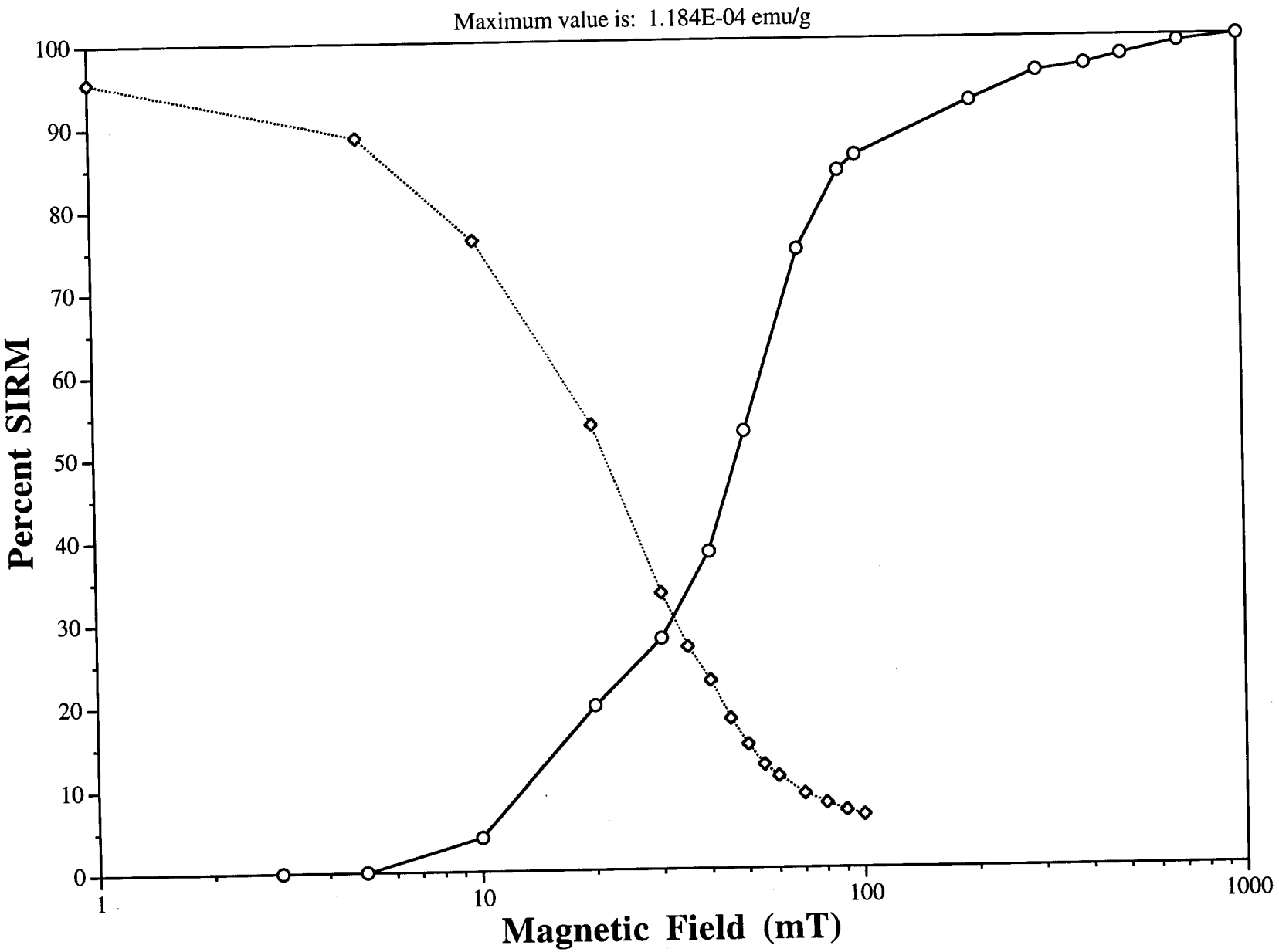
Maximum value is: 1.184E-04 emu/g
Percent SIRM
100
90
80
70
60
50
40
30
20
10
0
1
10
100
1000
Magnetic Field (mT)

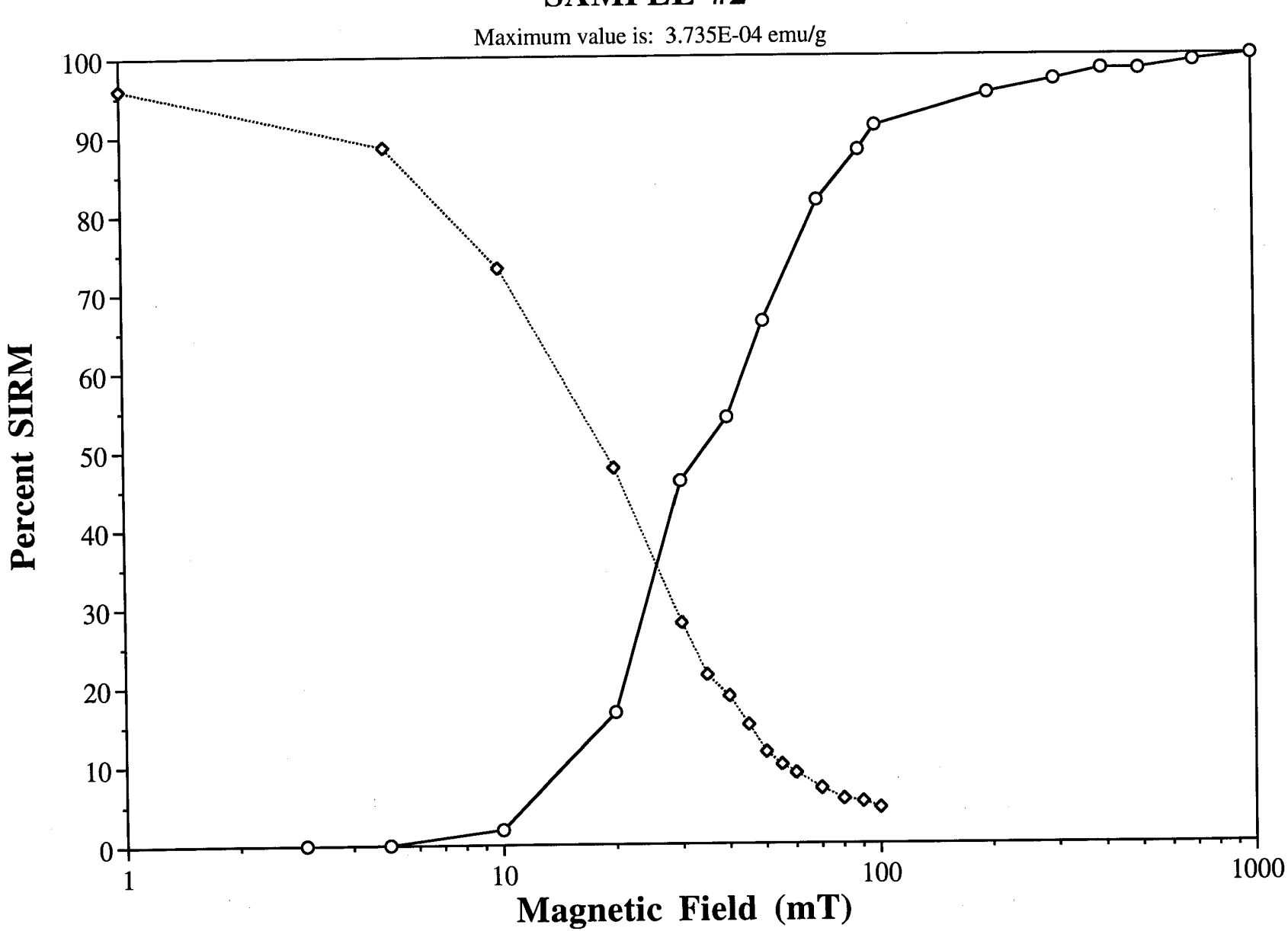
SAMPLE #2
Maximum value is: 3.735E-04 emu/g
Percent SIRM
100
90
80
70
60
50
40
30
20
10
0
1
10
100
1000
Magnetic Field (mT)

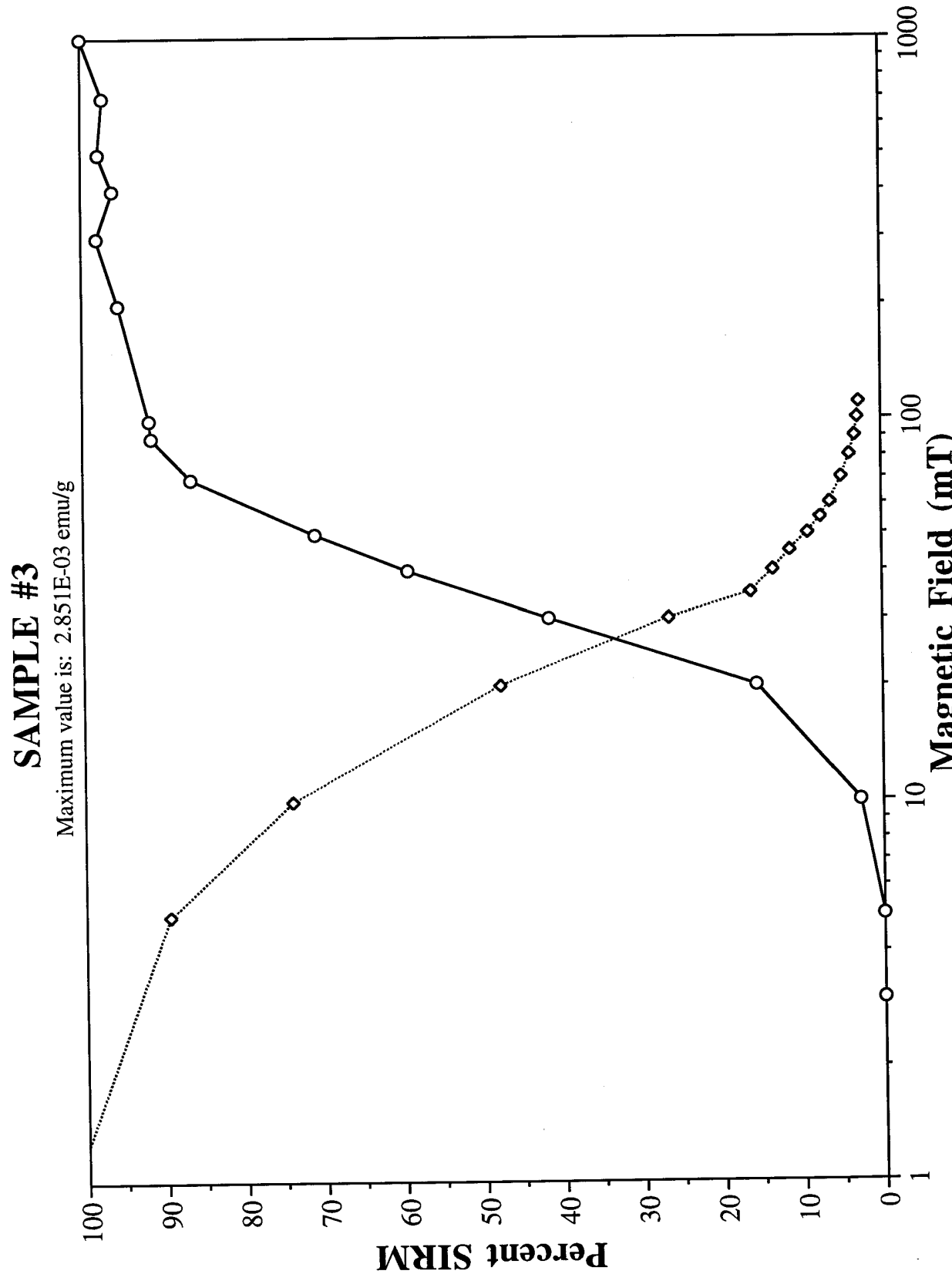
SAMPLE #3
Maximum value is: 2.851E-03 emu/g
Percent SIRM
100
90
80
70
60
50
40
30
20
10
0
1
10
100
1000
Magnetic Field (mT)

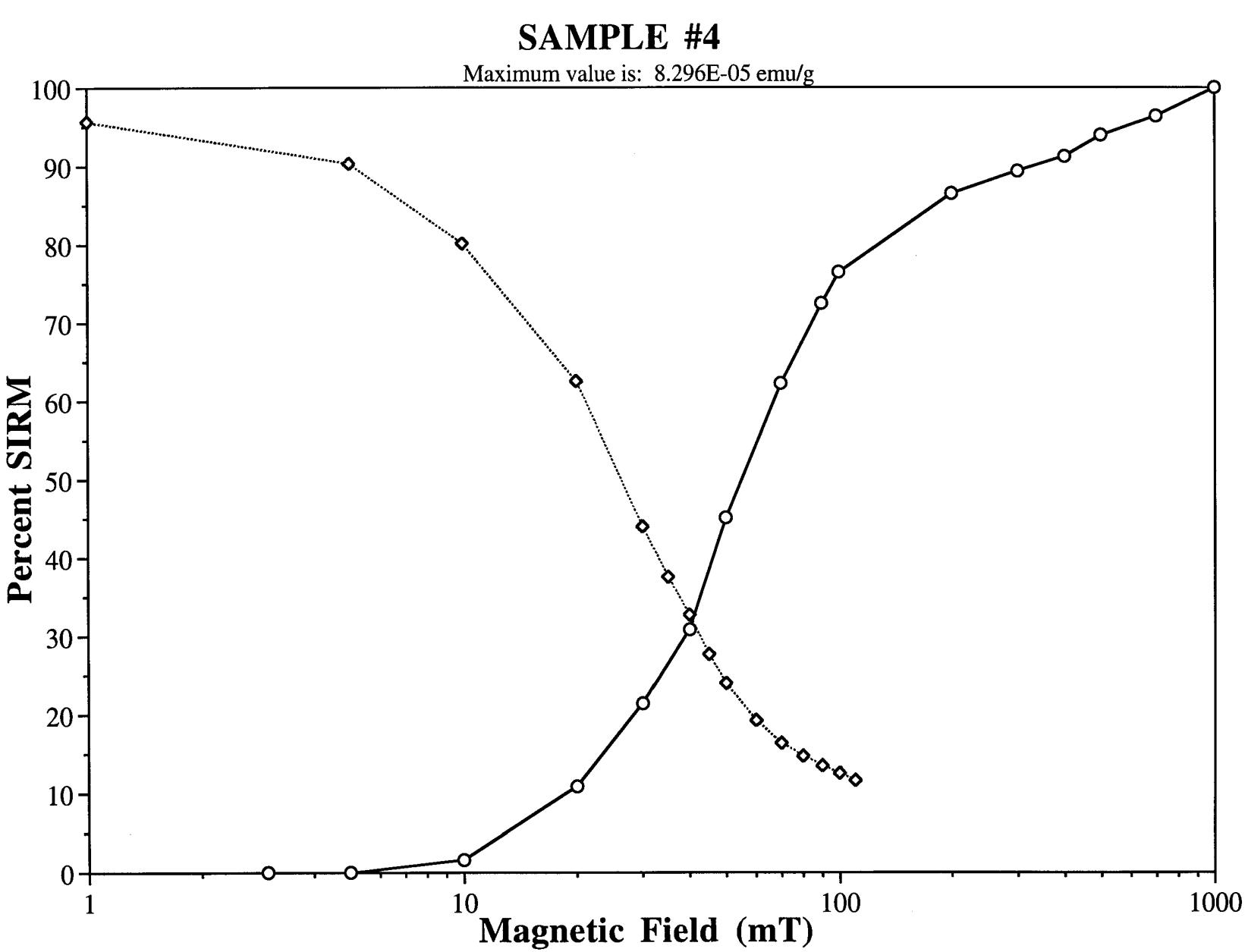
SAMPLE #4
Maximum value is: 8.296E-05 emu/g
Percent SIRM
100
90
80
70
60
50
40
30
20
10
0
1
10
100
1000
Magnetic Field (mT)

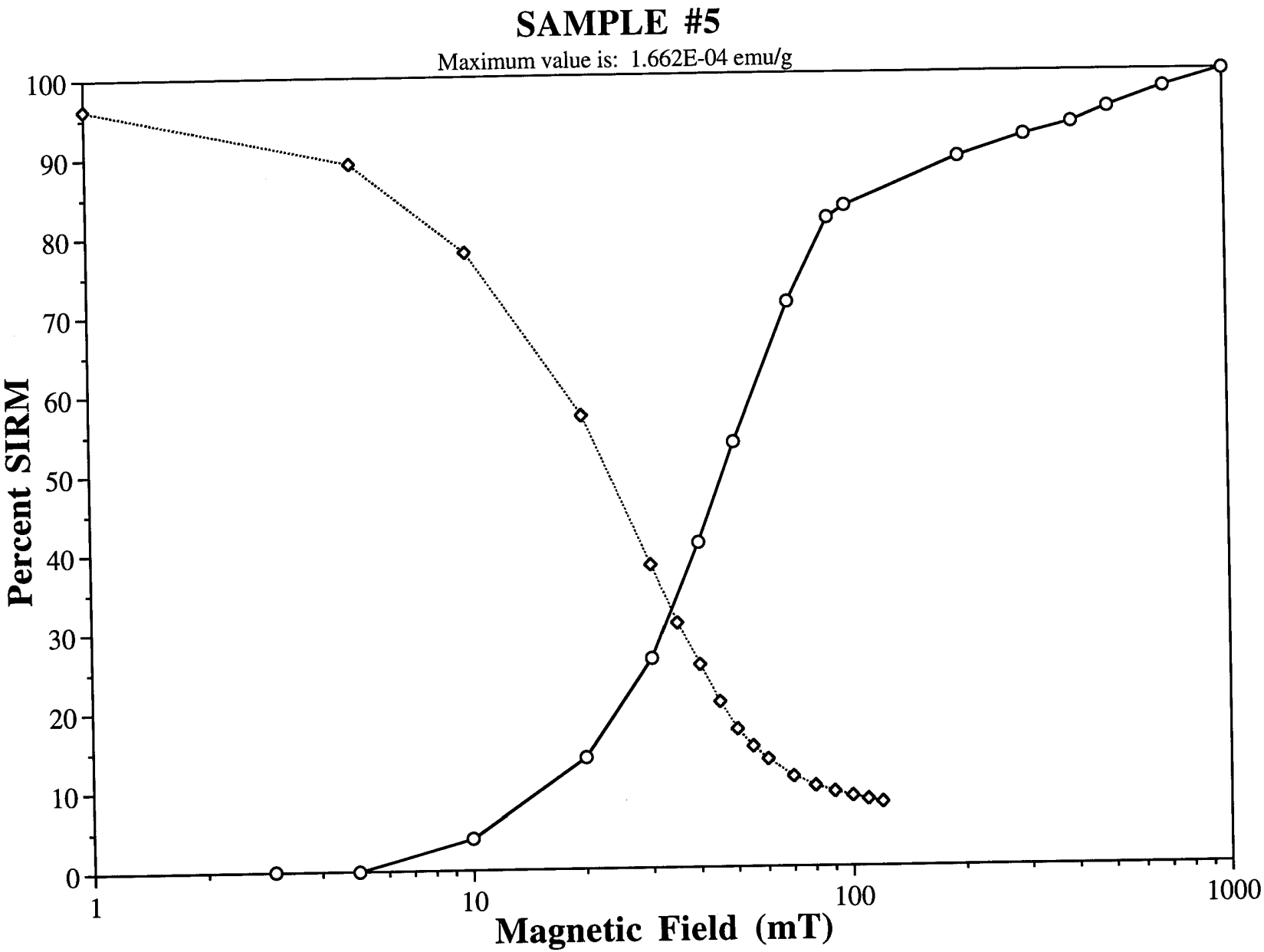
SAMPLE #5
Maximum value is: 1.662E-04 emu/g
Percent SIRM
100
90
80
70
60
50
40
30
20
10
0
1
10
100
1000
Magnetic Field (mT)

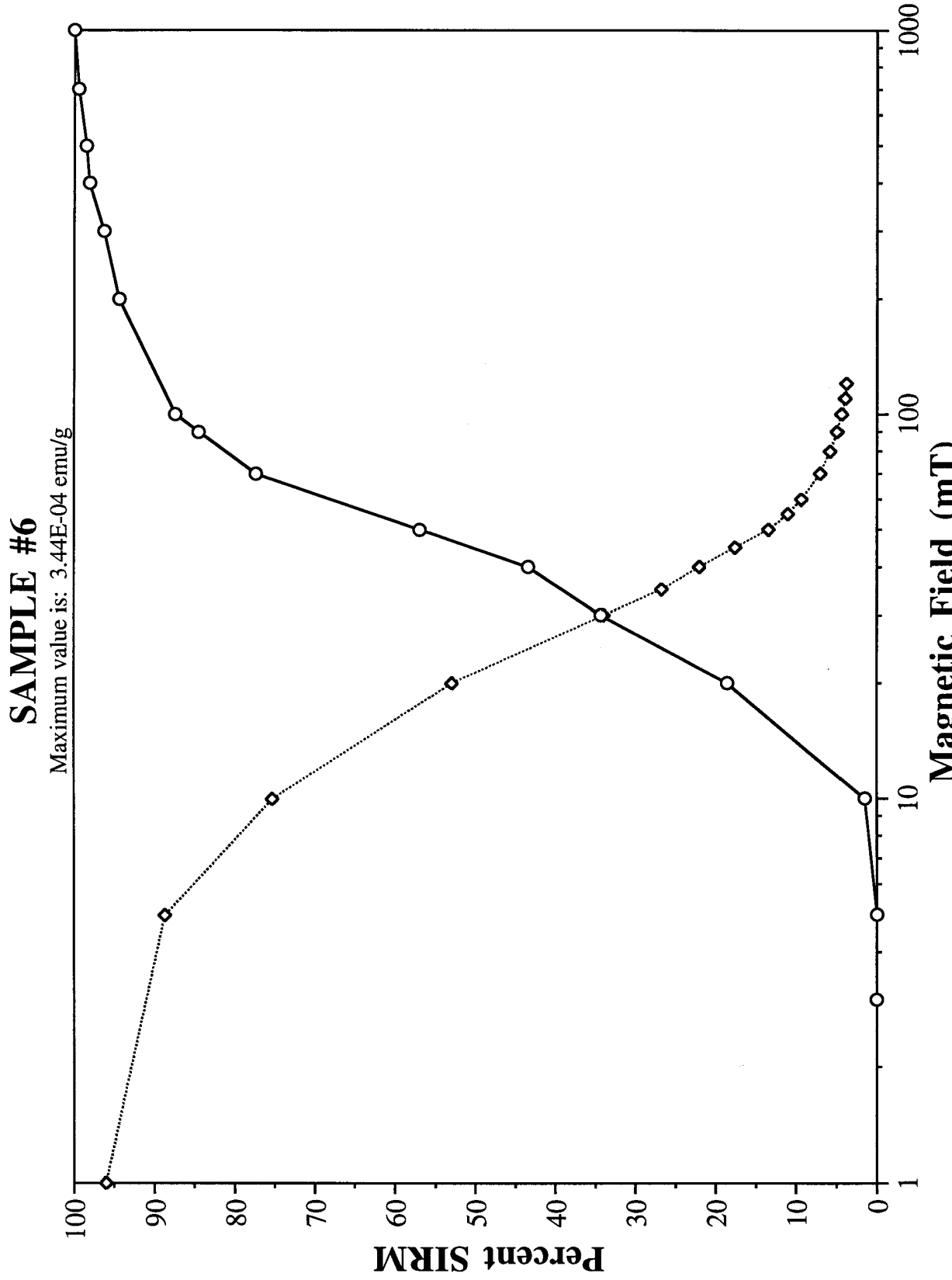
SAMPLE #6
Maximum value is: 3.44E-04 emu/g
Percent SIRM
100
90
80
70
60
50
40
30
20
10
0
1
10
100
1000
Magnetic Field (mT)

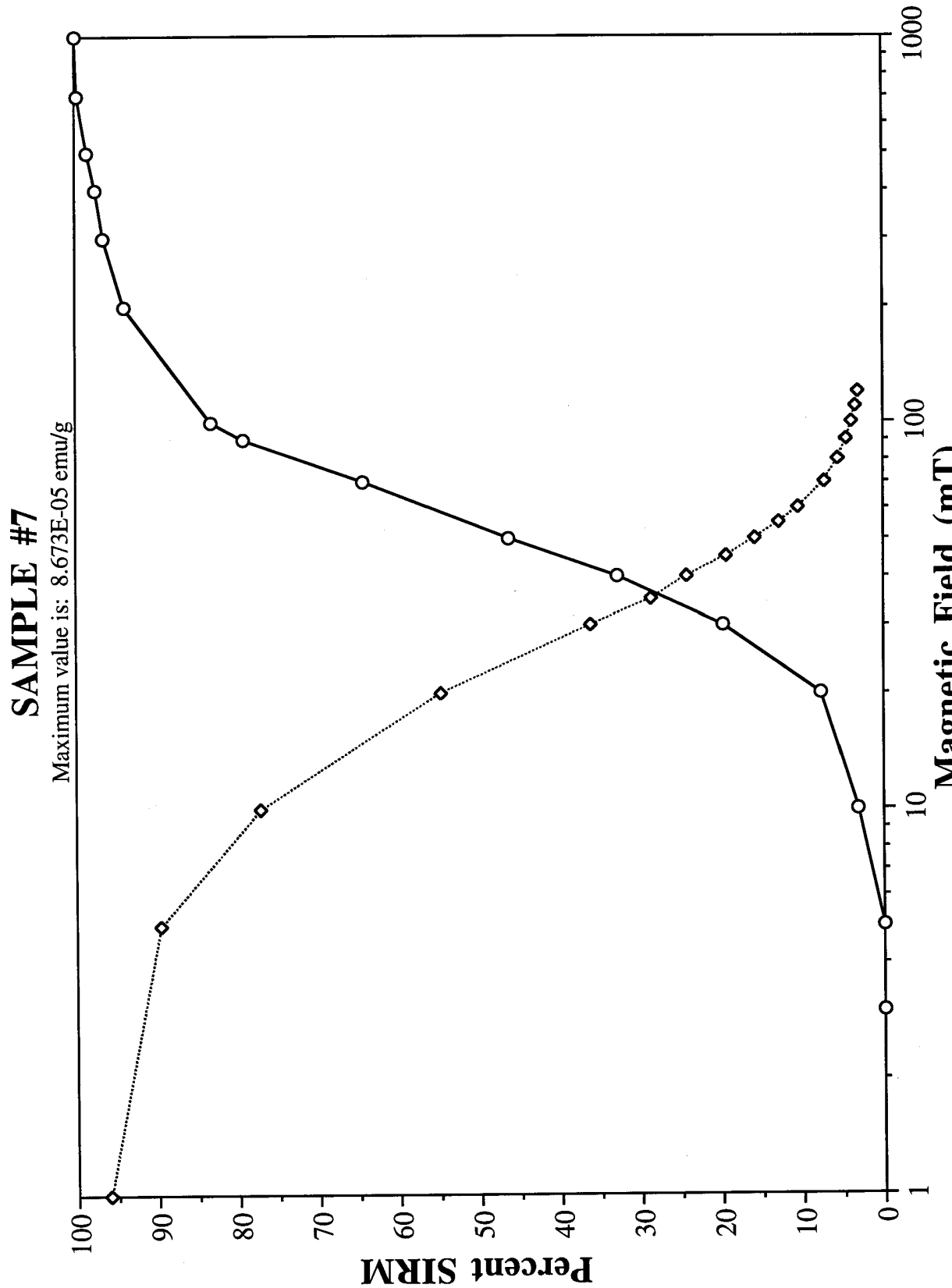
SAMPLE #7
Maximum value is: 8.673E-05 emu/g
Percent SIRM
100
90
80
70
60
50
40
30
20
10
0
1
10
100
1000
Magnetic Field (mT)

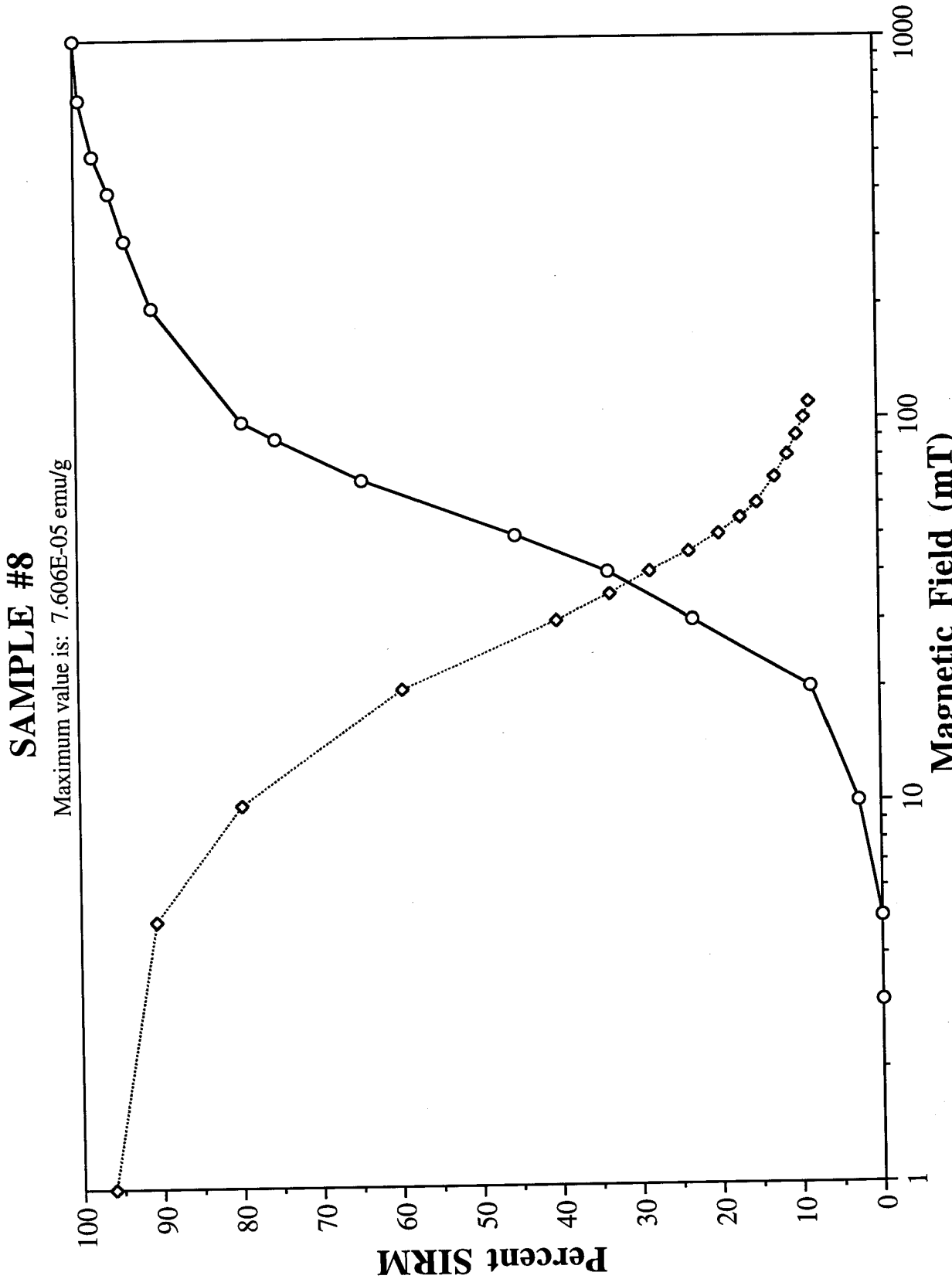
SAMPLE #8
Maximum value is: 7.606E-05 emu/g
Percent SIRM
100
90
80
70
60
50
40
30
20
10
0
1
10
100
1000
Magnetic Field (mT)

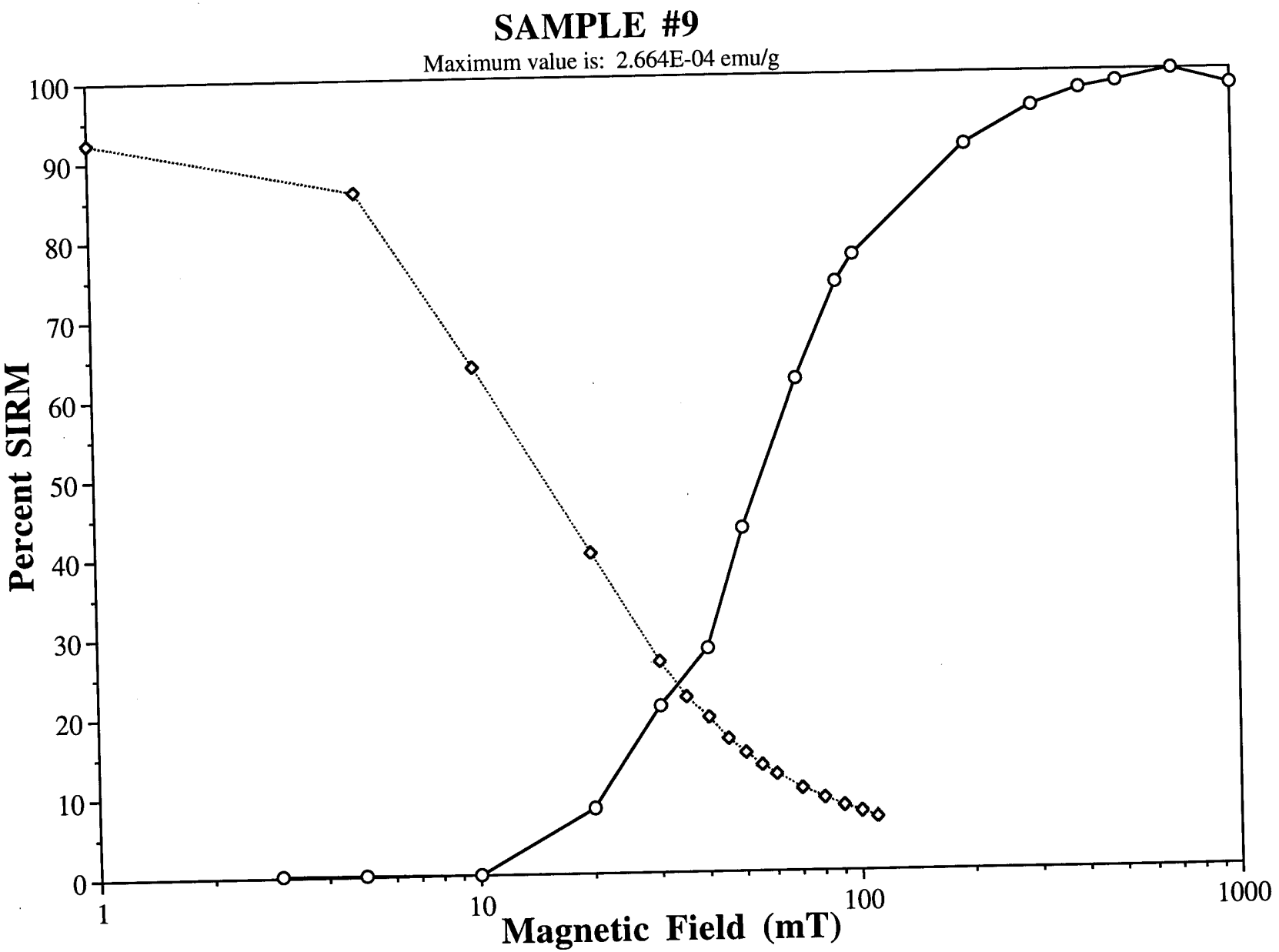
SAMPLE #9
Maximum value is: 2.664E-04 emu/g
Percent SIRM
100
90
80
70
60
50
40
30
20
10
0
1
10
100
1000
Magnetic Field (mT)

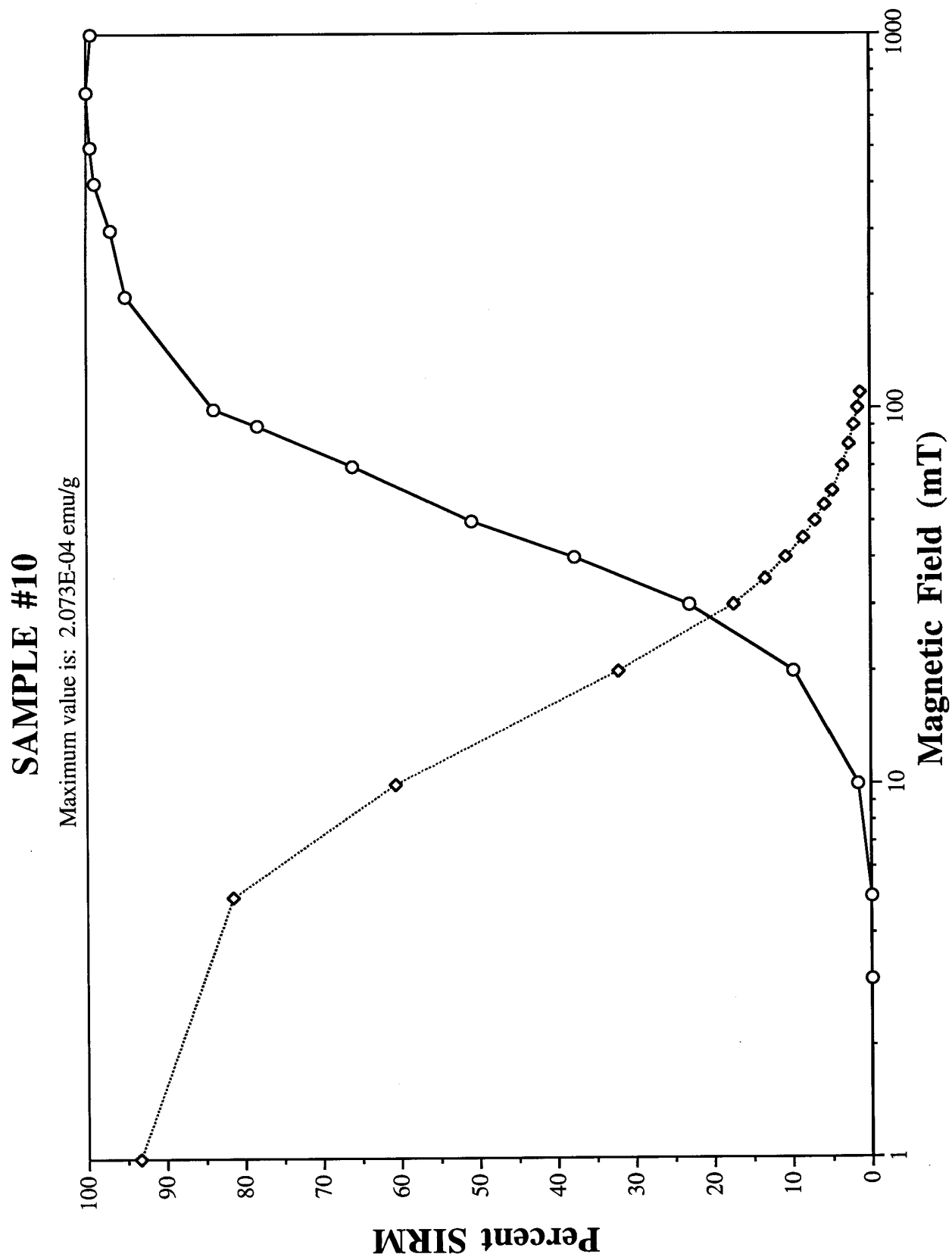
SAMPLE #10
Maximum value is: 2.073E-04 emu/g
Percent SIRM
100
90
80
70
60
50
40
30
20
10
0
1
10
100
1000
Magnetic Field (mT)

SAMPLE #11

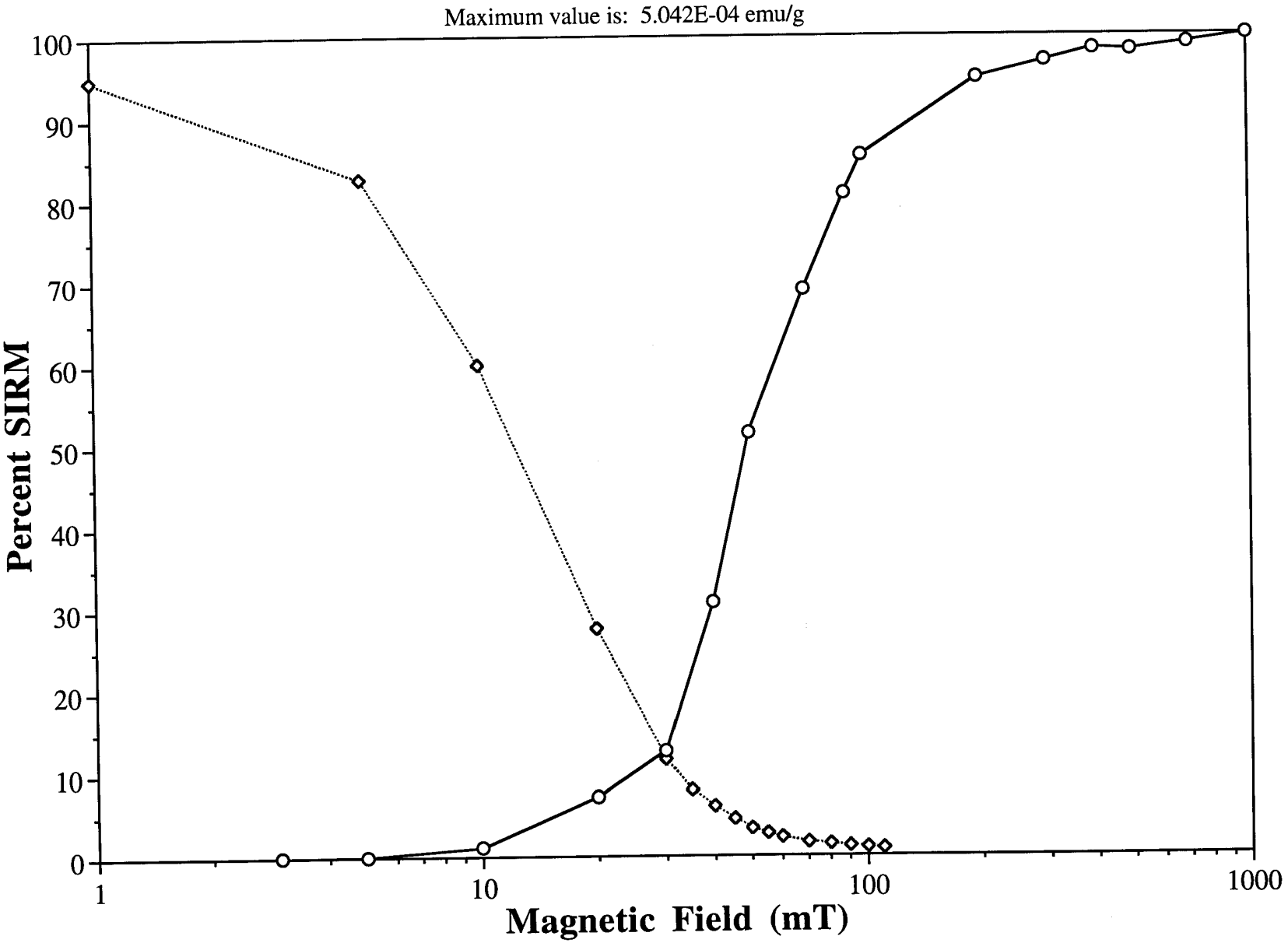
Maximum value is: 5.042E-04 emu/g
Percent SIRM
100
90
80
70
60
50
40
30
20
10
0
1
10
100
1000
Magnetic Field (mT)

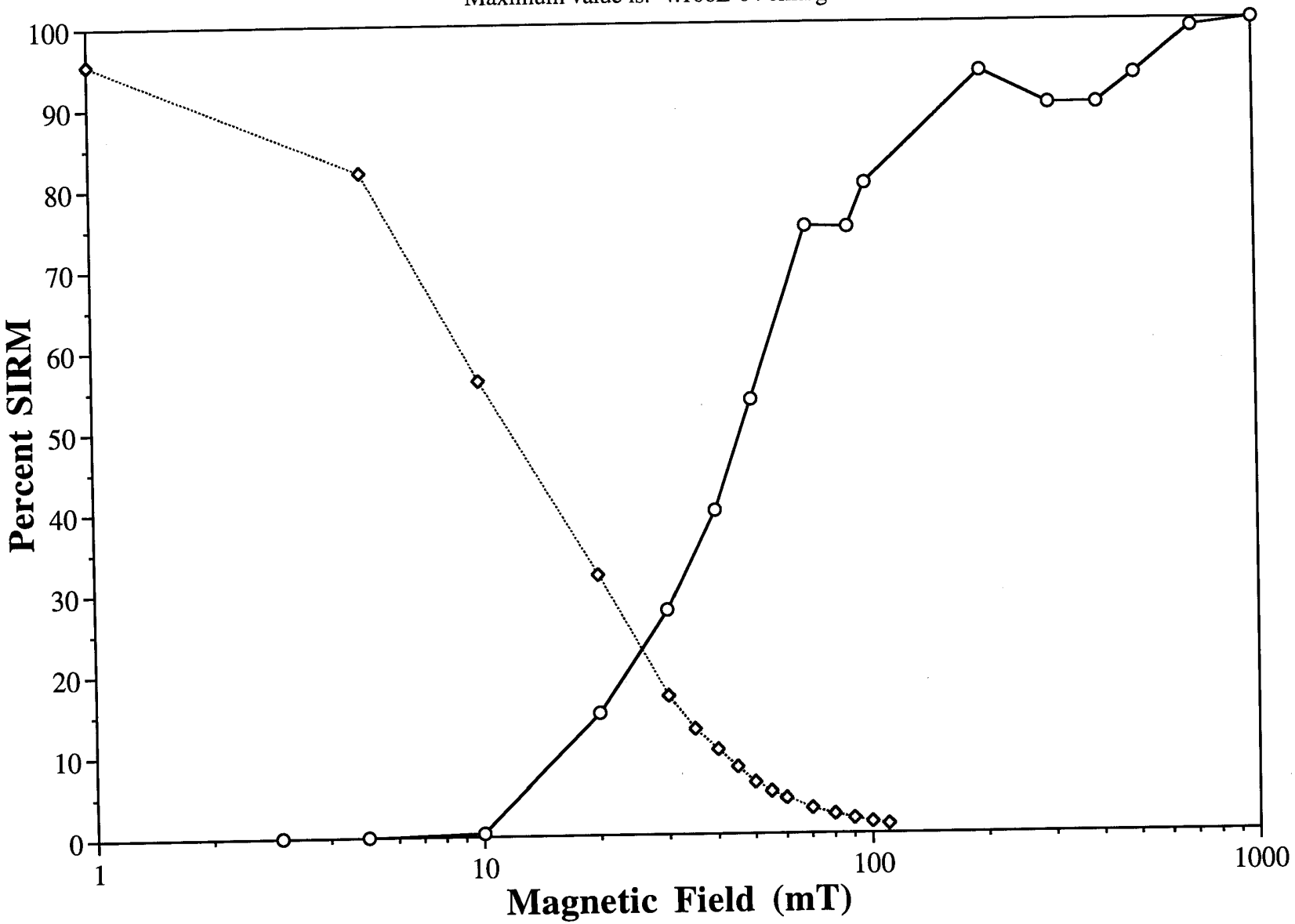
SAMPLE #12
Maximum value is: 4.106E-04 emu/g
Percent SIRM
100
90
80
70
60
50
40
30
20
10
0
1
10
100
1000
Magnetic Field (mT)

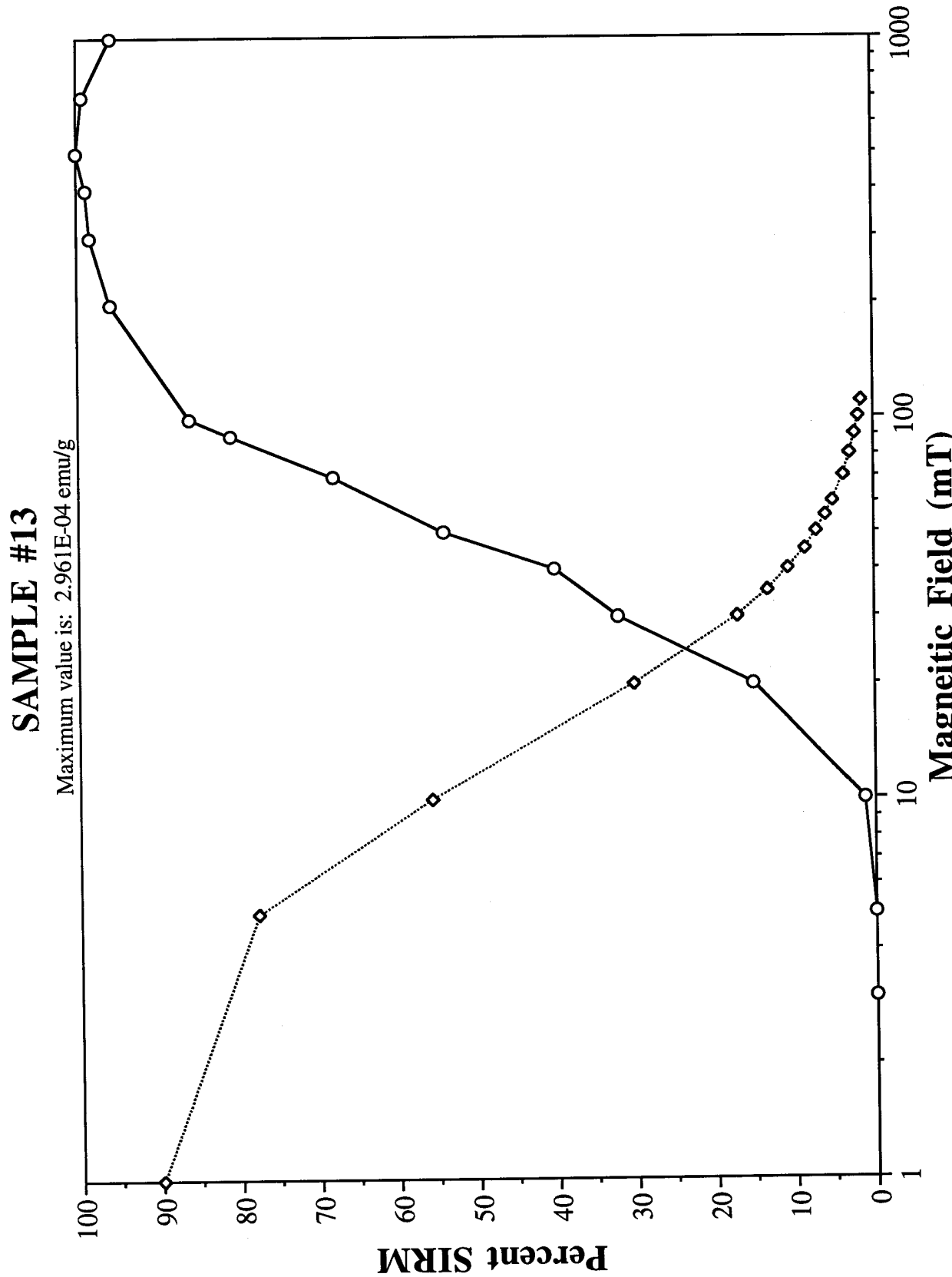
SAMPLE #13
Maximum value is: 2.961E-04 emu/g
Percent SIRM
100
90
80
70
60
50
40
30
20
10
0
1
10
100
1000
Magneitic Field (mT)

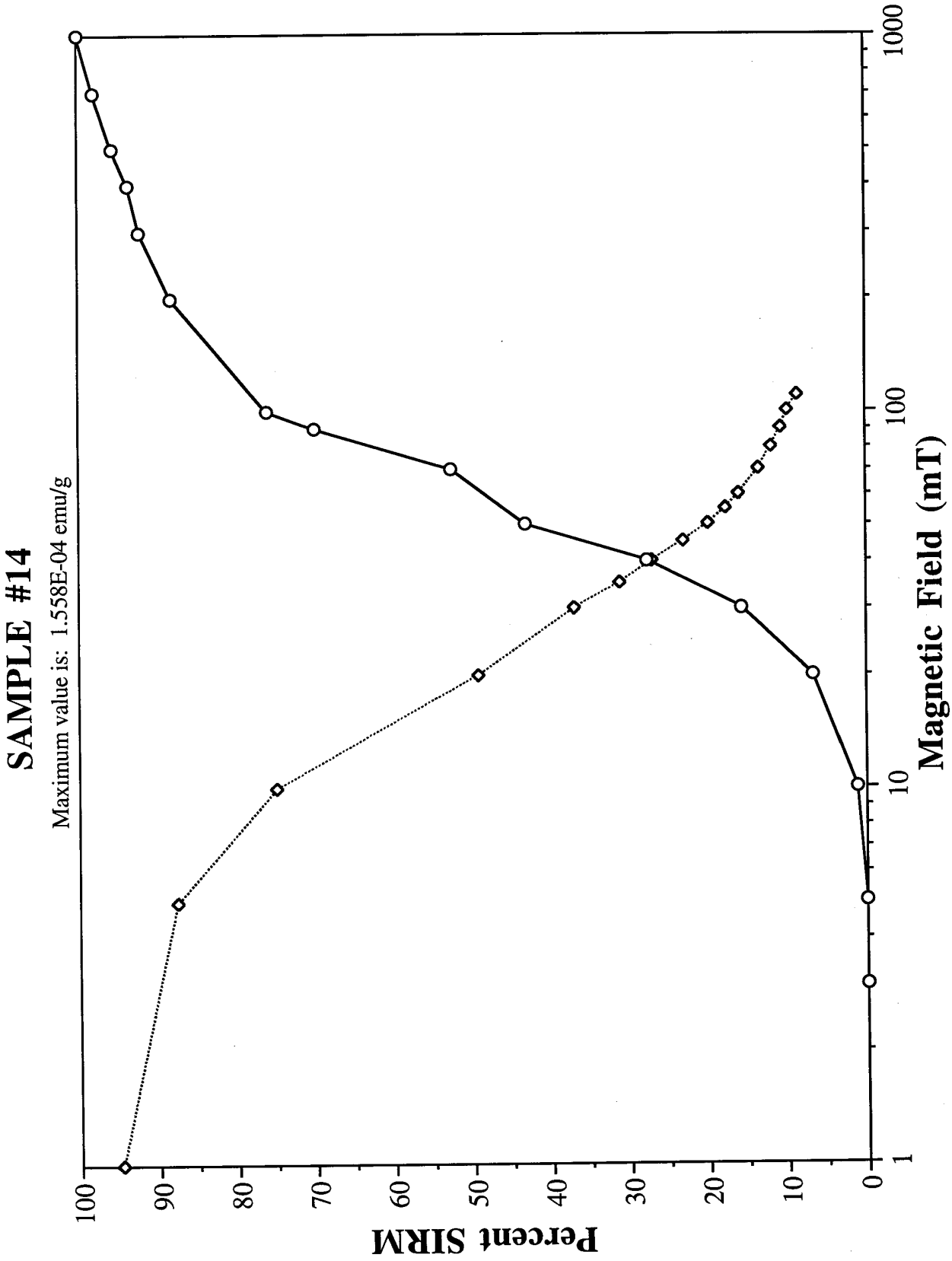
SAMPLE #14
Maximum value is: 1.558E-04 emu/g
Percent SIRM
100
90
80
70
60
50
40
30
20
10
0
1
10
100
1000
Magnetic Field (mT)

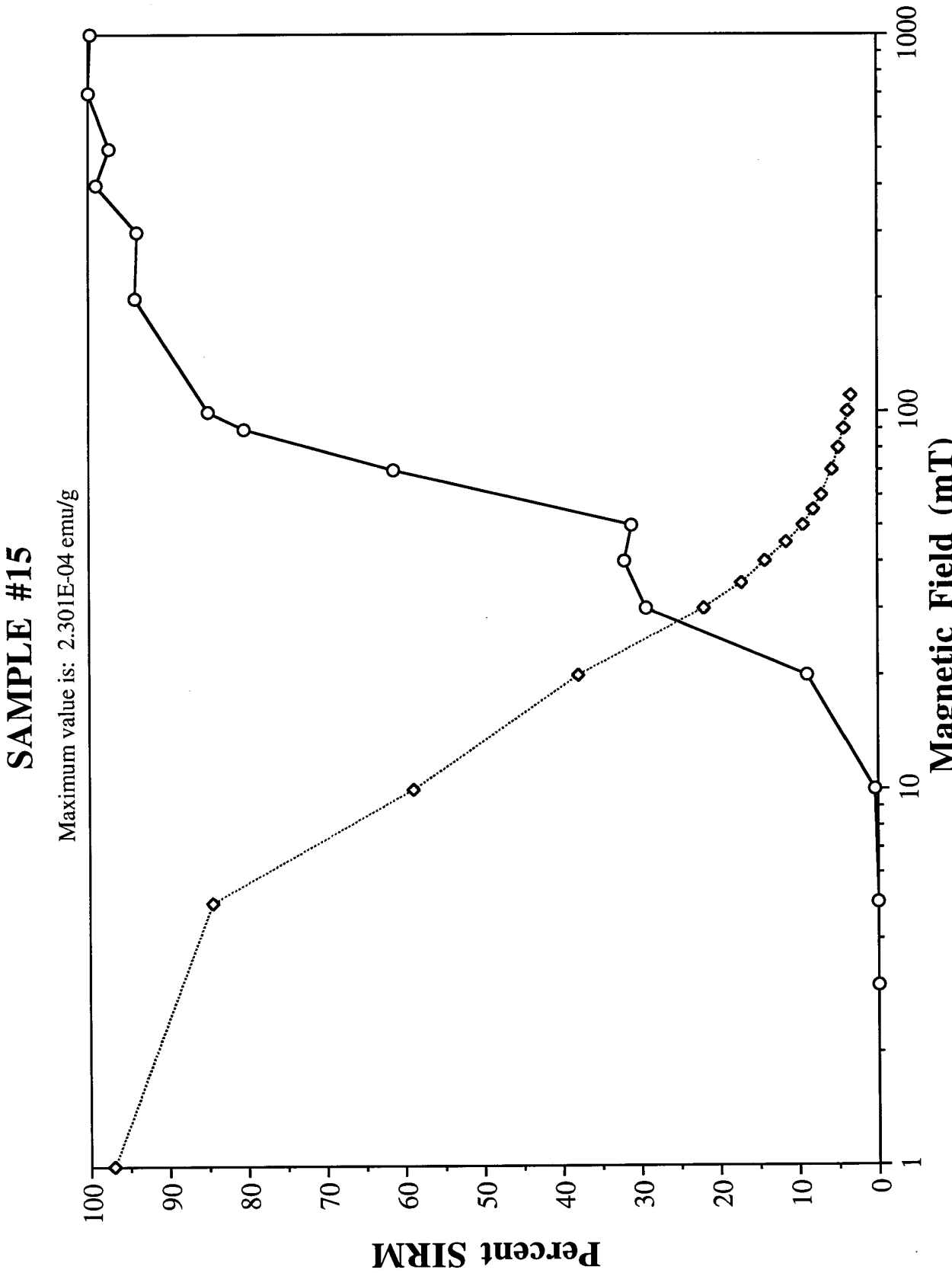
SAMPLE #15
Maximum value is: 2.301E-04 emu/g
Percent SIRM
100
90
80
70
60
50
40
30
20
10
0
1
10
100
1000
Magnetic Field (mT)

SAMPLE #16

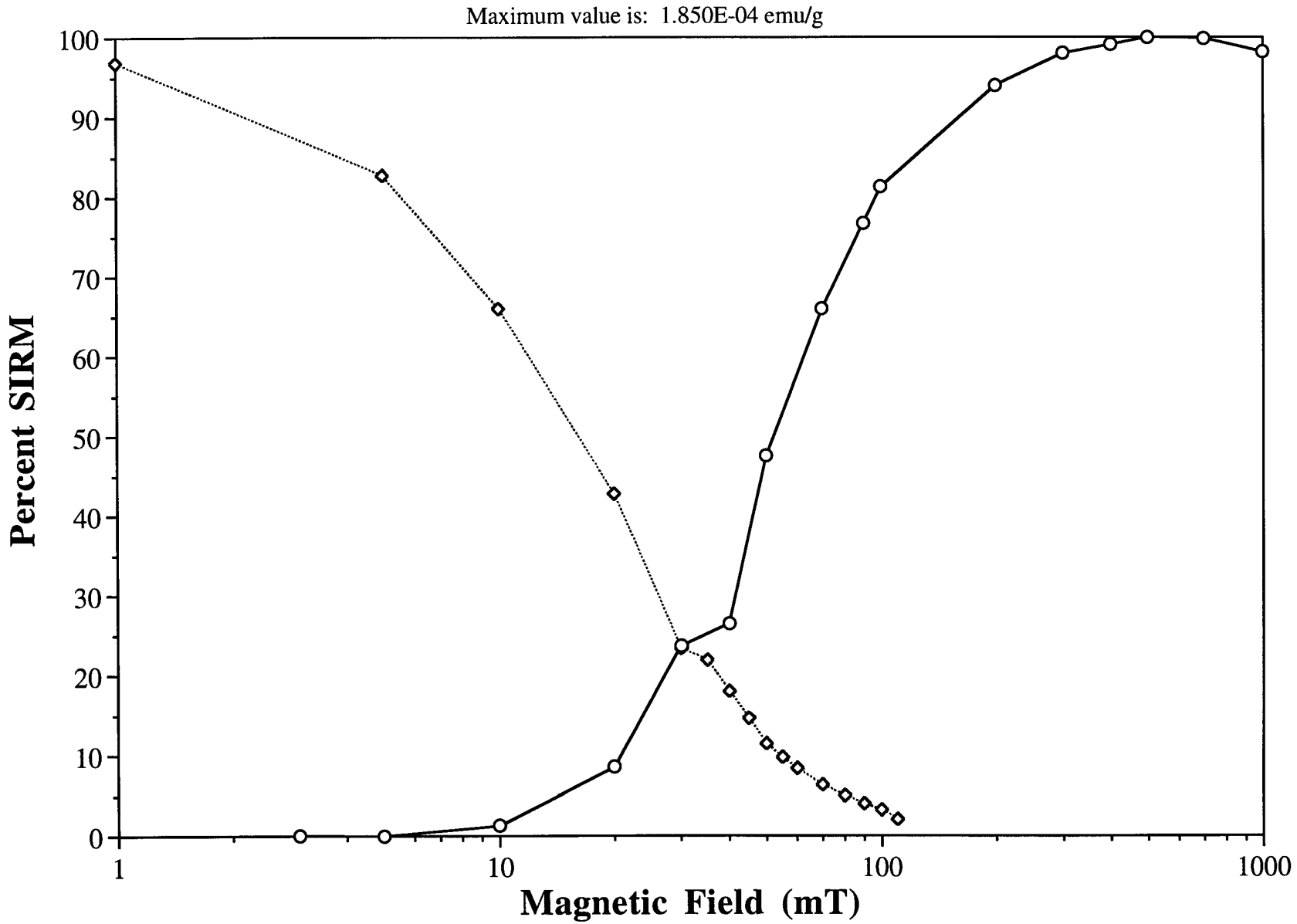
Maximum value is: 1.850E-04 emu/g
Percent SIRM
100
90
80
70
60
50
40
30
20
10
0
1
10
100
1000
Magnetic Field (mT)

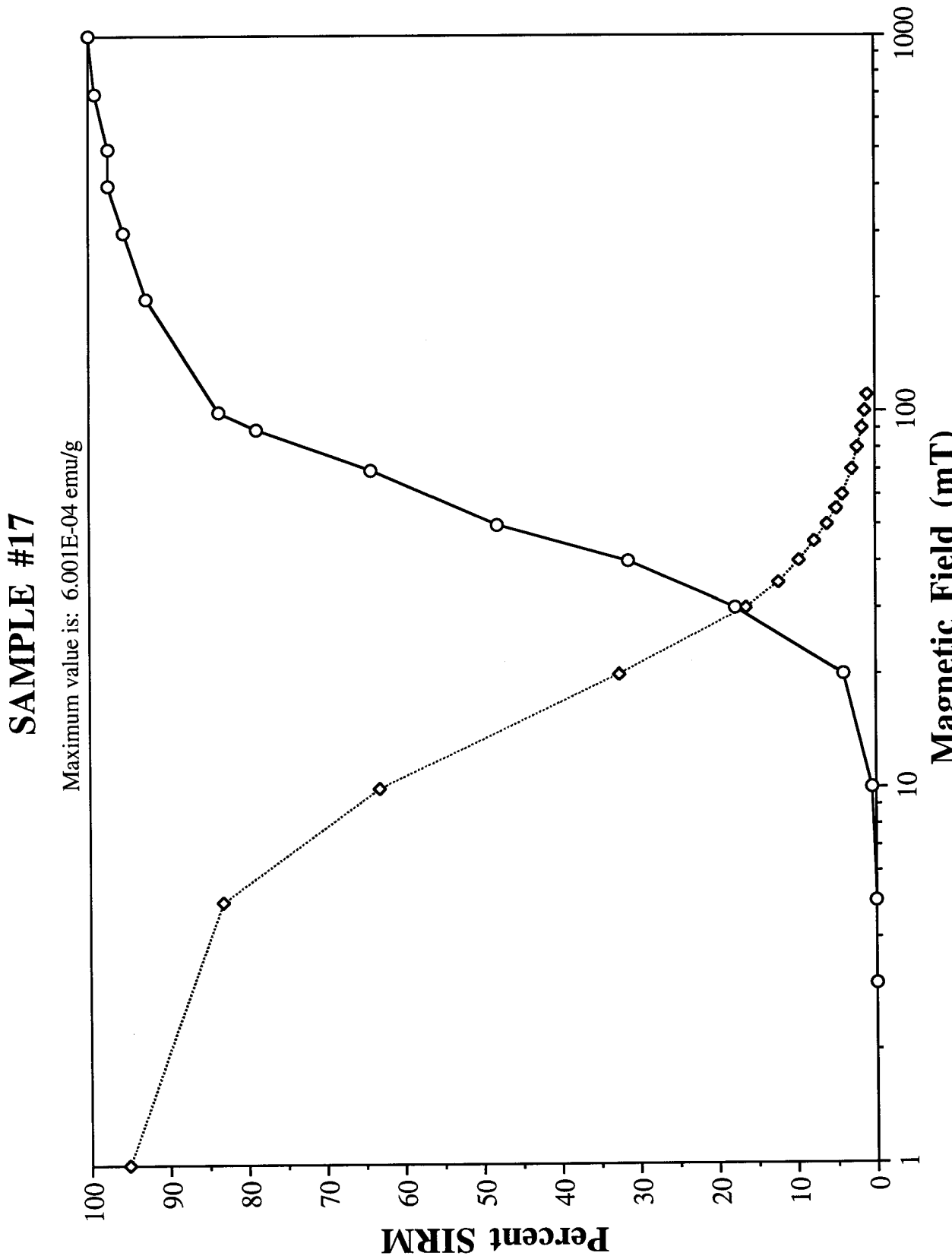
SAMPLE #17
Maximum value is: 6.001E-04 emu/g
Percent SIRM
100
90
80
70
60
50
40
30
20
10
0
1
10
100
1000
Magnetic Field (mT)

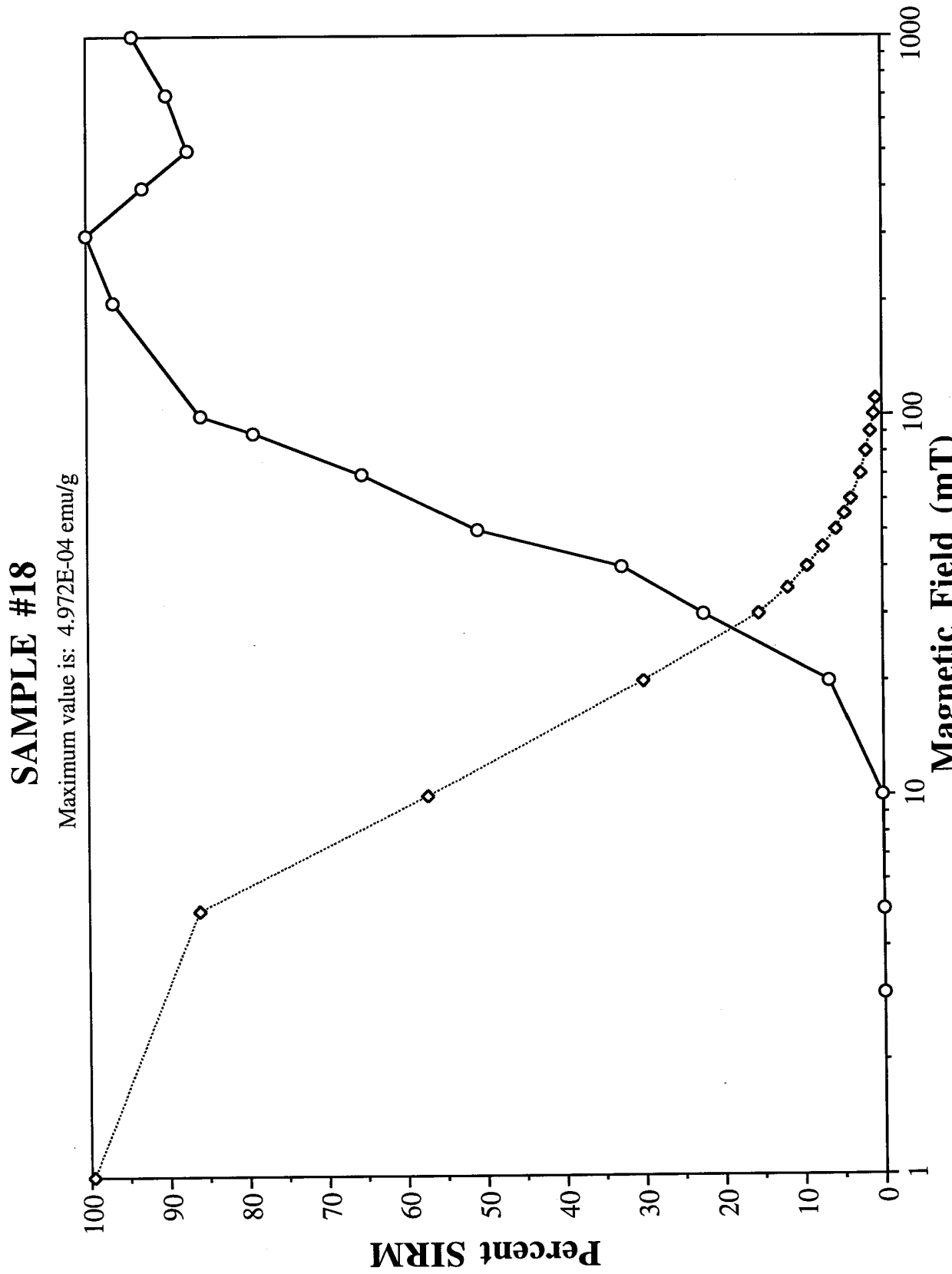
SAMPLE #18
Maximum value is: 4.972E-04 emu/g
Percent SIRM
100
90
80
70
60
50
40
30
20
10
0
1
10
100
1000
Magnetic Field (mT)

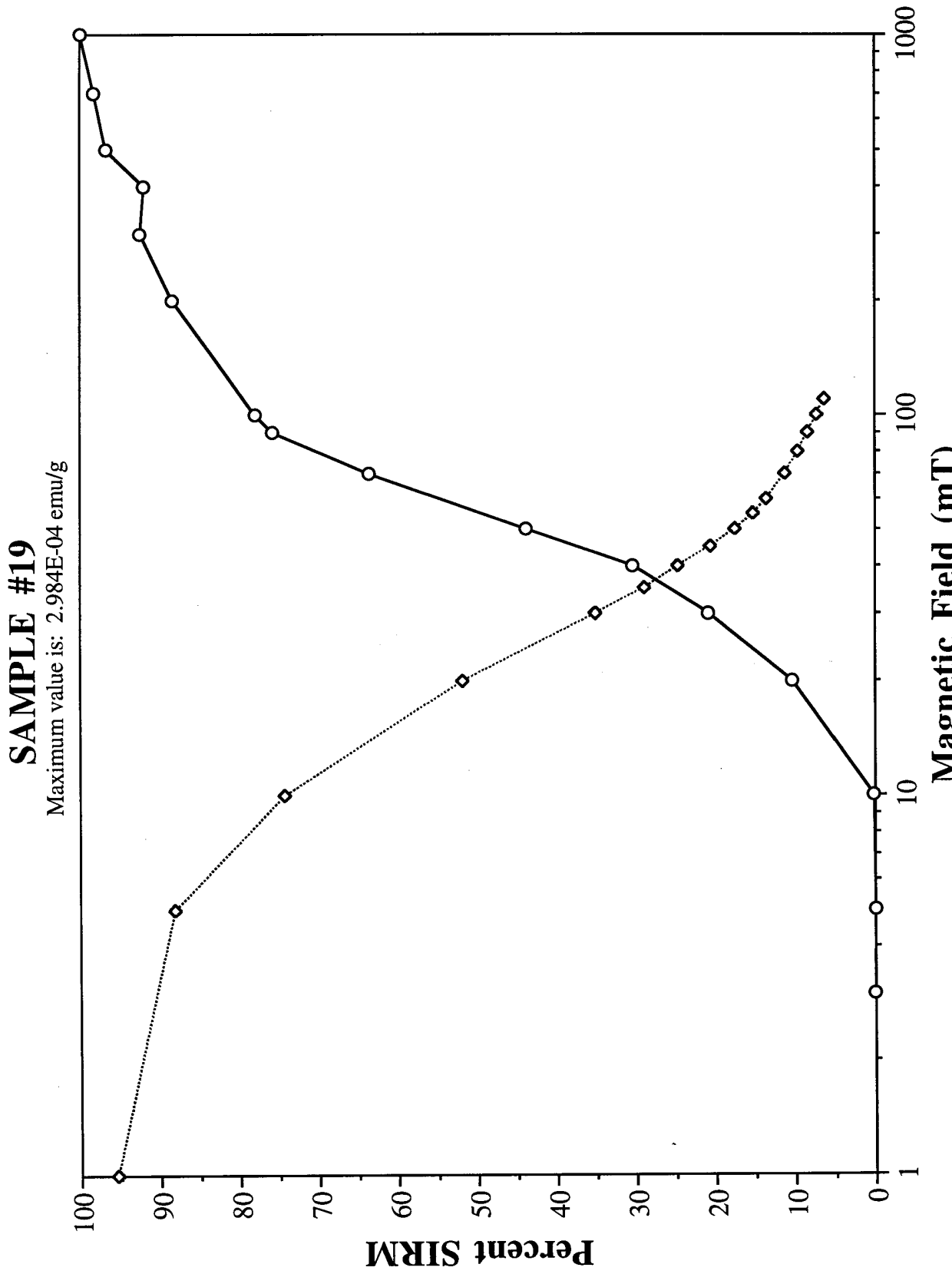
SAMPLE #19
Maximum value is: 2.984E-04 emu/g
Percent SIRM
100
90
80
70
60
50
40
30
20
10
0
1
10
100
1000
Magnetic Field (mT)

SAMPLE #20

Maximum value is: 1.723E-04 emu/g

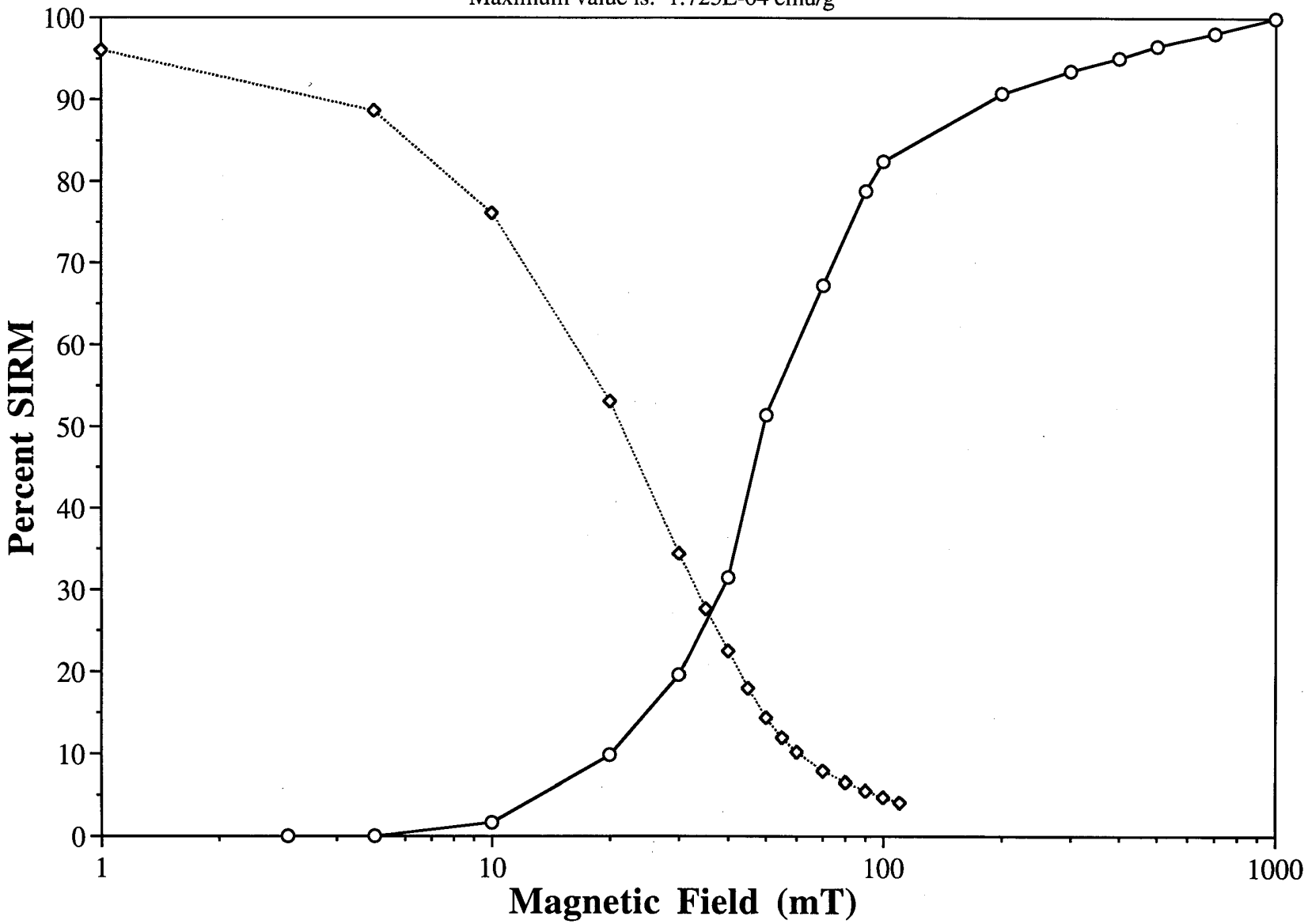

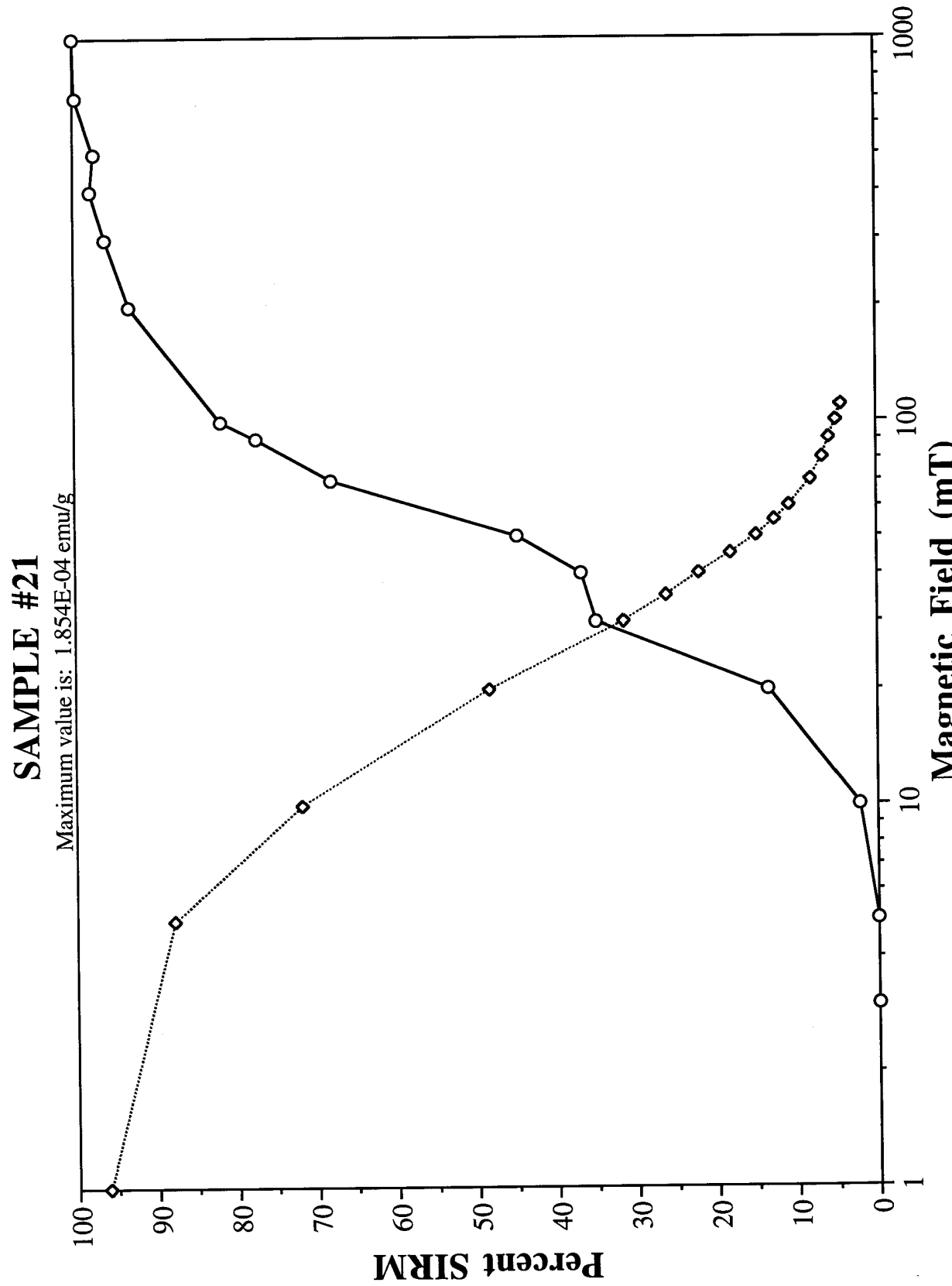
SAMPLE #21
Maximum value is: 1.854E-04 emu/g
Percent SIRM
100
90
80
70
60
50
40
30
20
10
0
1
10
100
1000
Magnetic Field (mT)

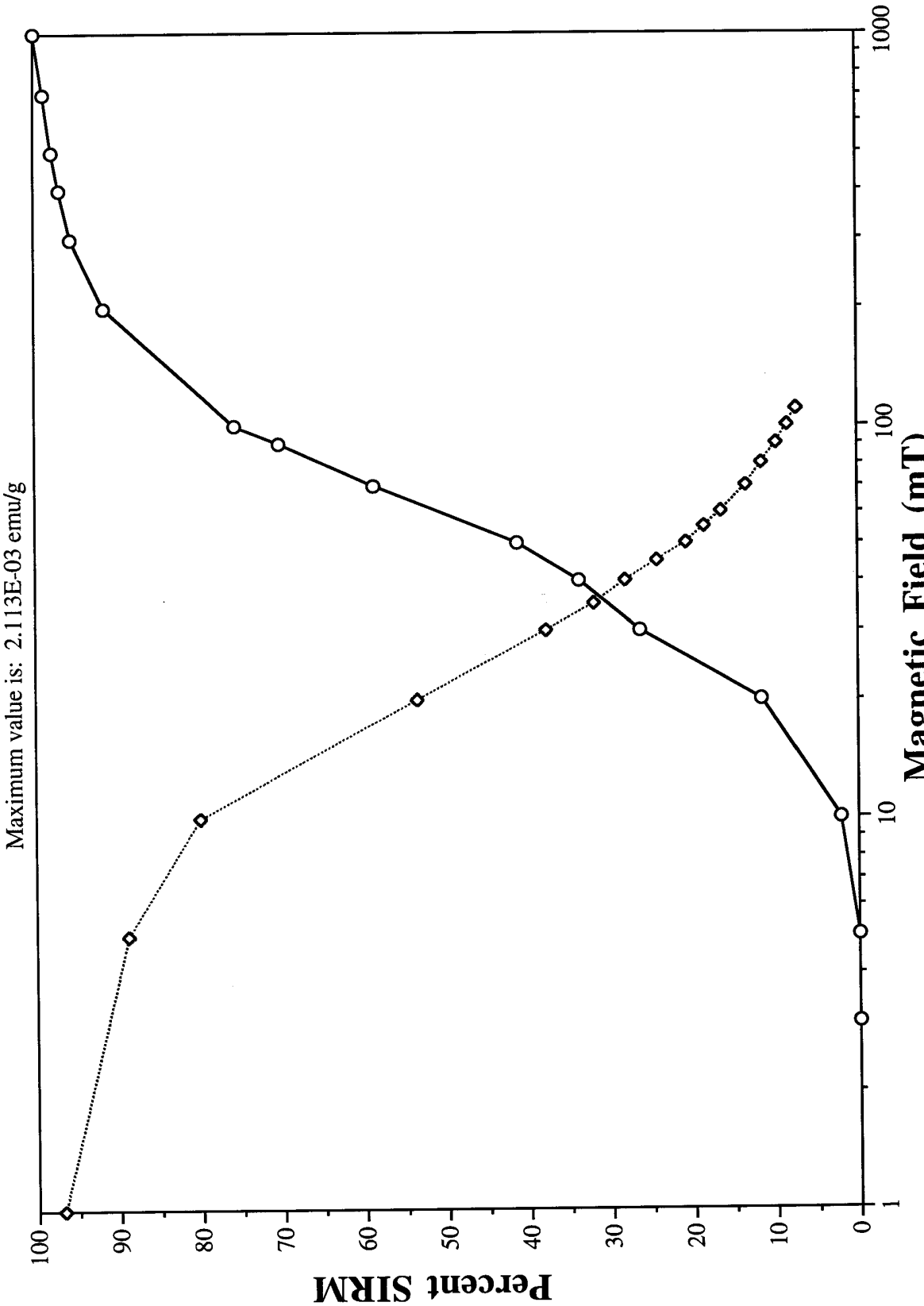
SAMPLE #22
Maximum value is: 2.113E-03 emu/g
Percent SIRM
100
90
80
70
60
50
40
30
20
10
0
1
10
100
1000
Magnetic Field (mT)

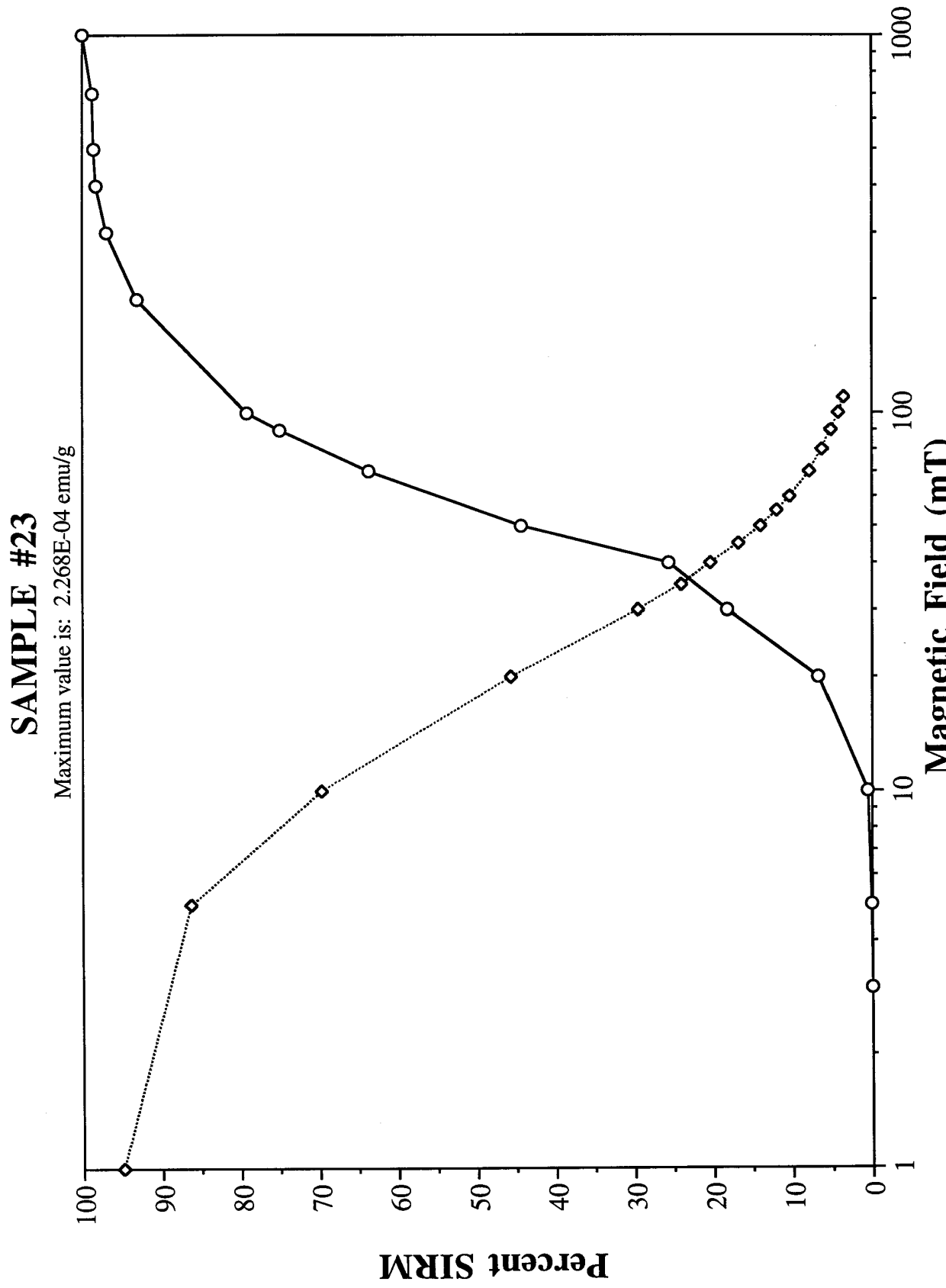
SAMPLE #23
Maximum value is: 2.268E-04 emu/g
Percent SIRM
100
90
80
70
60
50
40
30
20
10
0
1
10
100
1000
Magnetic Field (mT)

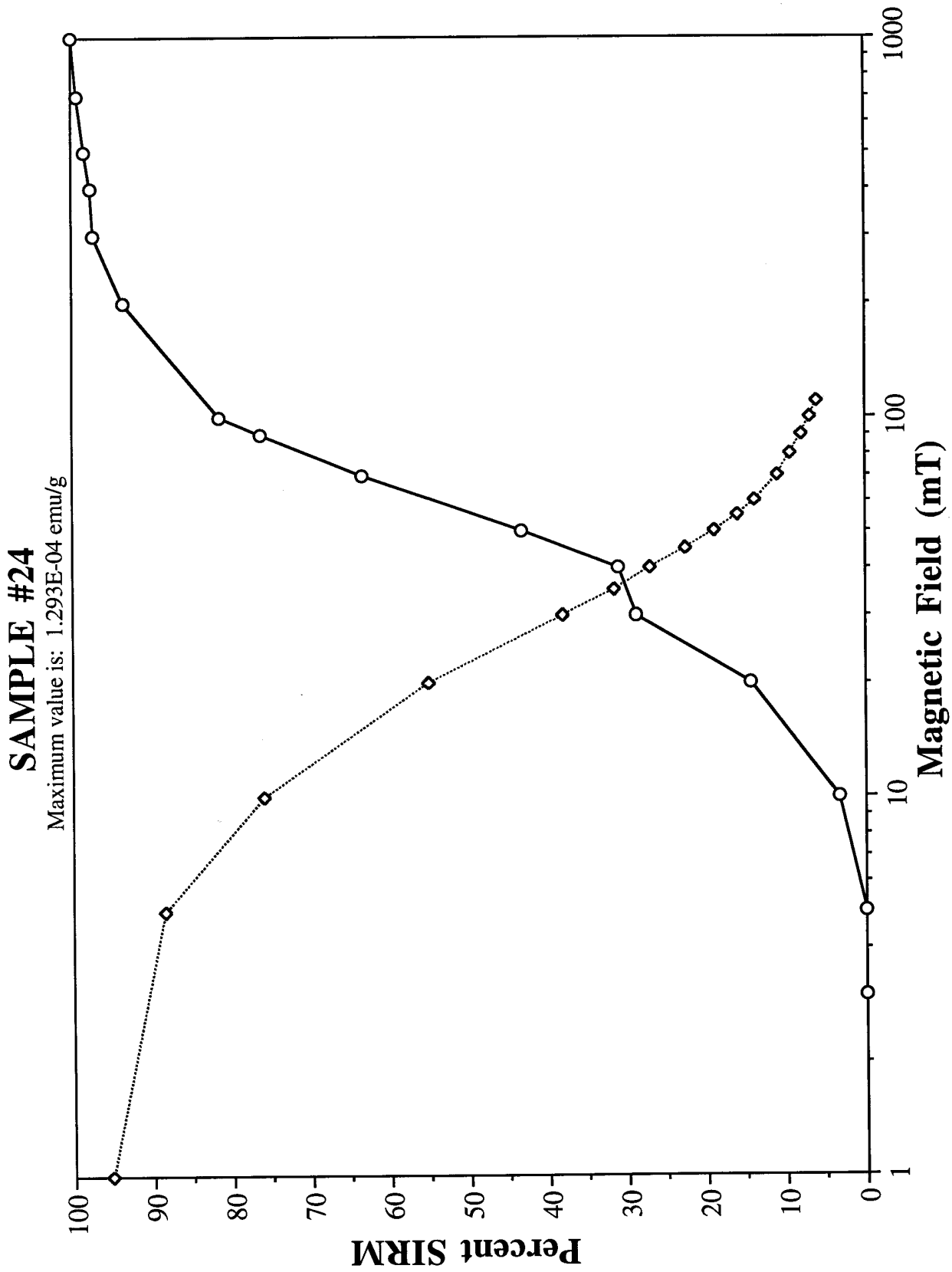
SAMPLE #24
Maximum value is: 1.293E-04 emu/g
Percent SIRM
100
90
80
70
60
50
40
30
20
10
0
1
10
100
1000
Magnetic Field (mT)

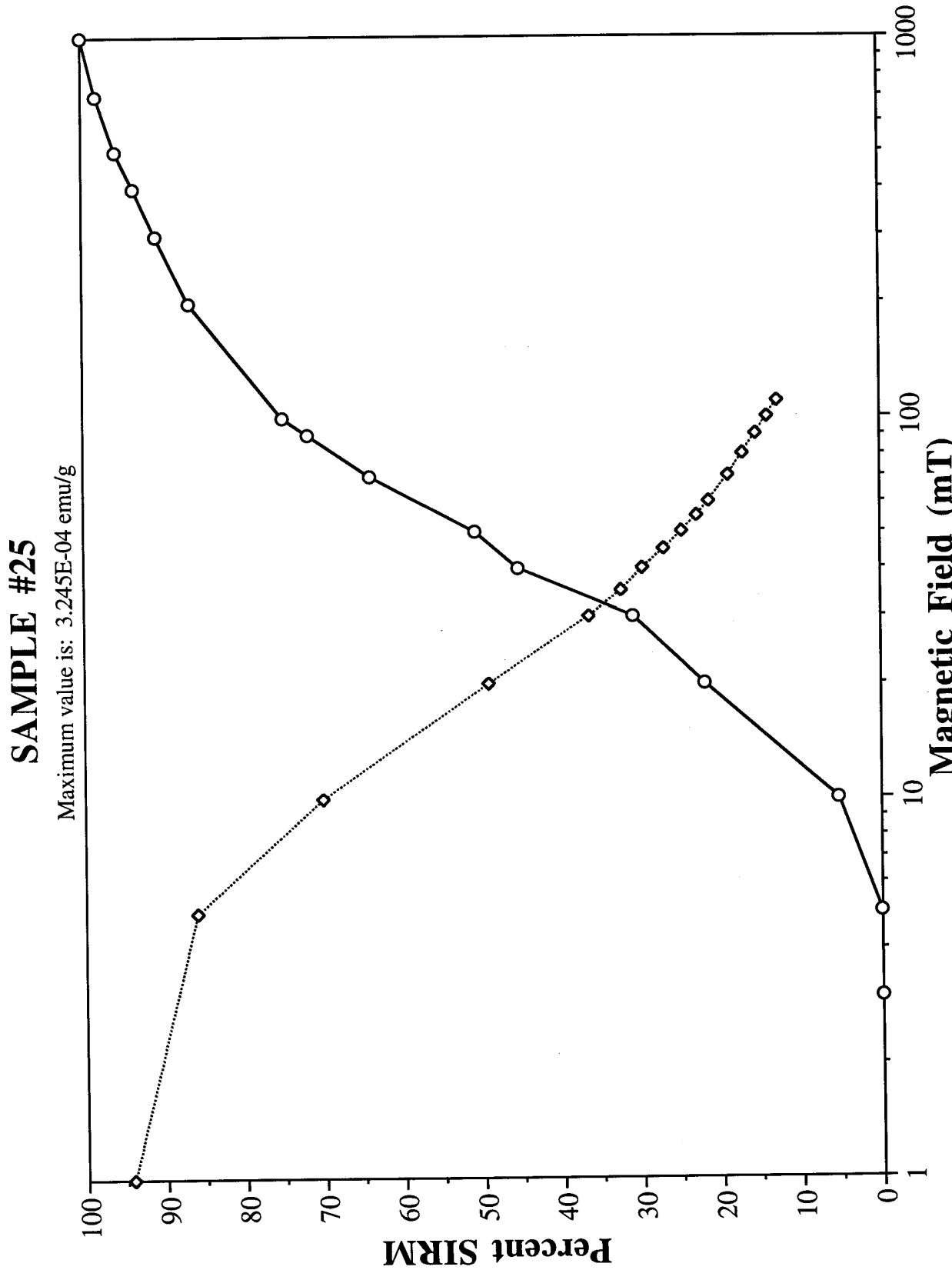
SAMPLE #25
Maximum value is: 3.245E-04 emu/g
Percent SIRM
100
90
80
70
60
50
40
30
20
10
0
1
10
100
1000
Magnetic Field (mT)

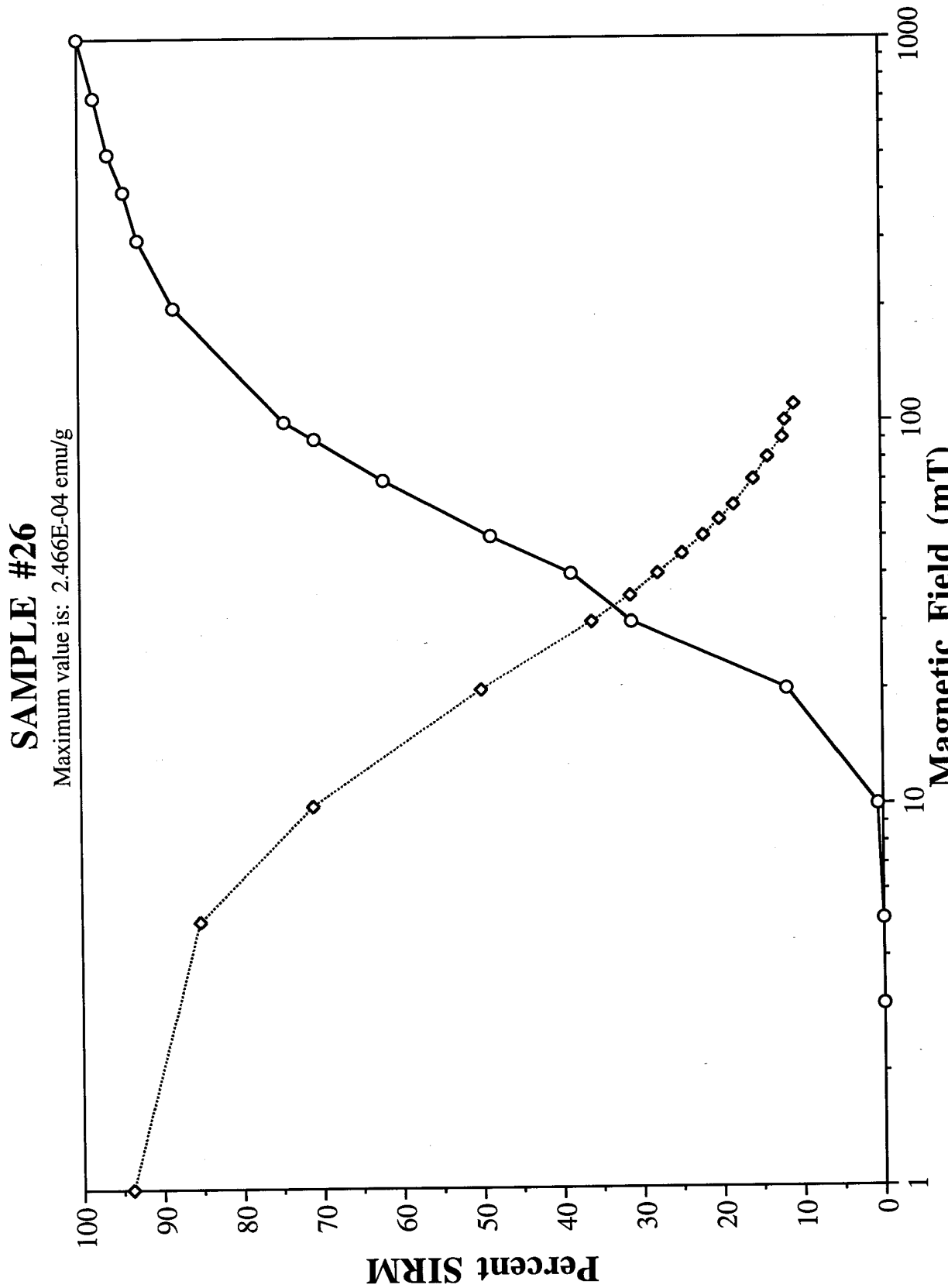
SAMPLE #26
Maximum value is: 2.466E-04 emu/g
Percent SIRM
100
90
80
70
60
50
40
30
20
10
0
1
10
100
1000
Magnetic Field (mT)

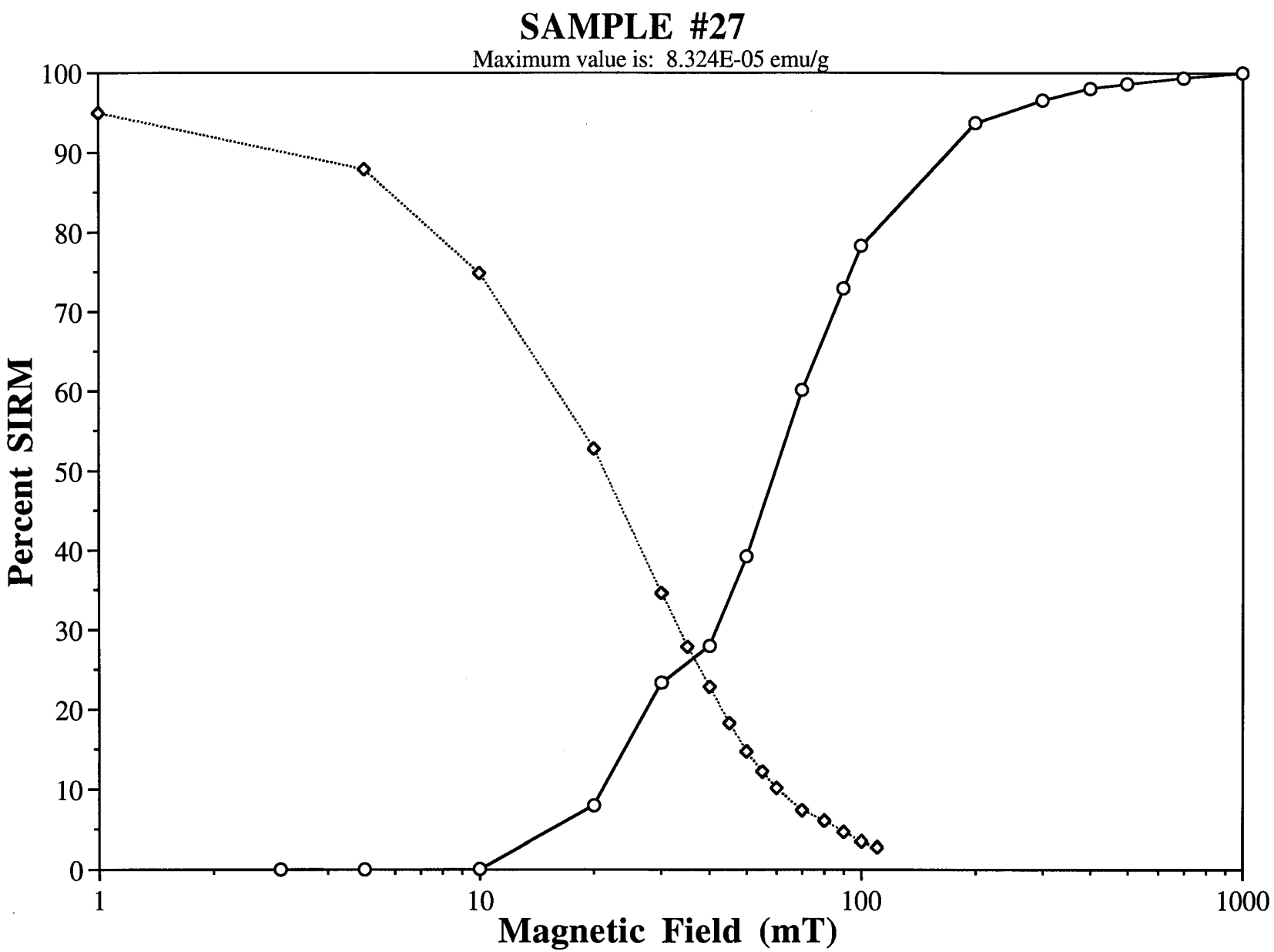
SAMPLE #27
Maximum value is: 8.324E-05 emu/g
Percent SIRM
100
90
80
70
60
50
40
30
20
10
0
1
10
100
1000
Magnetic Field (mT)

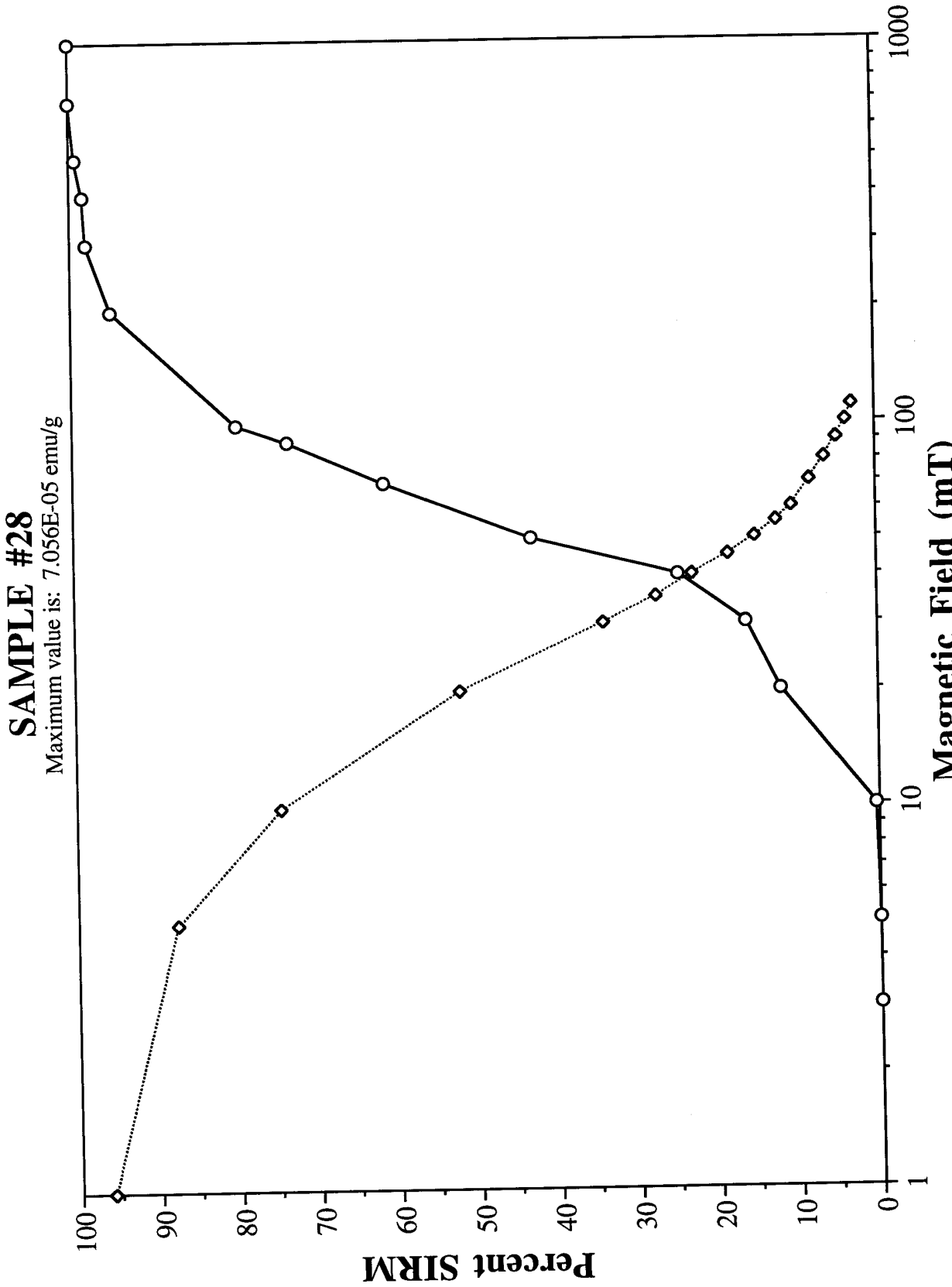
SAMPLE #28
Maximum value is: 7.056E-05 emu/g
Percent SIRM
100
90
80
70
60
50
40
30
20
10
0
1
10
100
1000
Magnetic Field (mT)

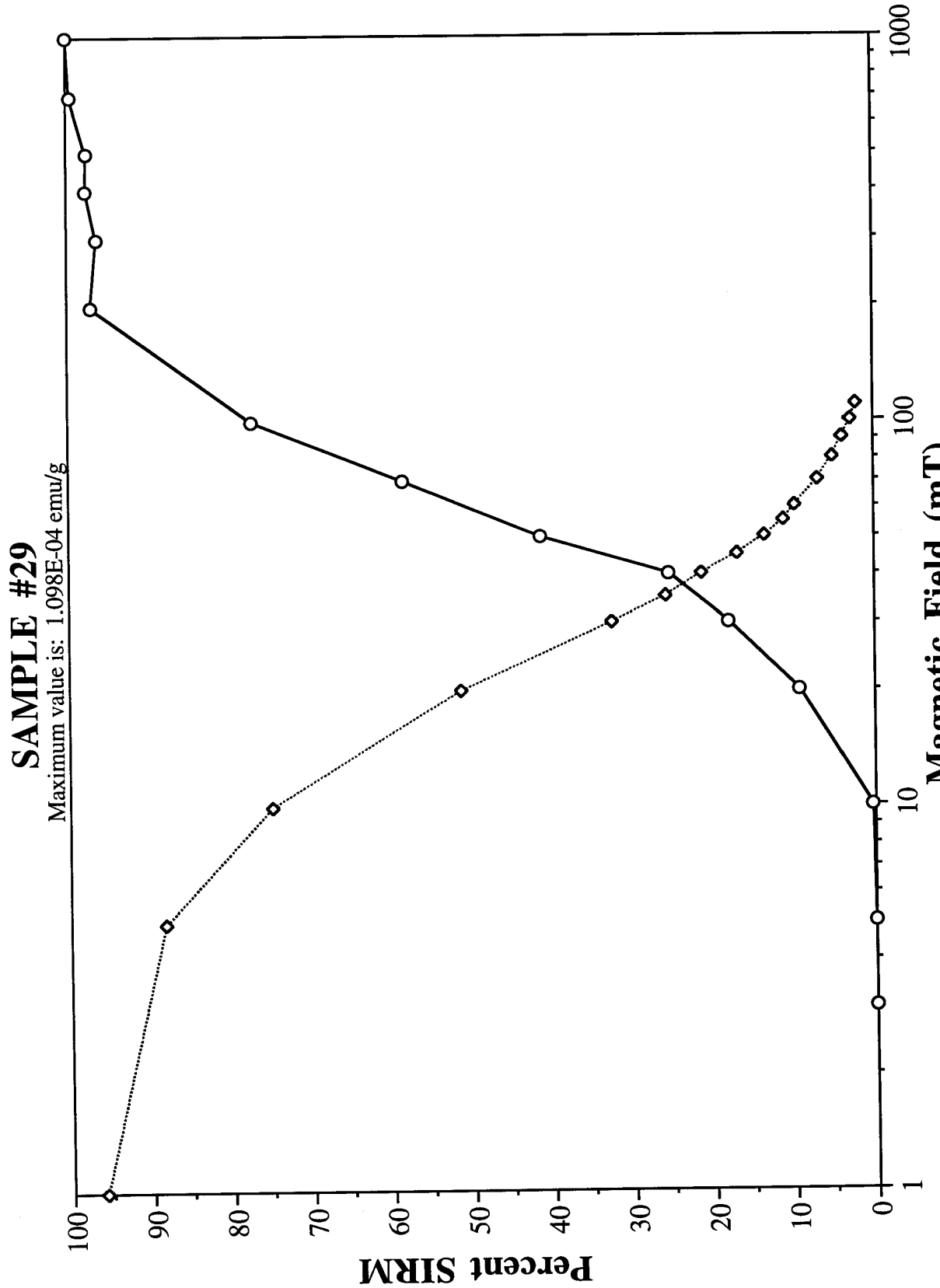
SAMPLE #29
Maximum value is: 1.098E-04 emu/g
Percent SIRM
100
90
80
70
60
50
40
30
20
10
0
1
10
100
1000
Magnetic Field (mT)

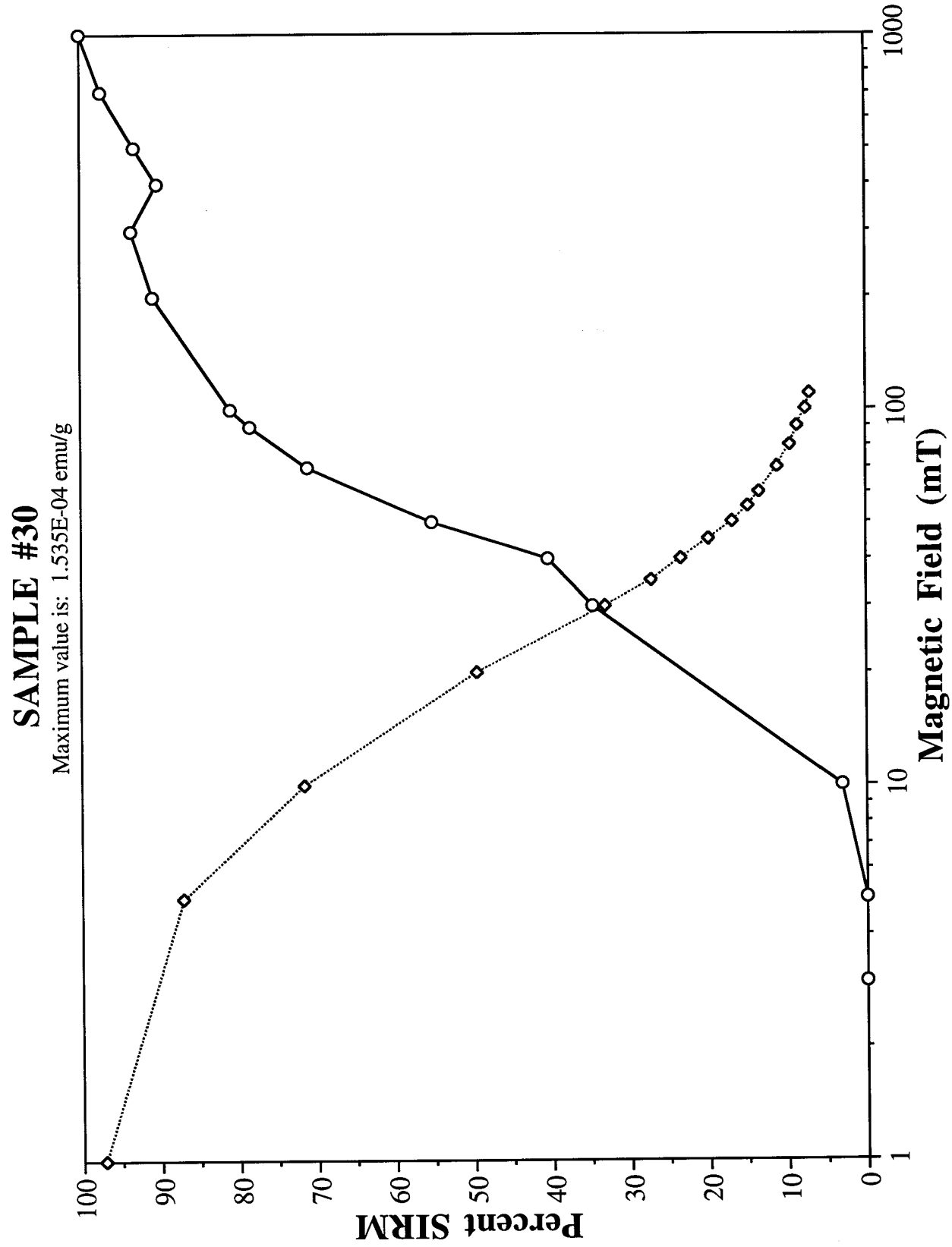
SAMPLE #30
Maximum value is: 1.535E-04 emu/g
Percent SIRM
100
90
80
70
60
50
40
30
20
10
0
1
10
100
1000
Magnetic Field (mT)

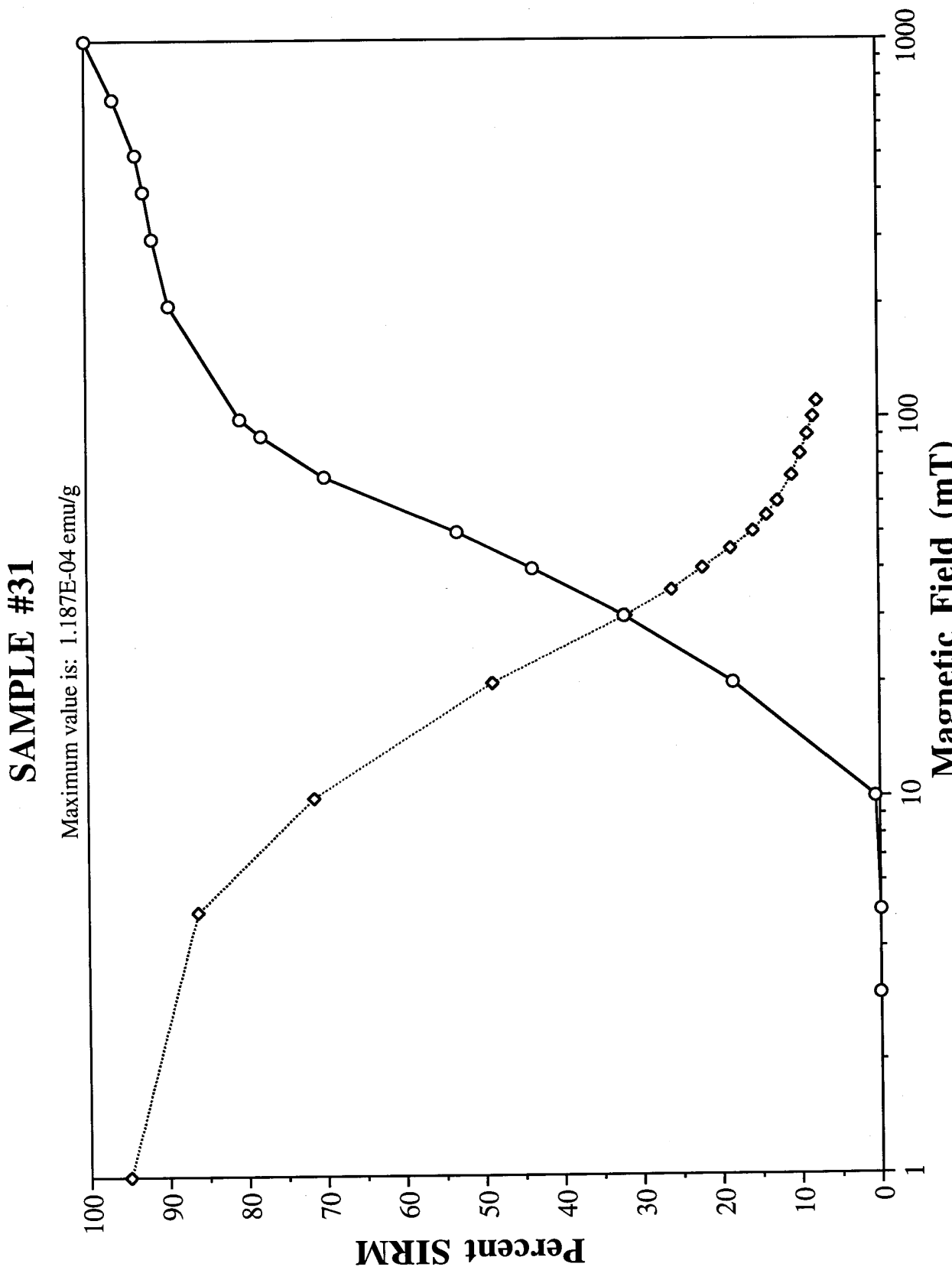
SAMPLE #31
Maximum value is: 1.187E-04 emu/g
Percent SIRM
100
90
80
70
60
50
40
30
20
10
0
1
10
100
1000
Magnetic Field (mT)

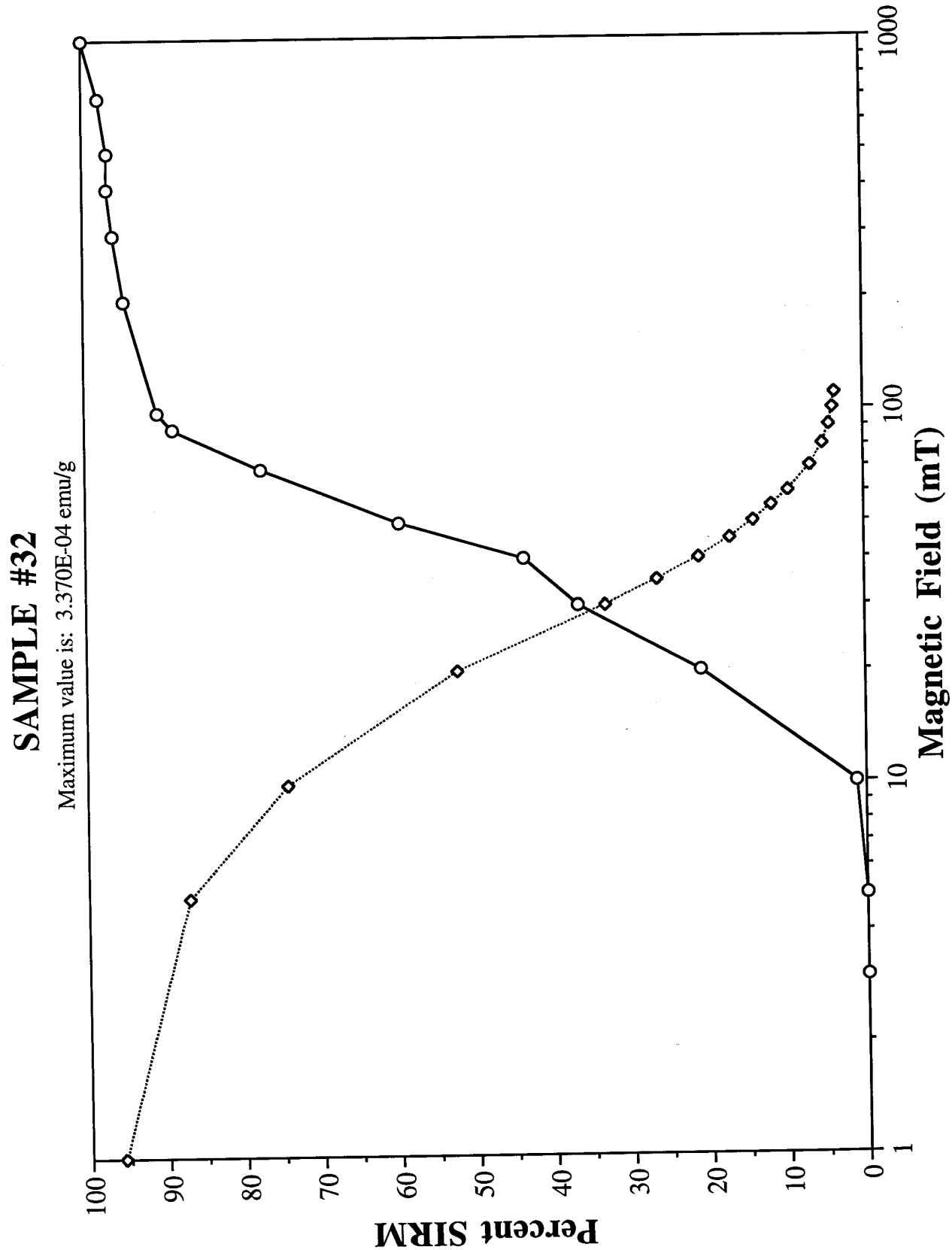
SAMPLE #32
Maximum value is: 3.370E-04 emu/g
Percent SIRM
100
90
80
70
60
50
40
30
20
10
0
1
10
100
1000
Magnetic Field (mT)

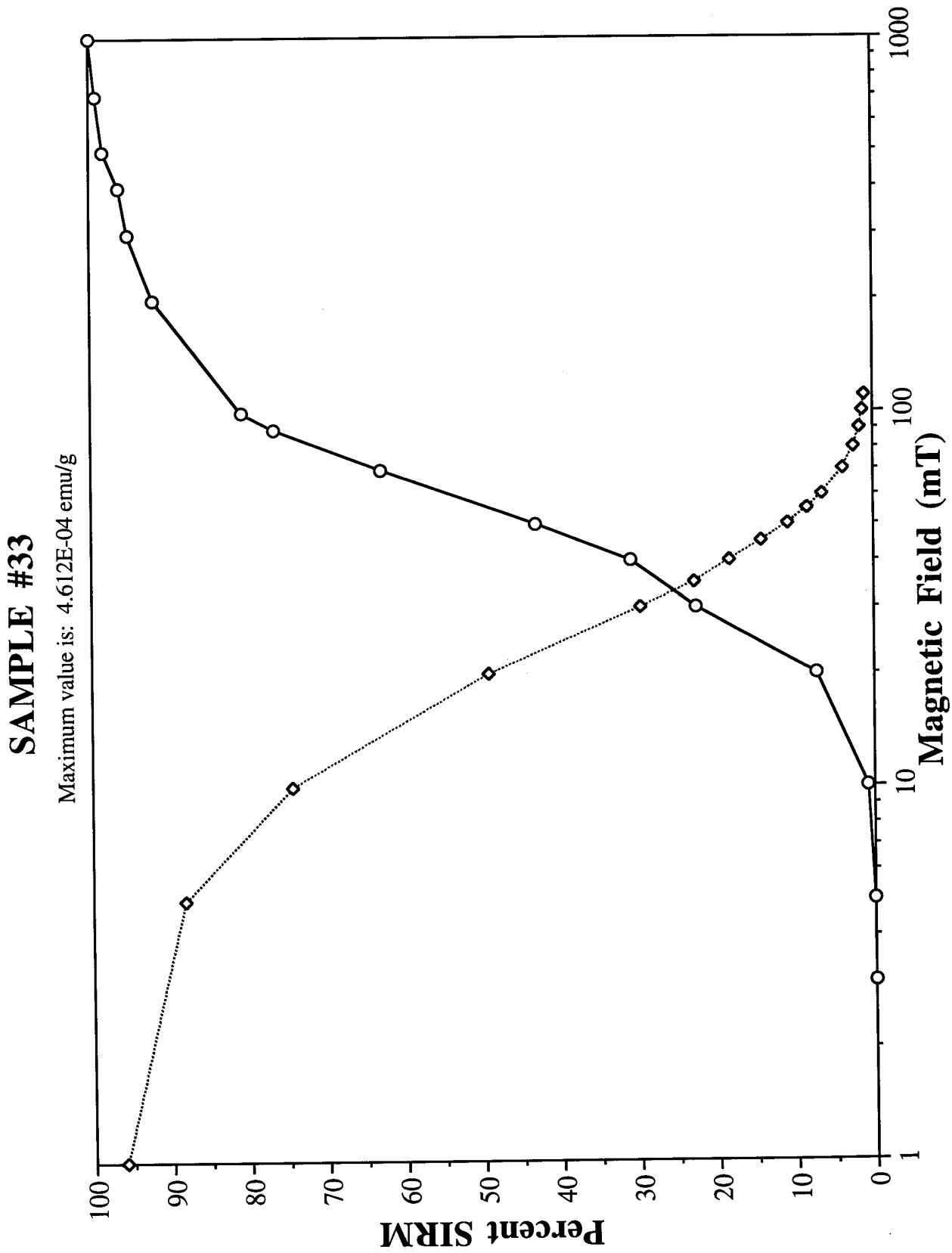
SAMPLE #33
Maximum value is: 4.612E-04 emu/g
Percent SIRM
100
90
80
70
60
50
40
30
20
10
0
1
10
100
1000
Magnetic Field (mT)

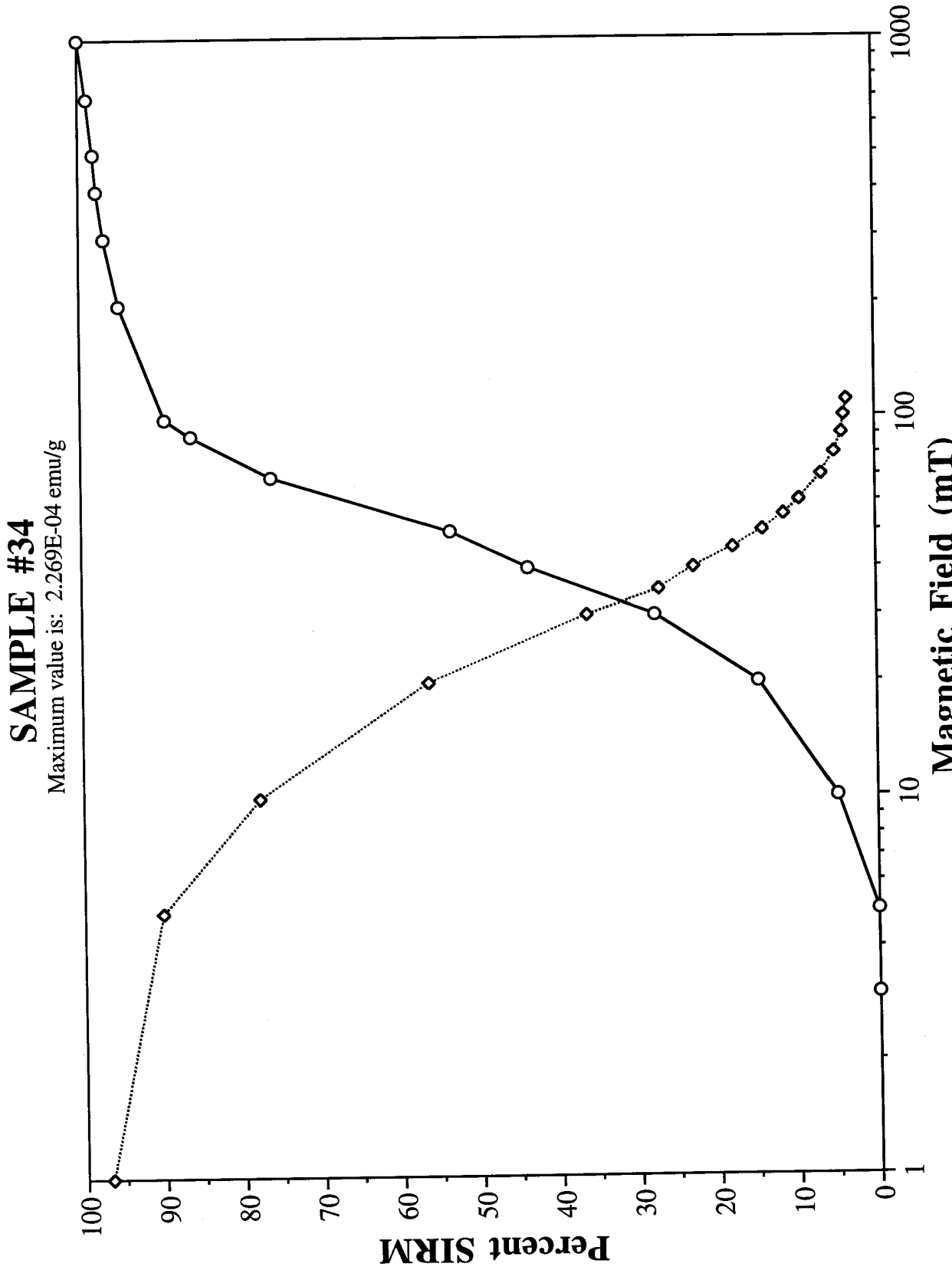
SAMPLE #34
Maximum value is: 2.269E-04 emu/g
Percent SIRM
100
90
80
70
60
50
40
30
20
10
0
1
10
100
1000
Magnetic Field (mT)

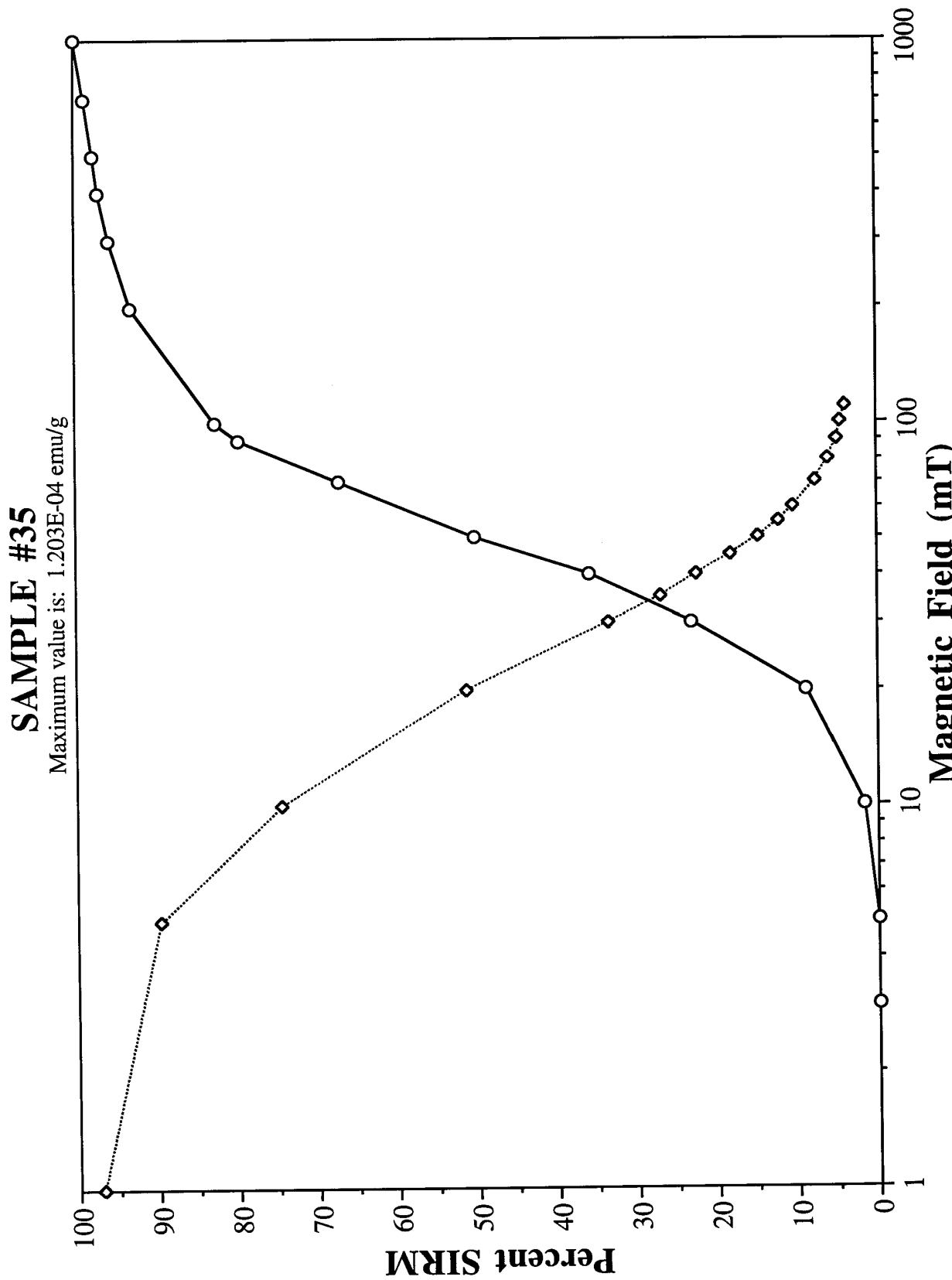
SAMPLE #35
Maximum value is: 1.203E-04 emu/g
Percent SIRM
100
90
80
70
60
50
40
30
20
10
0
1
10
100
1000
Magnetic Field (mT)

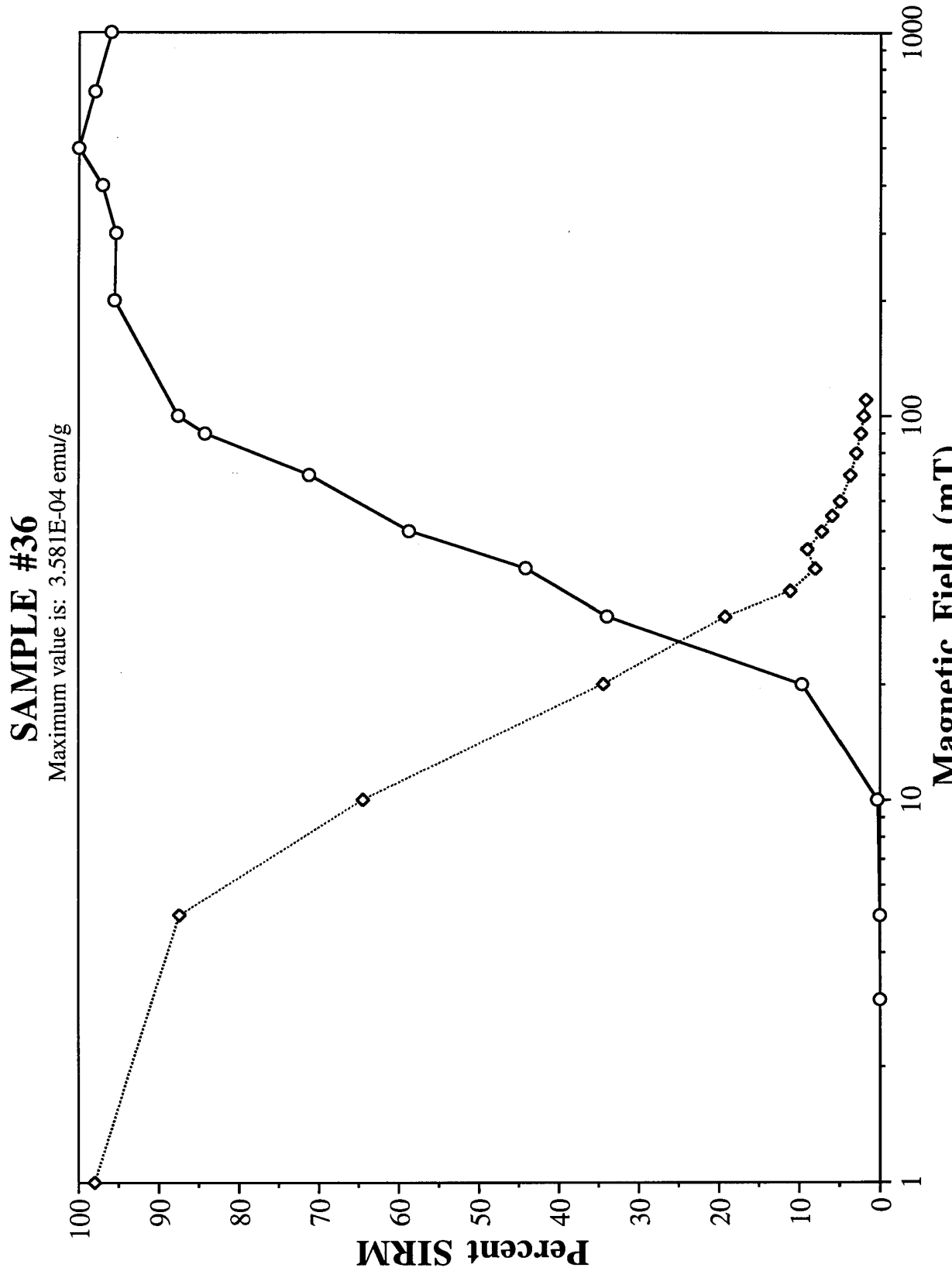
SAMPLE #36
Maximum value is: 3.581E-04 emu/g
Percent SIRM
100
90
80
70
60
50
40
30
20
10
0
1
10
100
1000
Magnetic Field (mT)

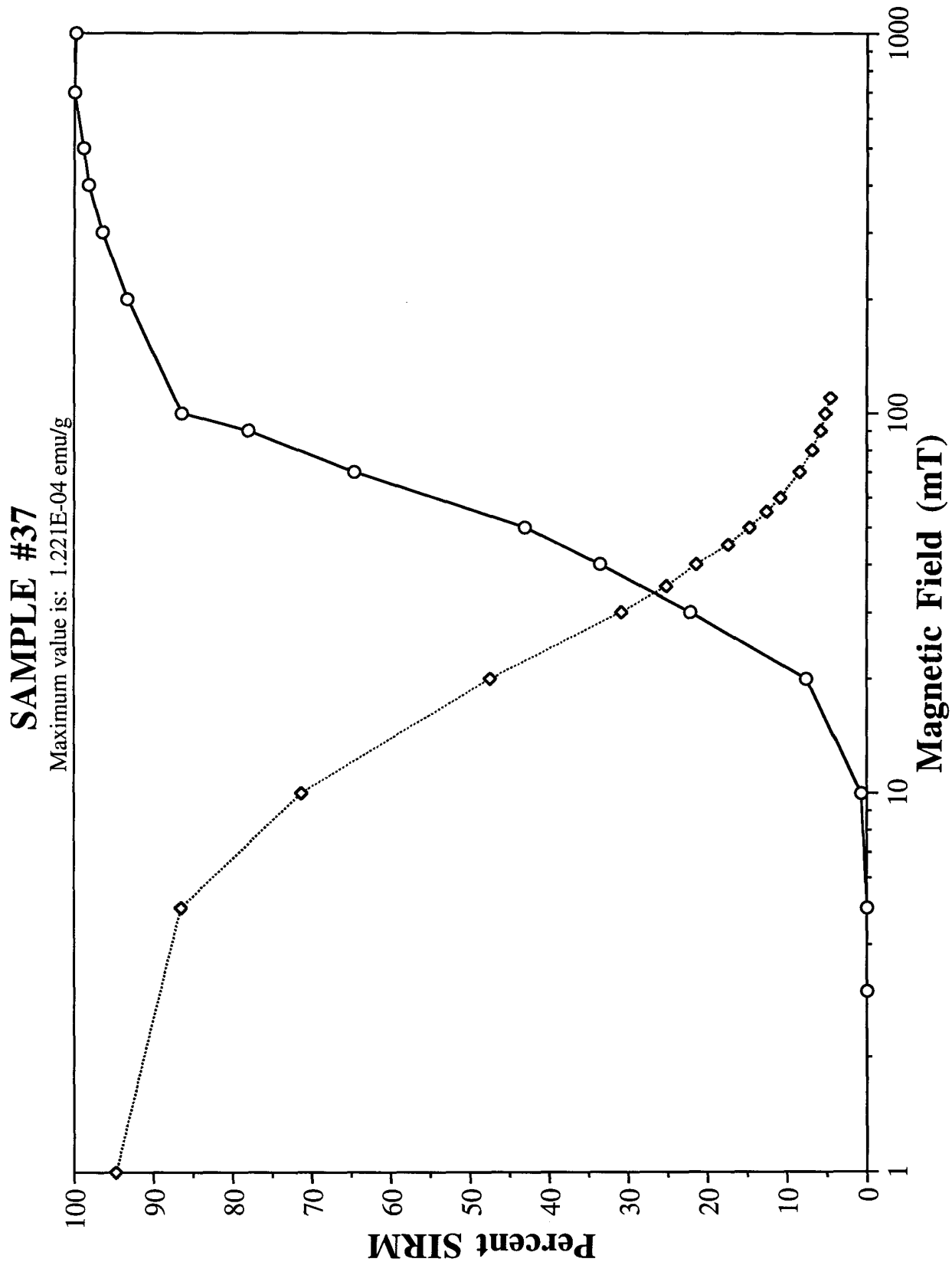
SAMPLE #37
Maximum value is: 1.221E-04 emu/g
Percent SIRM
100
90
80
70
60
50
40
30
20
10
0
1
10
100
1000
Magnetic Field (mT)

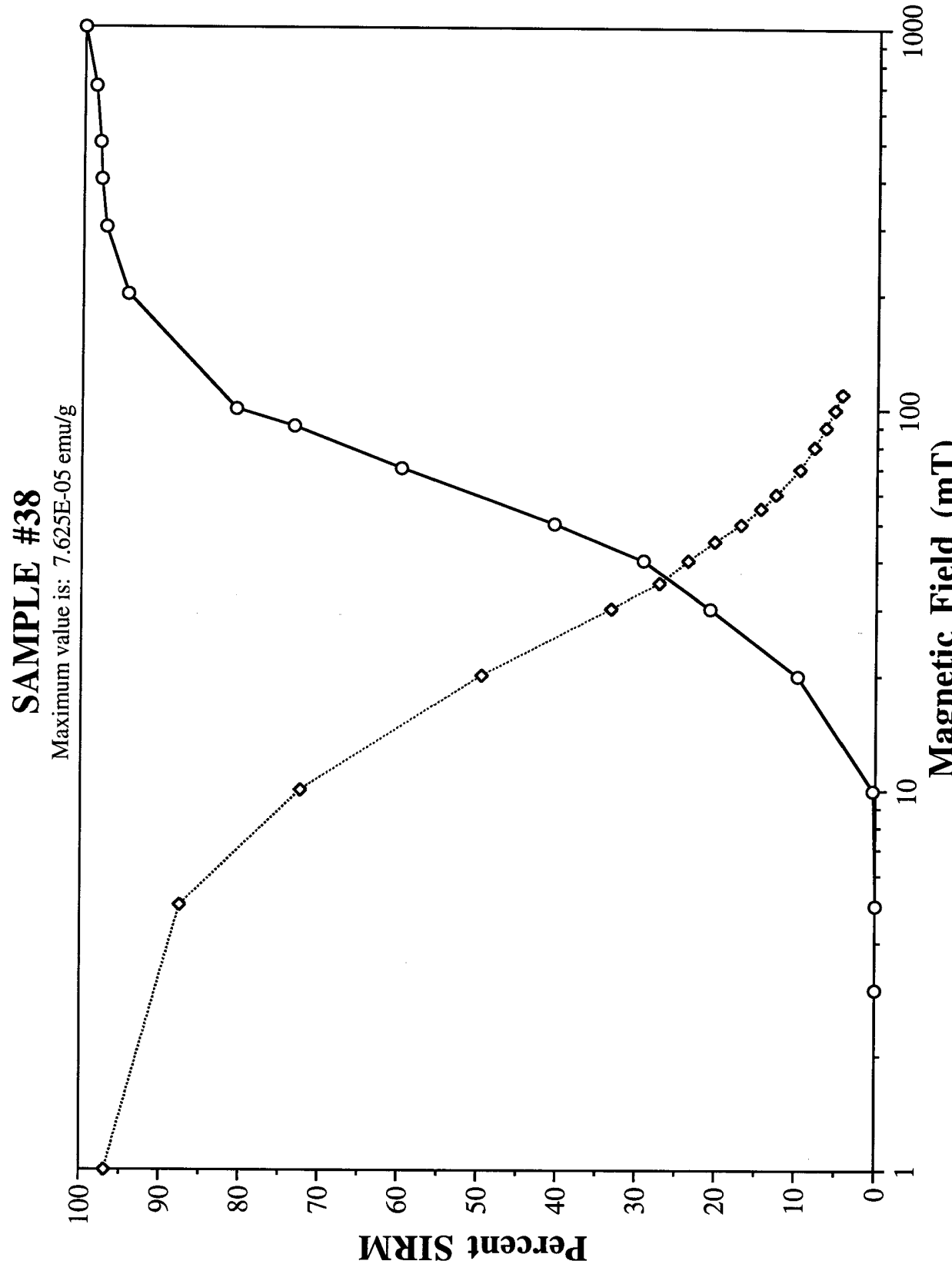
SAMPLE #38
Maximum value is: 7.625E-05 emu/g
Percent SIRM
100
90
80
70
60
50
40
30
20
10
0
1
10
100
1000
Magnetic Field (mT)

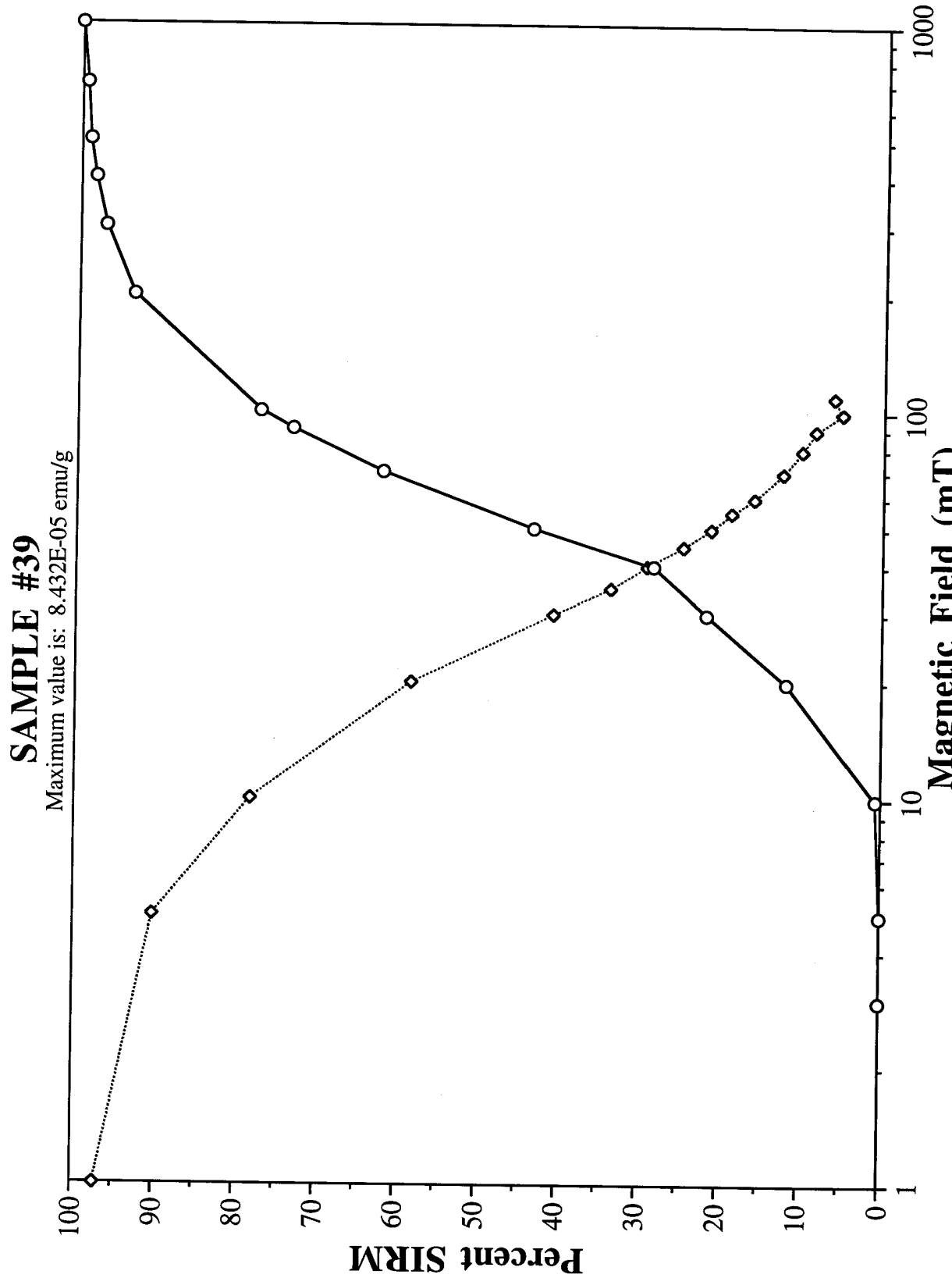
SAMPLE #39
Maximum value is: 8.432E-05 emu/g
Percent SIRM
100
90
80
70
60
50
40
30
20
10
0
1
10
100
1000
Magnetic Field (mT)

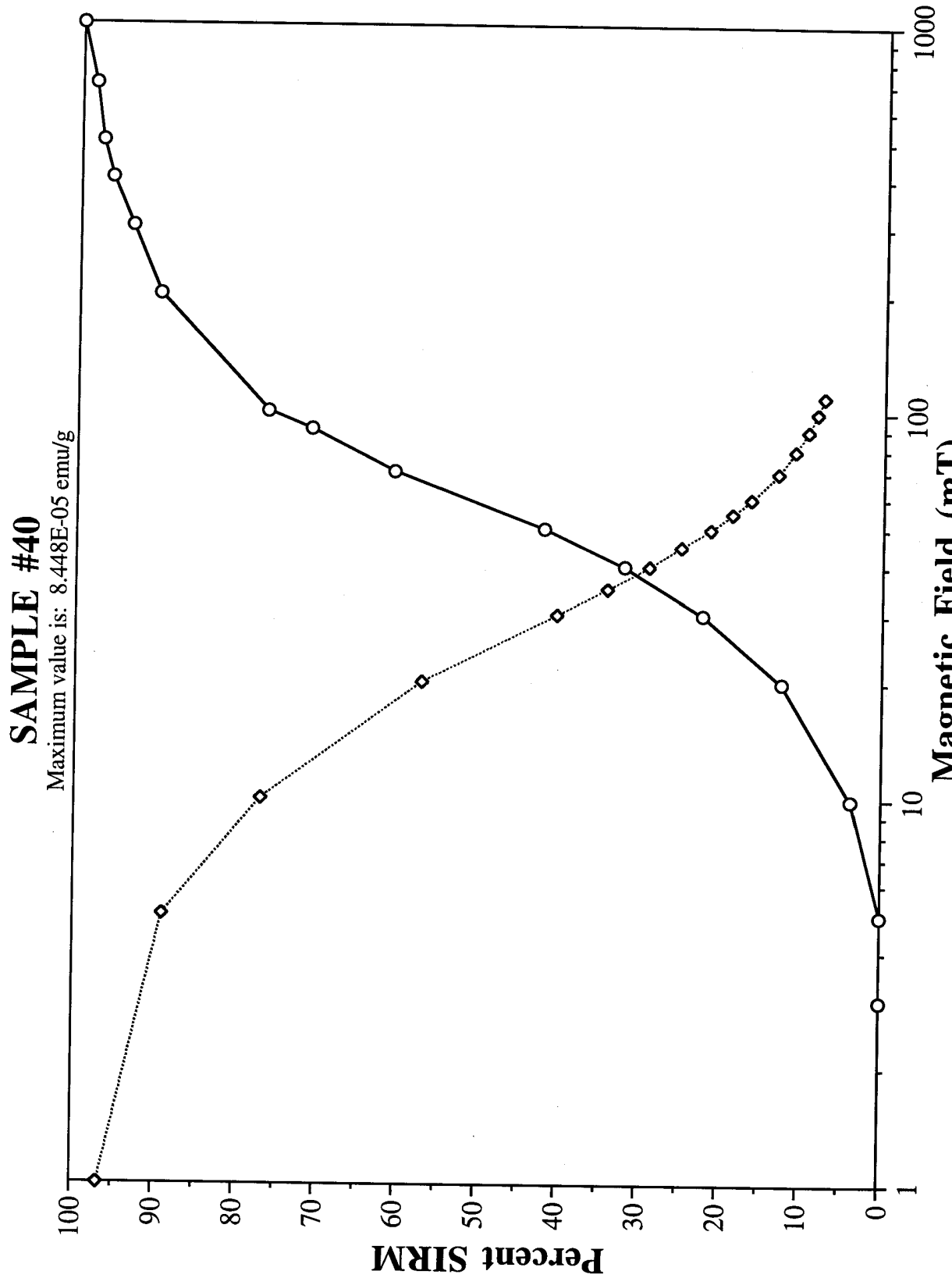
SAMPLE #40
Maximum value is: 8.448E-05 emu/g
Percent SIRM
100
90
80
70
60
50
40
30
20
10
0
1
10
100
1000
Magnetic Field (mT)

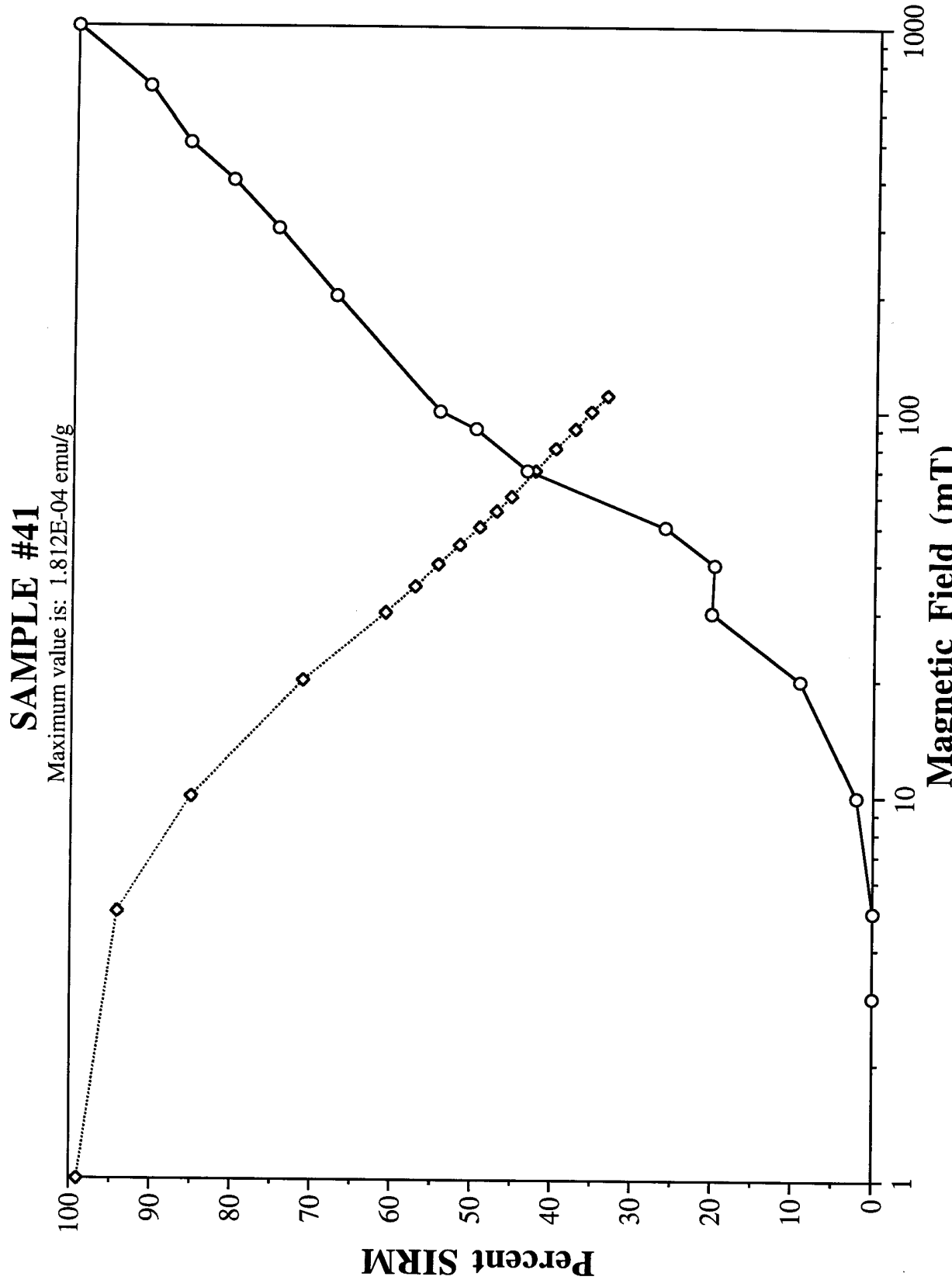
SAMPLE #41
Maximum value is: 1.812E-04 emu/g
Percent SIRM
100
90
80
70
60
50
40
30
20
10
0
1
10
100
1000
Magnetic Field (mT)

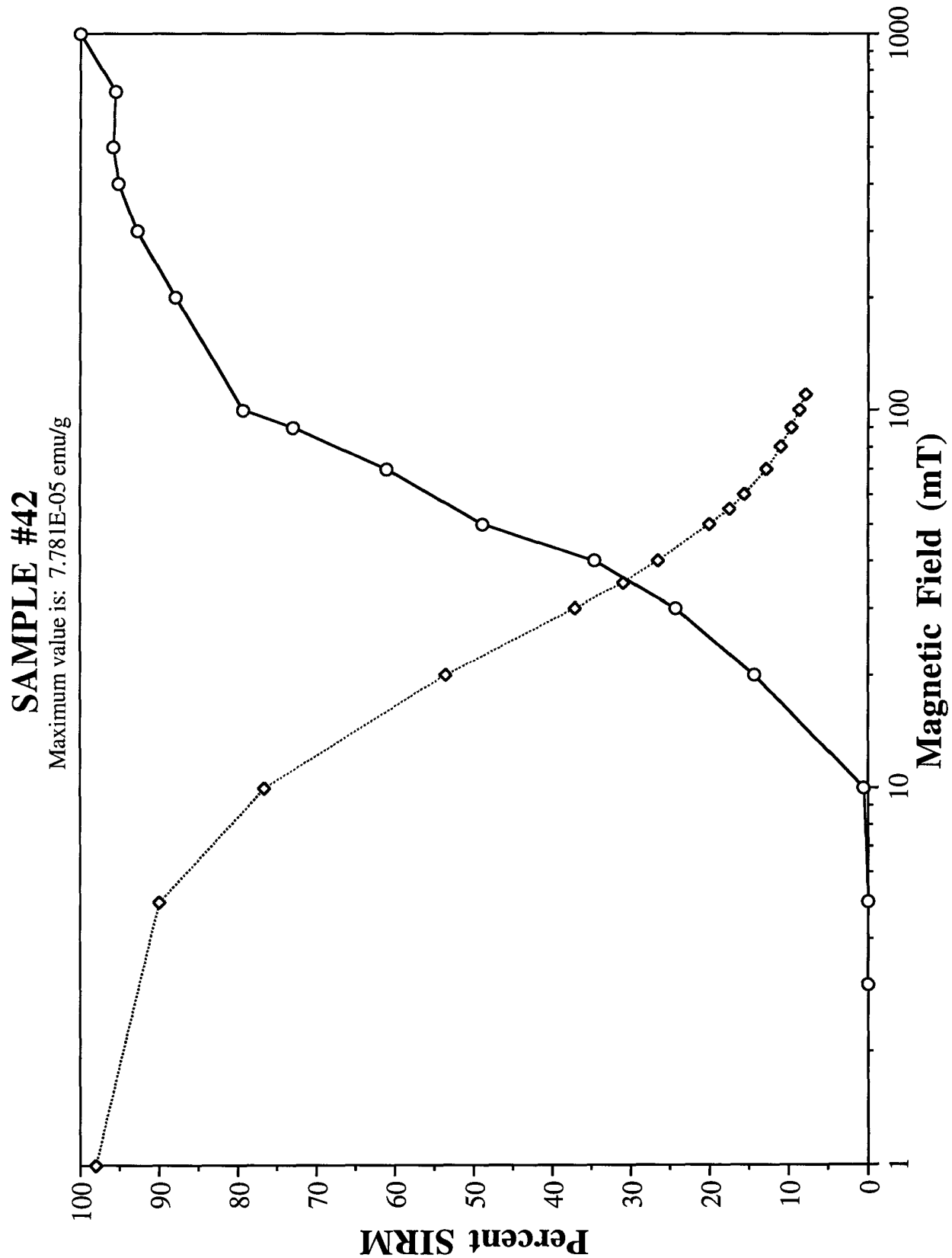
SAMPLE #42
Maximum value is: 7.781E-05 emu/g
Percent SIRM
100
90
80
70
60
50
40
30
20
10
0
1
10
100
1000
Magnetic Field (mT)

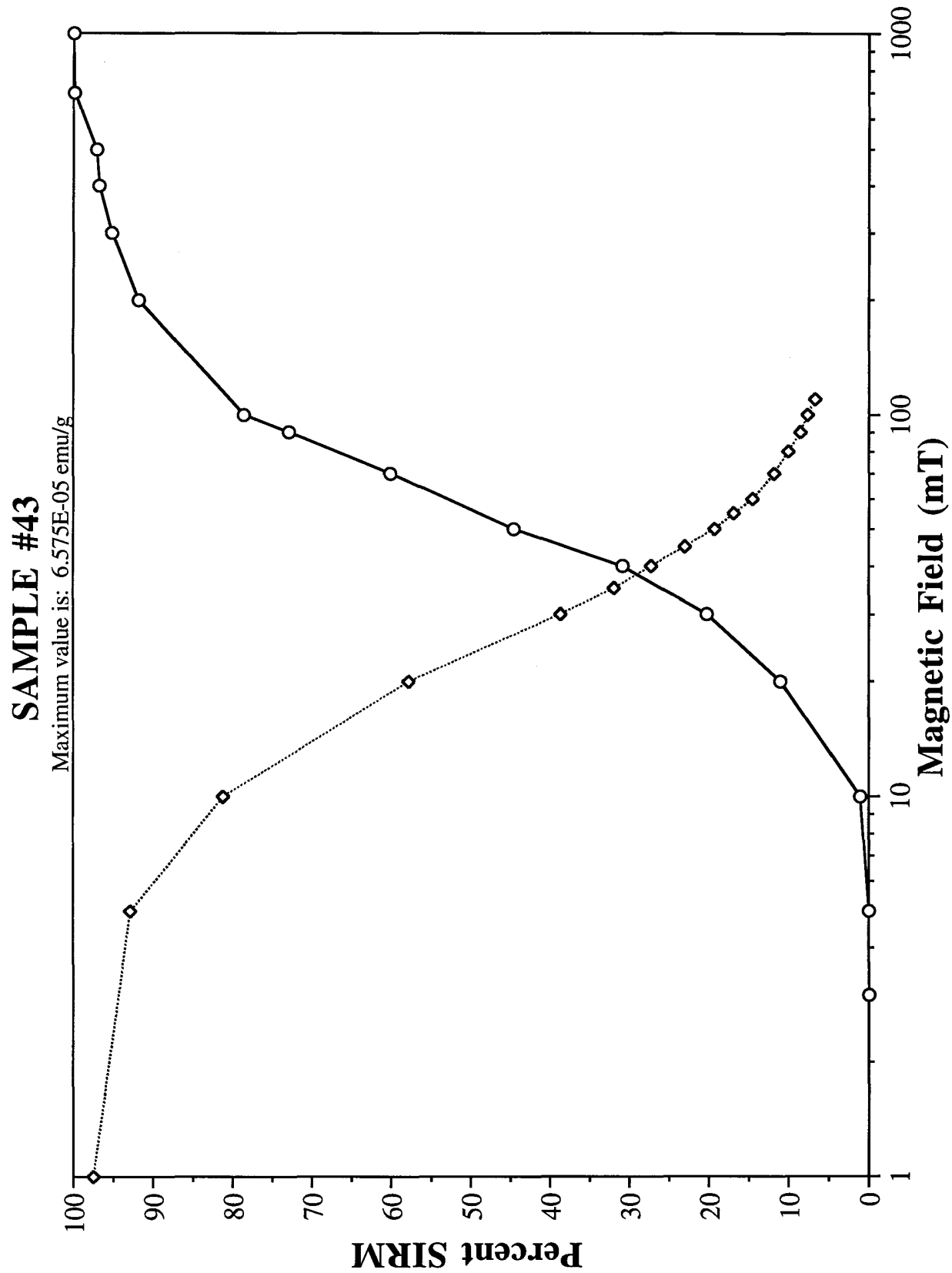
SAMPLE #43
Maximum value is: 6.575E-05 emu/g
Percent SIRM
100
90
80
70
60
50
40
30
20
10
0
1
10
100
1000
Magnetic Field (mT)

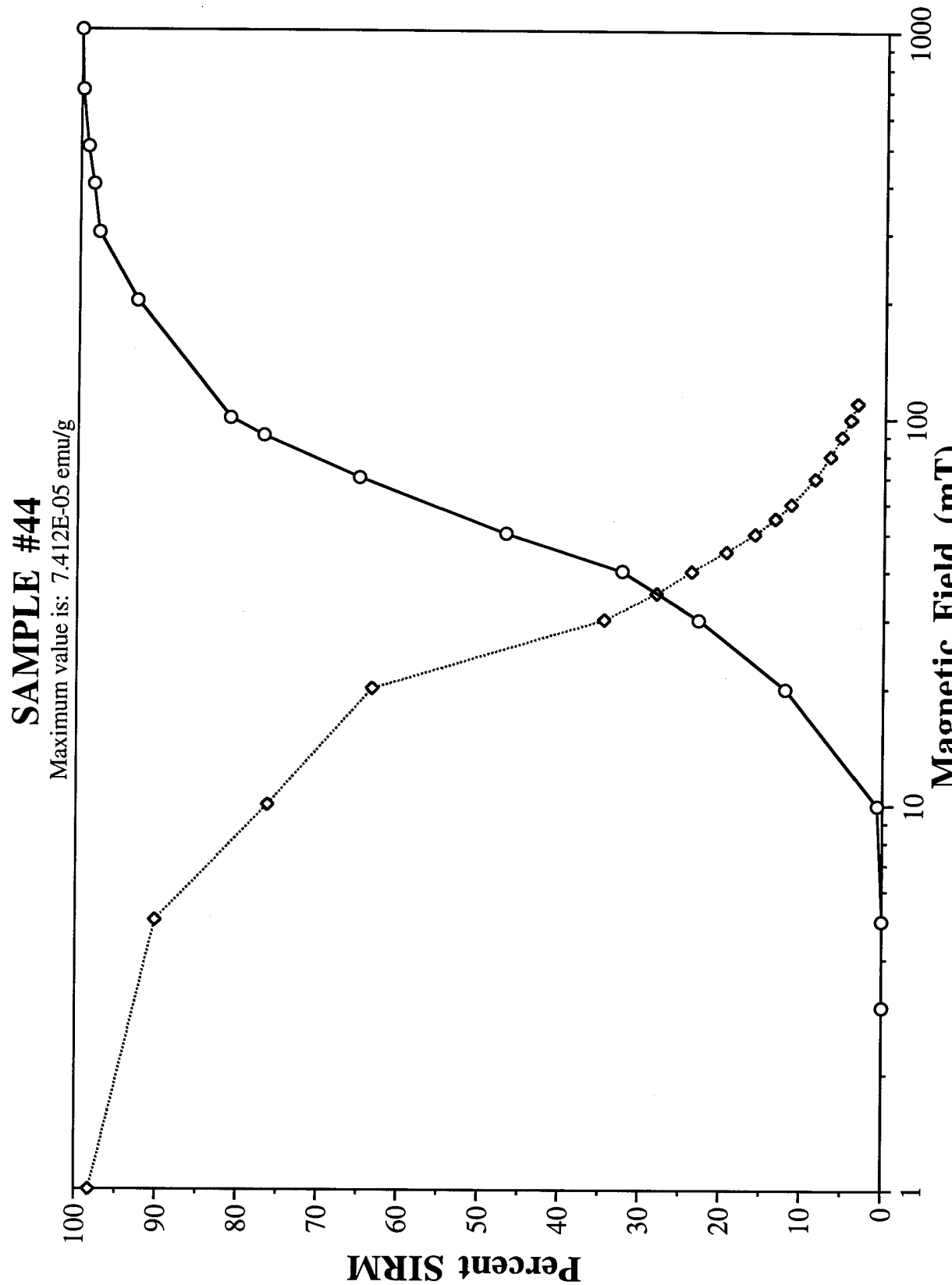
SAMPLE #44
Maximum value is: 7.412E-05 emu/g
Percent SIRM
100
90
80
70
60
50
40
30
20
10
0
1
10
100
1000
Magnetic Field (mT)

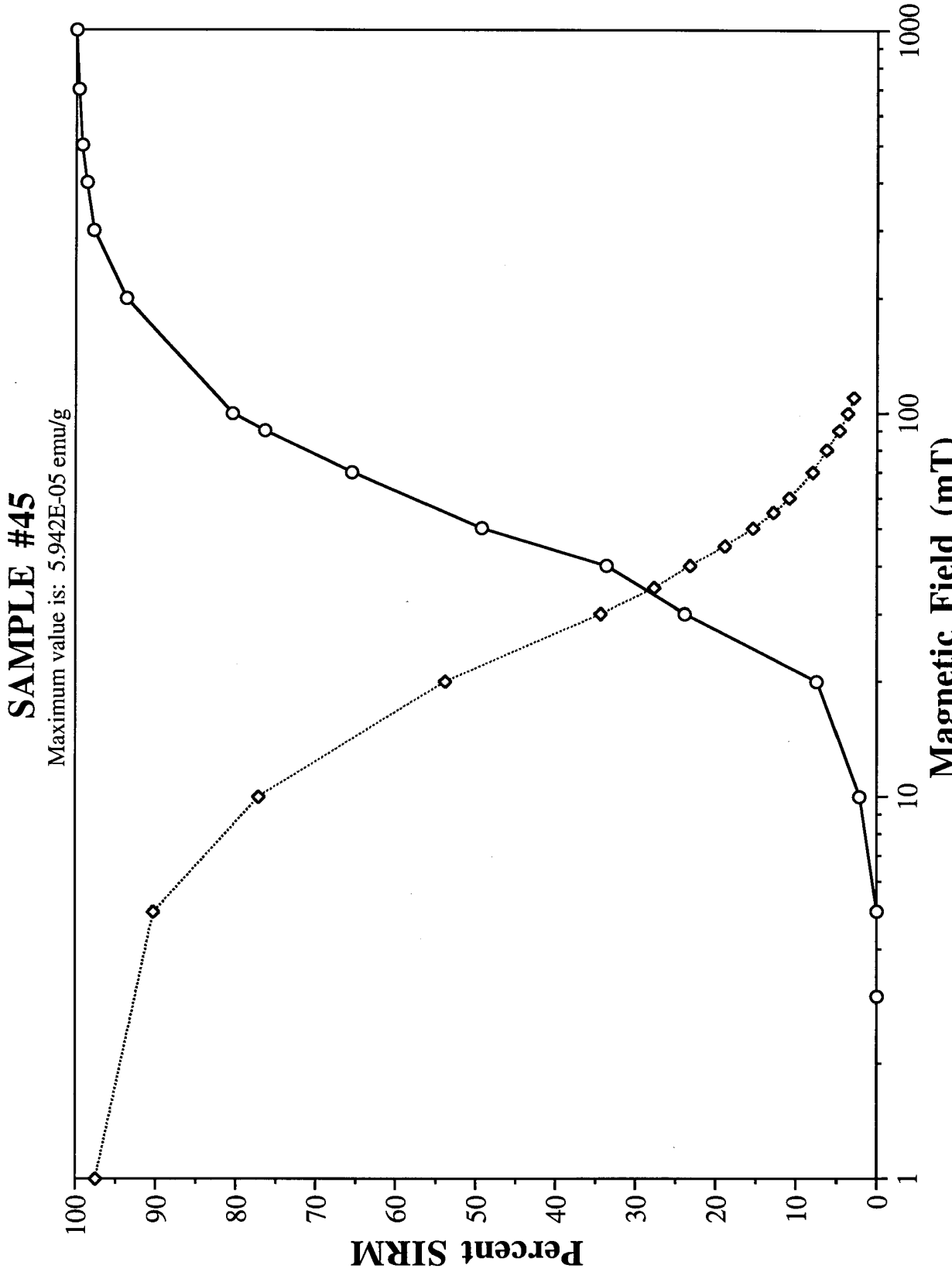
SAMPLE #45
Maximum value is: 5.942E-05 emu/g
Percent SIRM
100
90
80
70
60
50
40
30
20
10
0
1
10
100
1000
Magnetic Field (mT)

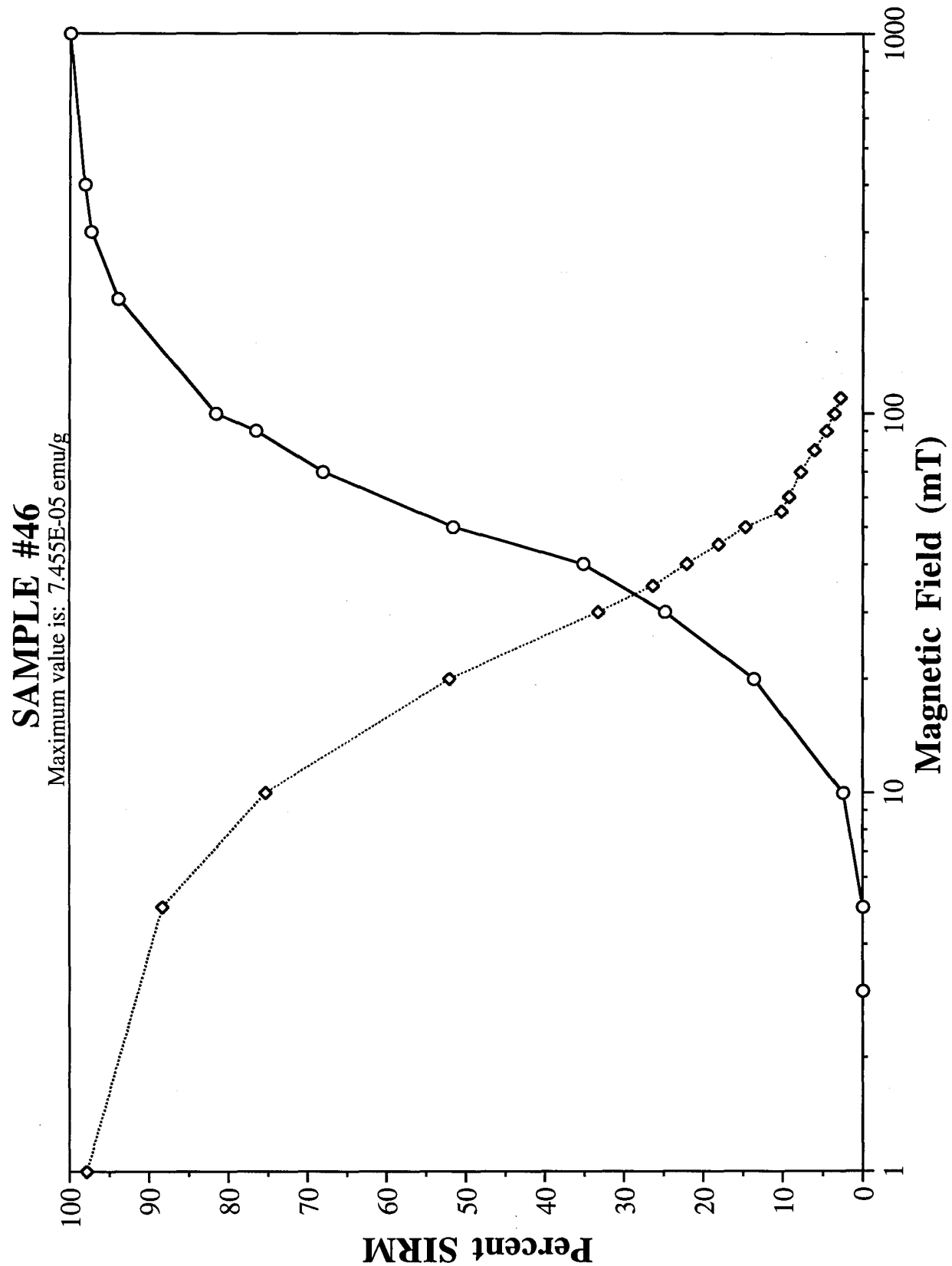
SAMPLE #46
Maximum value is: 7.455E-05 emu/g
Percent SIRM
100
90
80
70
60
50
40
30
20
10
0
1
10
100
1000
Magnetic Field (mT)

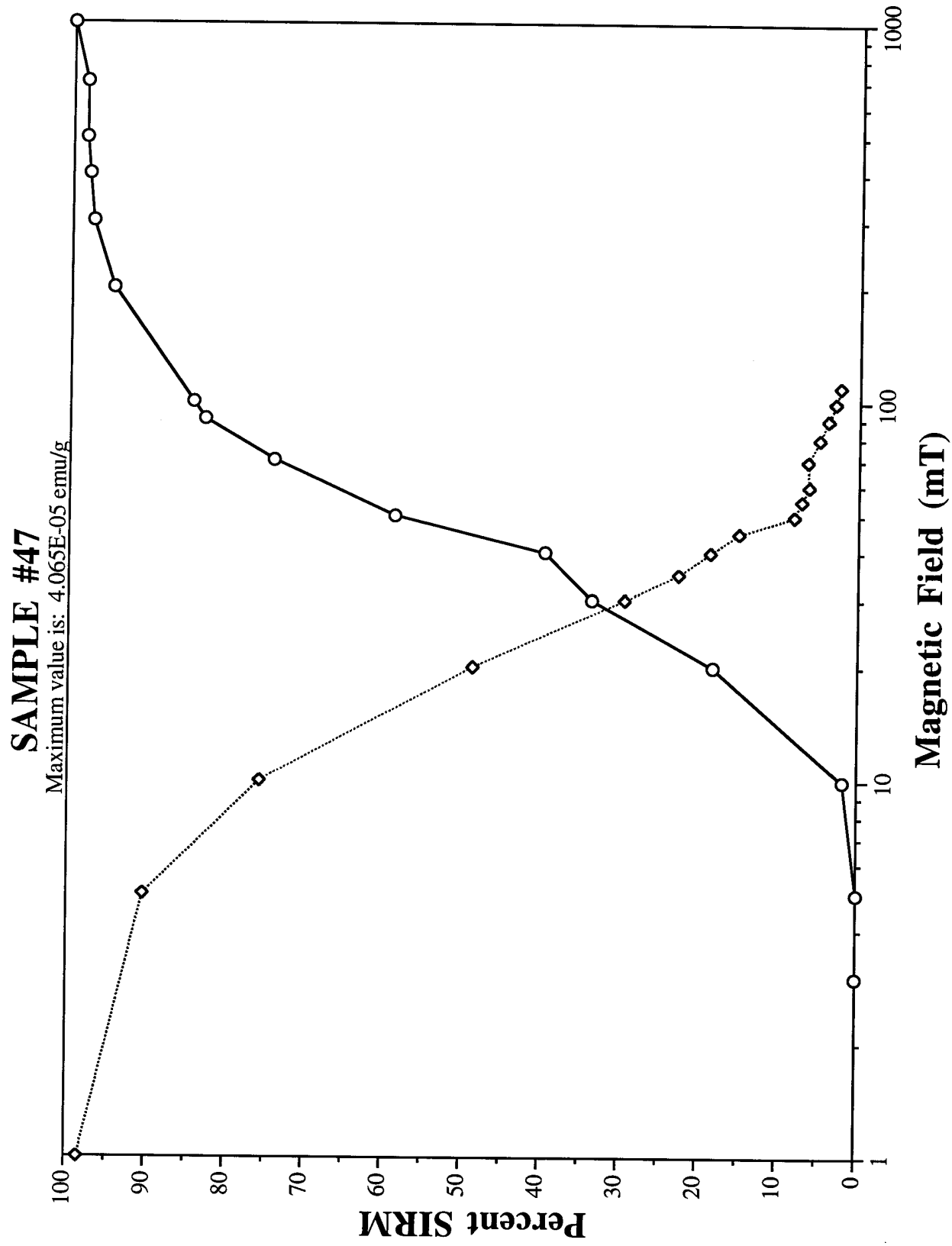
SAMPLE #47
Maximum value is: 4.065E-05 emu/g
Percent SIRM
100
90
80
70
60
50
40
30
20
10
0
1
10
100
1000
Magnetic Field (mT)

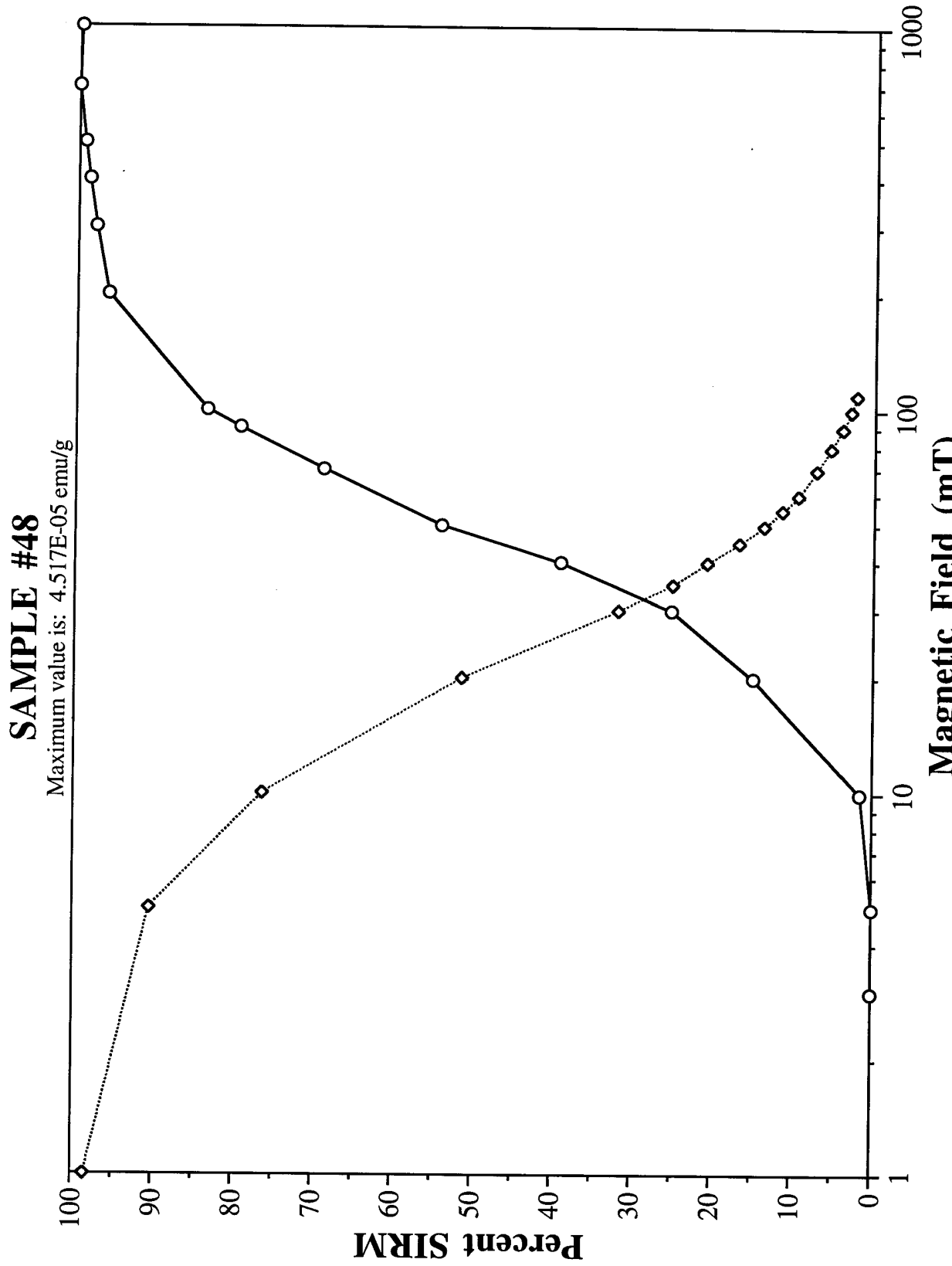
SAMPLE #48
Maximum value is: 4.517E-05 emu/g
Percent SIRM
100
90
80
70
60
50
40
30
20
10
0
1
10
100
1000
Magnetic Field (mT)

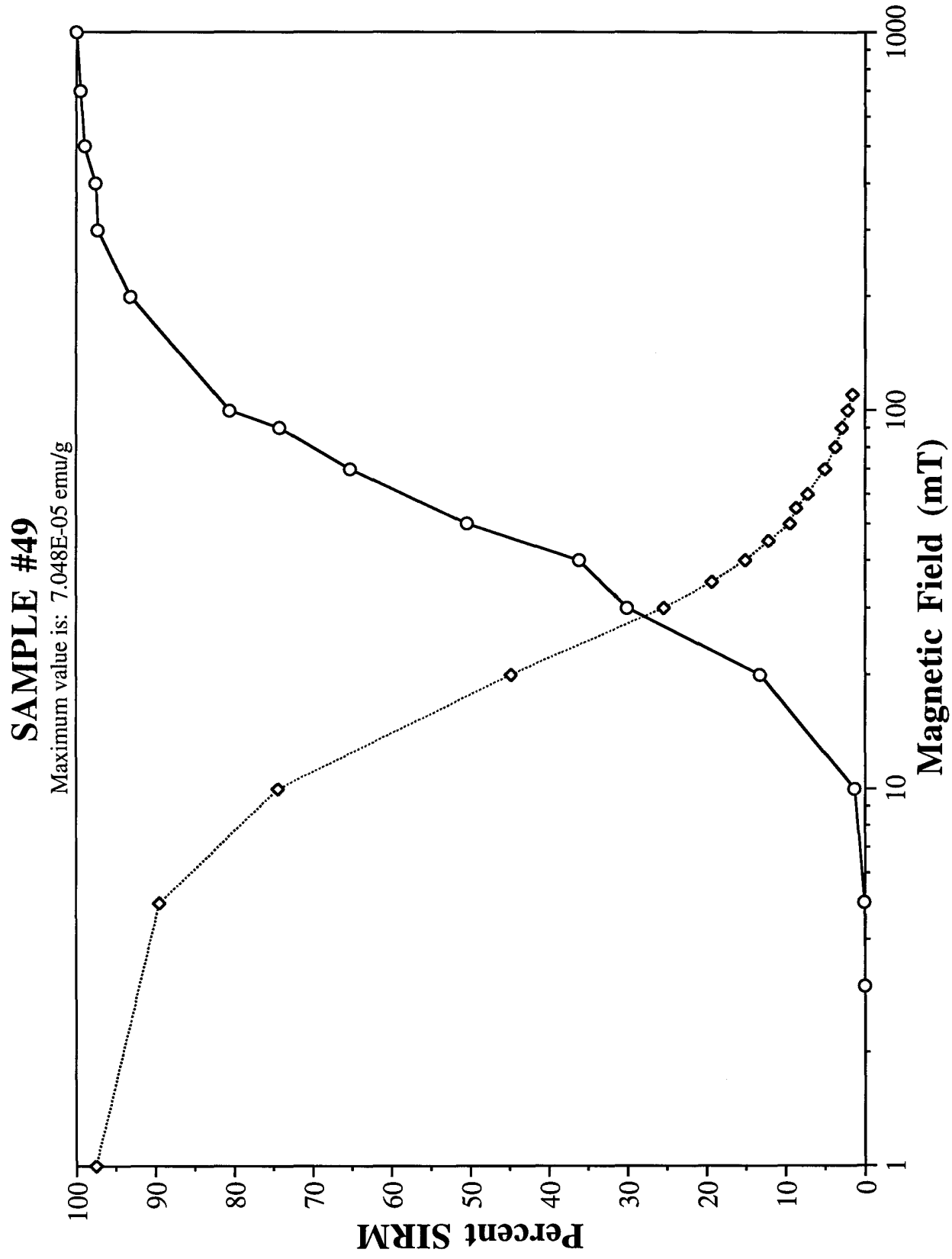
SAMPLE #49
Maximum value is: 7.048E-05 emu/g
Percent SIRM
100
90
80
70
60
50
40
30
20
10
0
1
10
100
1000
Magnetic Field (mT)

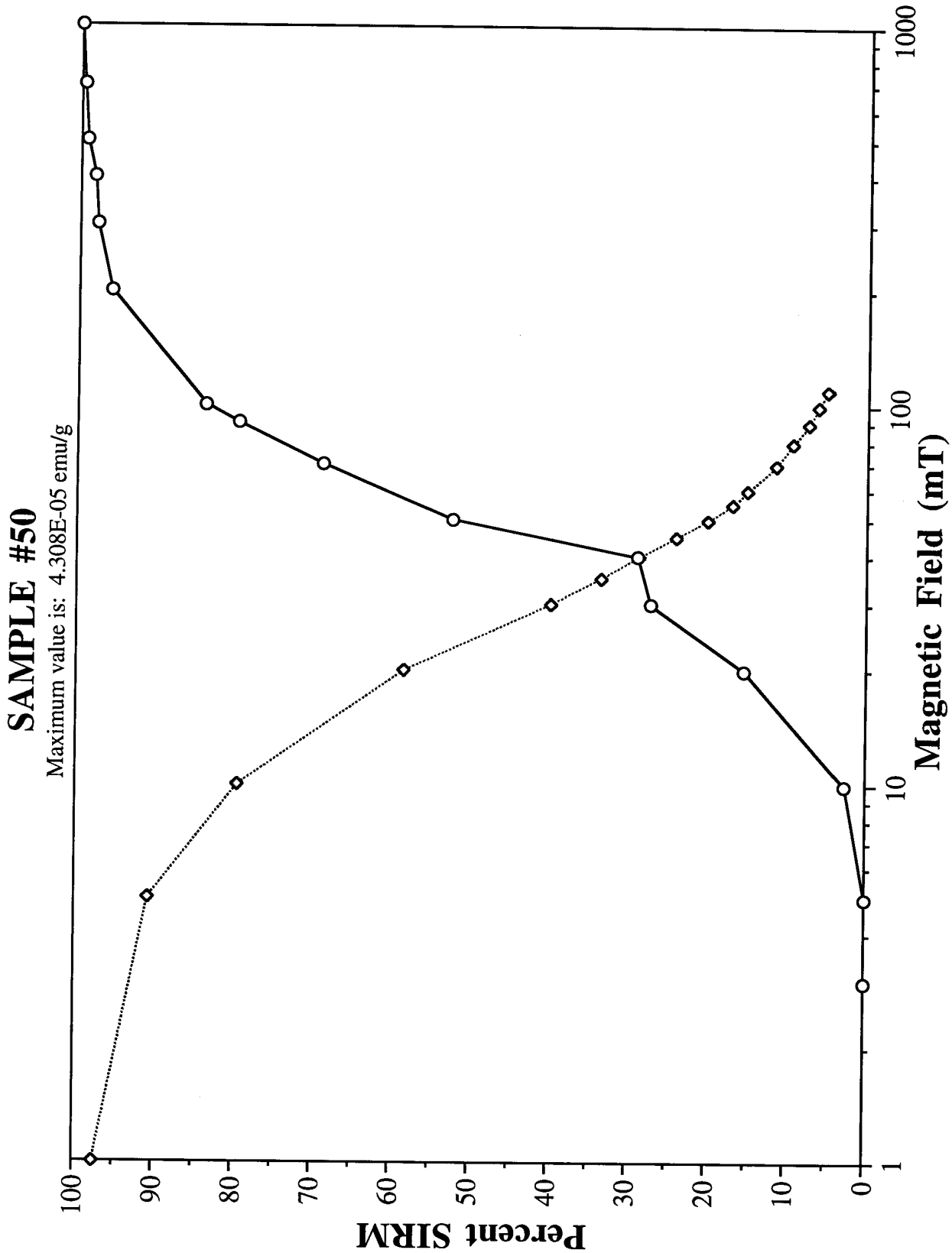
SAMPLE #50
Maximum value is: 4.308E-05 emu/g
Percent SIRM
100
90
80
70
60
50
40
30
20
10
0
1
10
100
1000
Magnetic Field (mT)

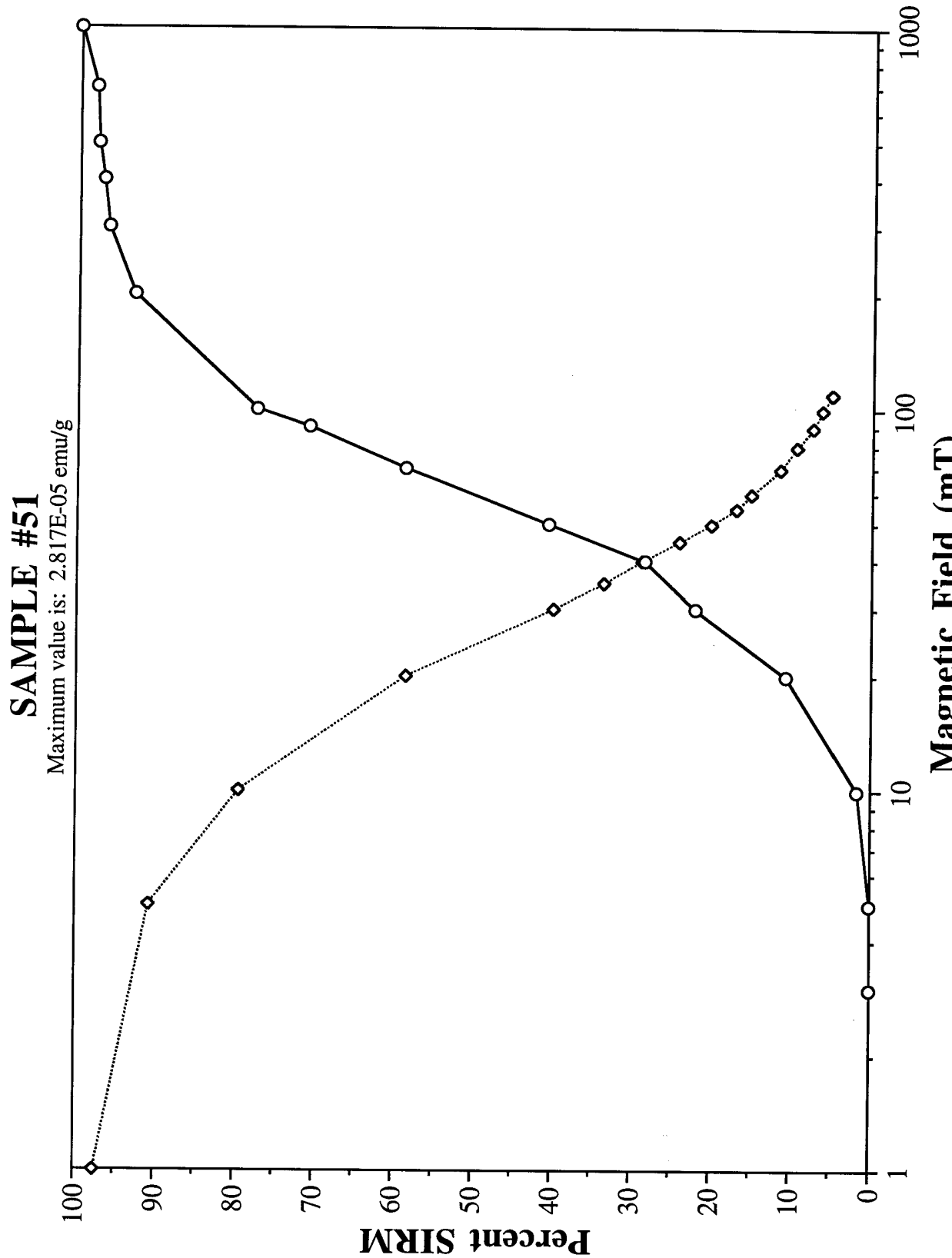
SAMPLE #51
Maximum value is: 2.817E-05 emu/g
Percent SIRM
100
90
80
70
60
50
40
30
20
10
0
1
10
100
1000
Magnetic Field (mT)

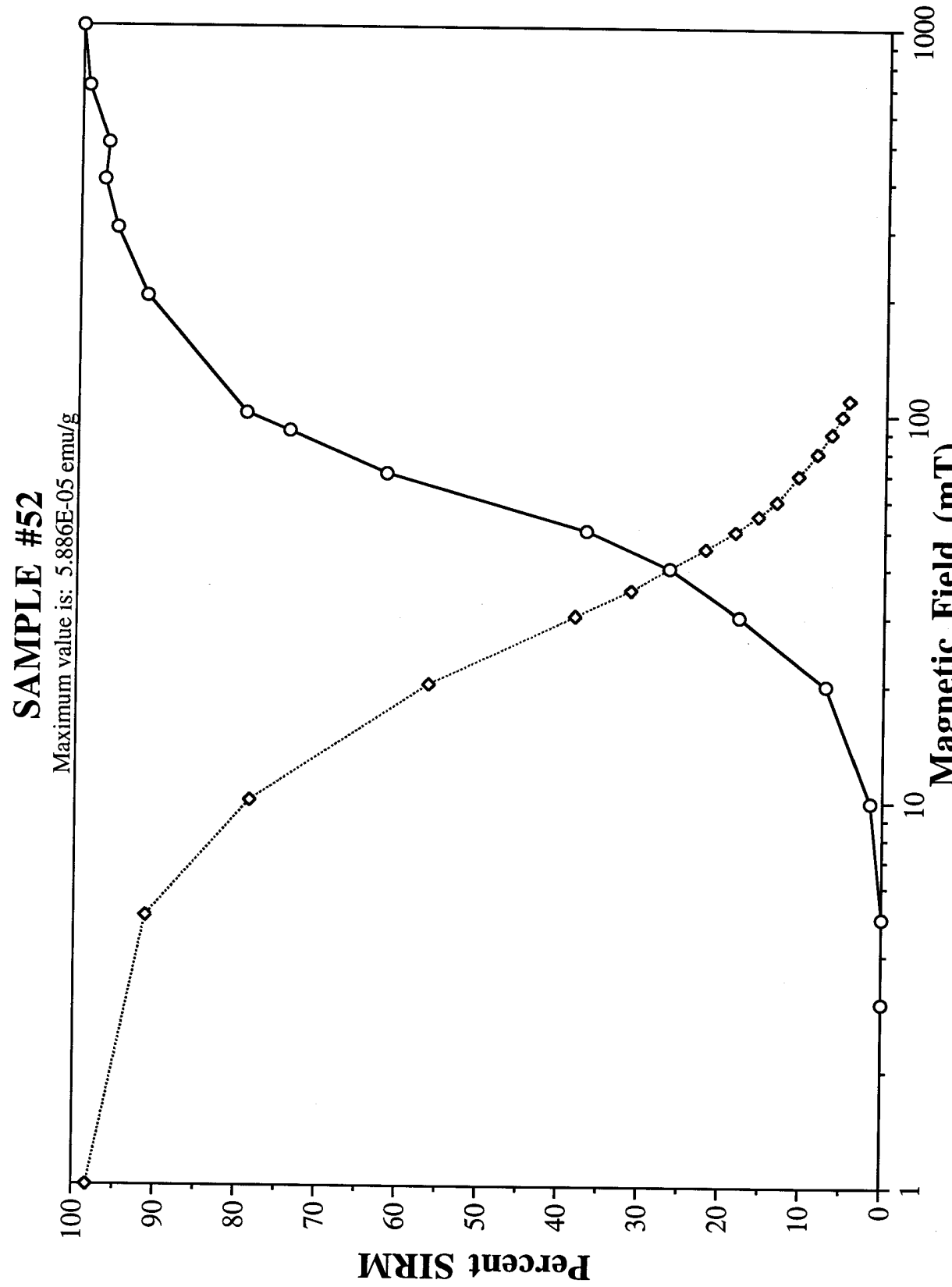
SAMPLE #52
Maximum value is: 5.886E-05 emu/g
Percent SIRM
100
90
80
70
60
50
40
30
20
10
0
1
10
100
1000
Magnetic Field (mT)

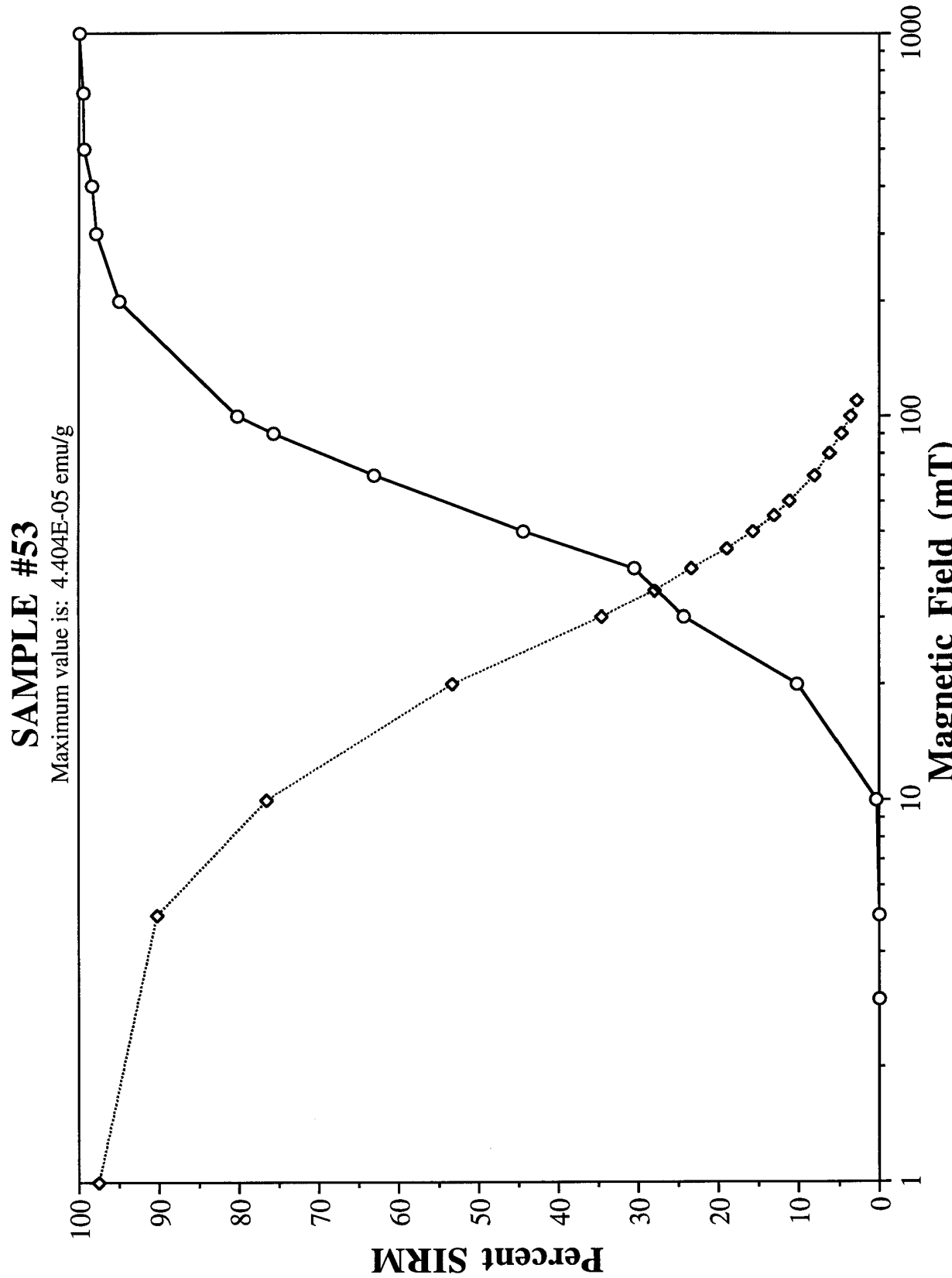
SAMPLE #53
Maximum value is: 4.404E-05 emu/g
Percent SIRM
100
90
80
70
60
50
40
30
20
10
0
1
10
100
1000
Magnetic Field (mT)

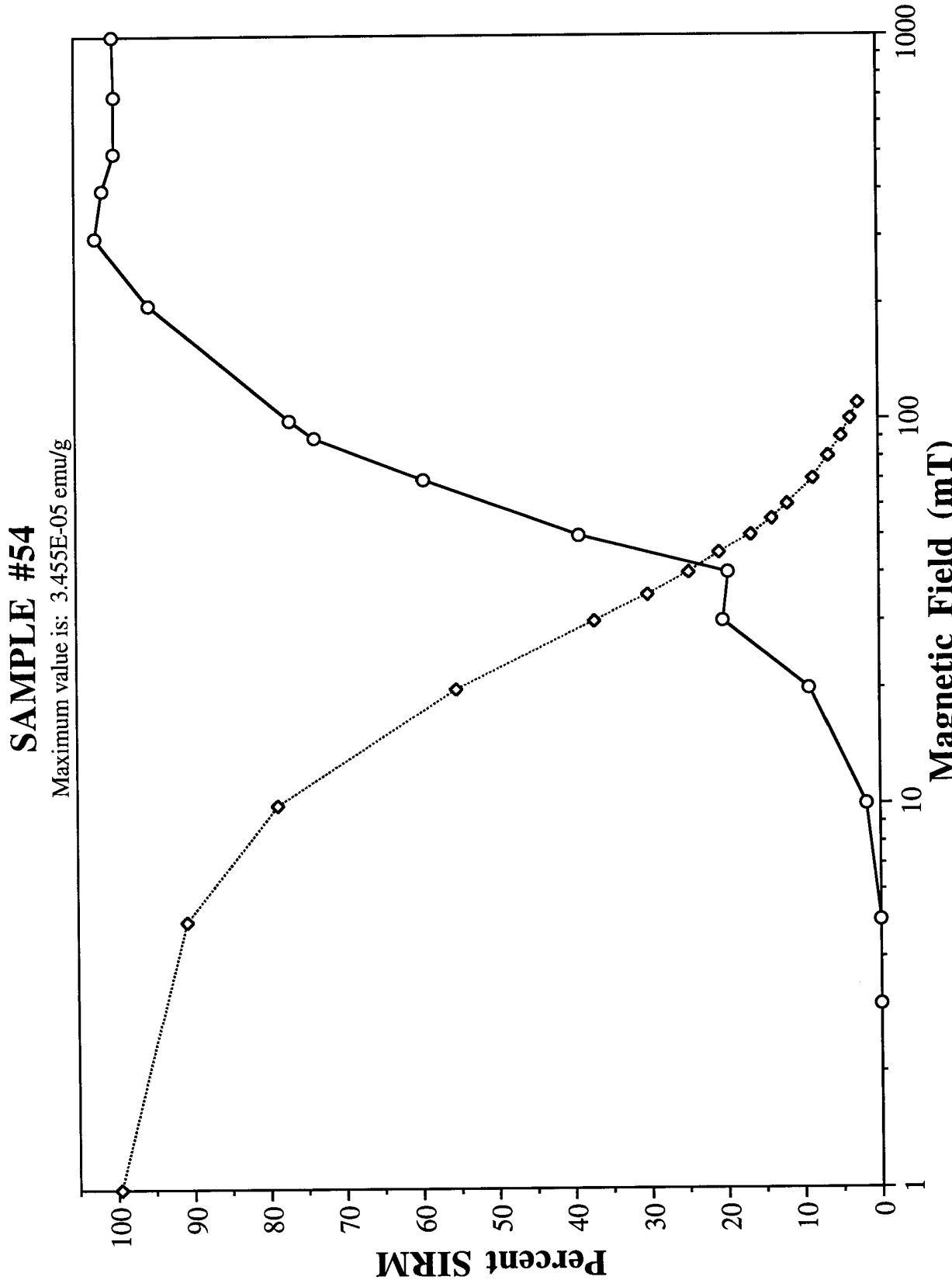
SAMPLE #54
Maximum value is: 3.455E-05 emu/g
Percent SIRM
100
90
80
70
60
50
40
30
20
10
0
1
10
100
1000
Magnetic Field (mT)

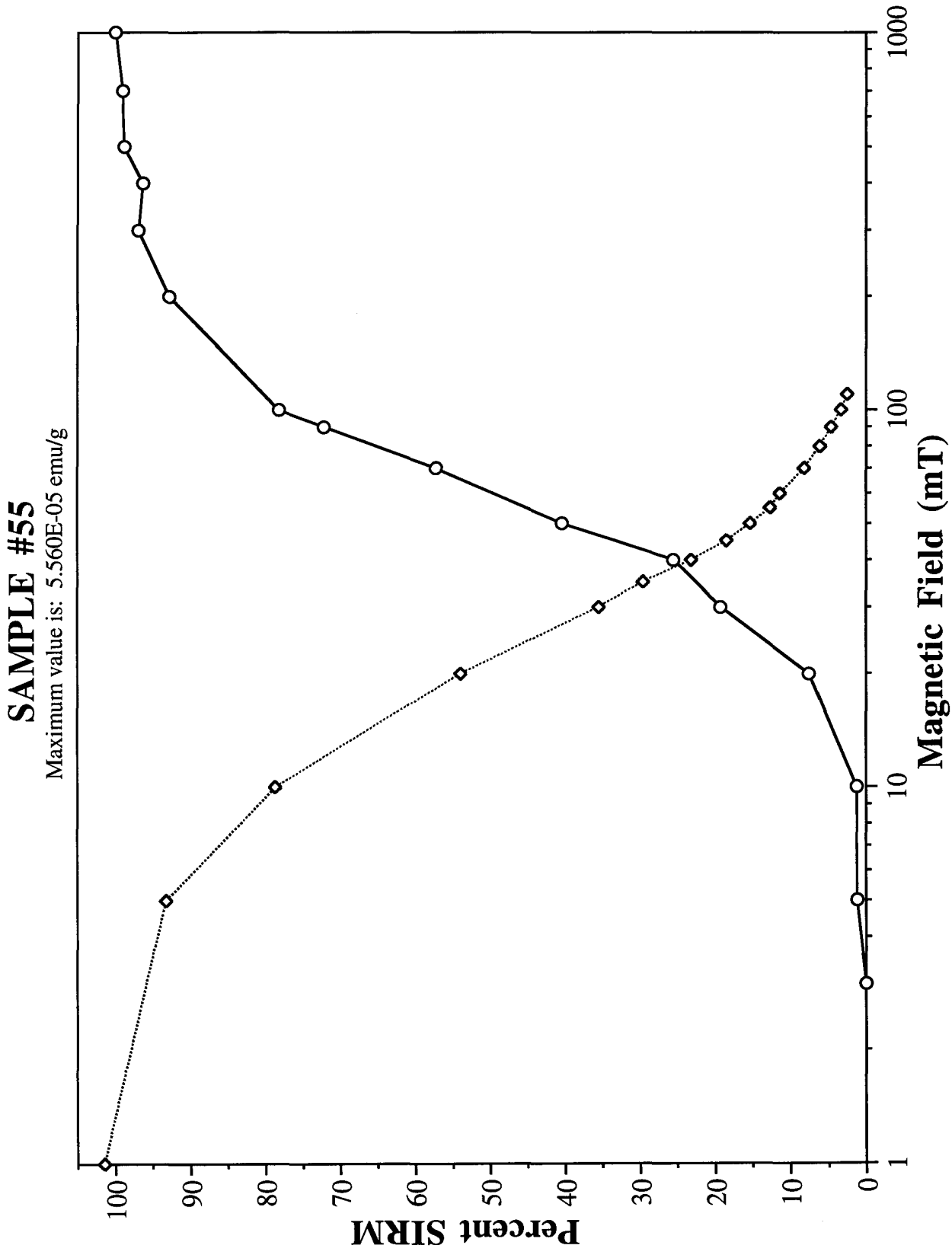
SAMPLE #55
Maximum value is: 5.560E-05 emu/g
Percent SIRM
100
90
80
70
60
50
40
30
20
10
0
1
10
100
1000
Magnetic Field (mT)

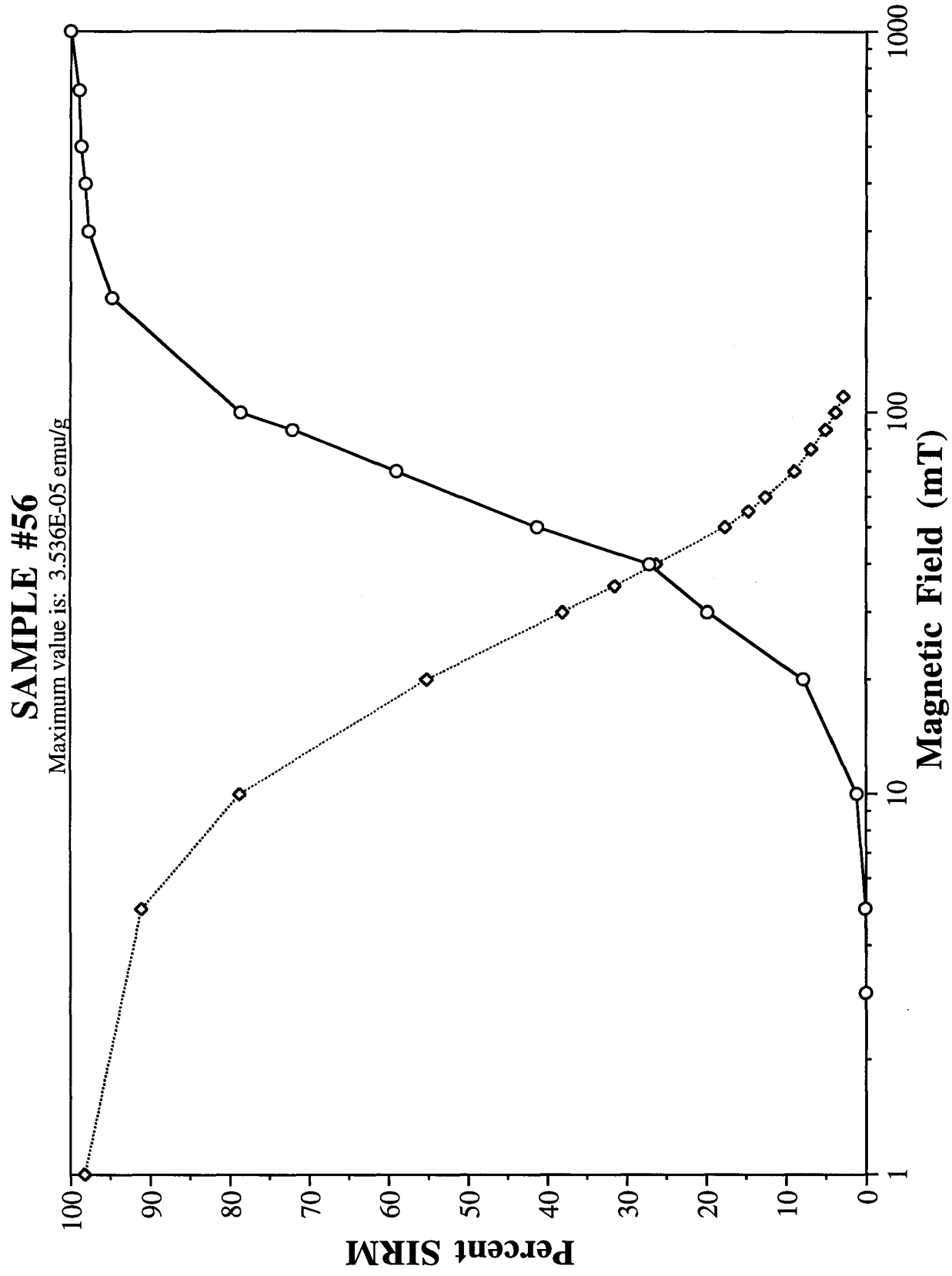
SAMPLE #56
Maximum value is: 3.536E-05 emu/g
Percent SIRM
100
90
80
70
60
50
40
30
20
10
0
1
10
100
1000
Magnetic Field (mT)

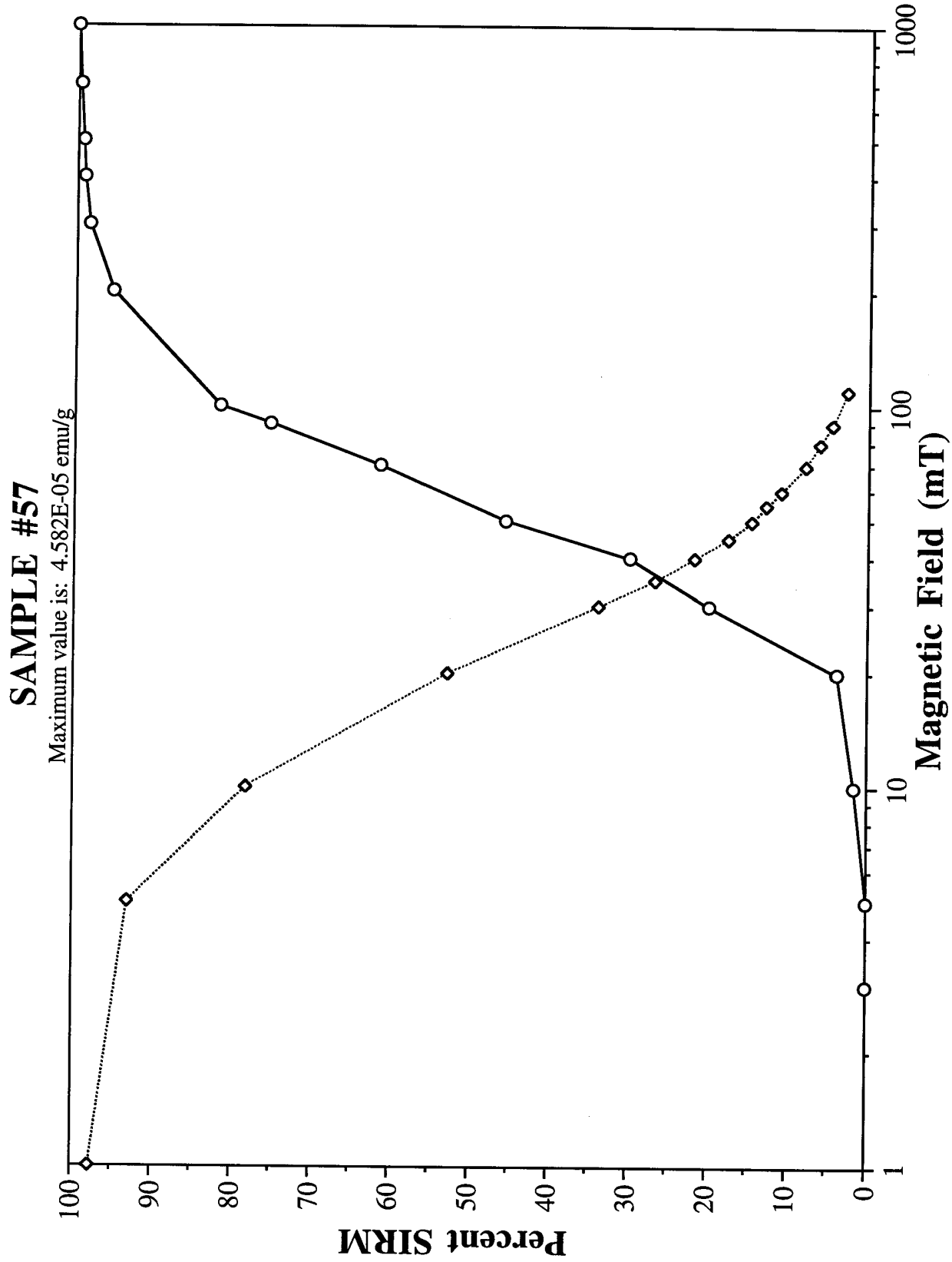
SAMPLE #57
Maximum value is: 4.582E-05 emu/g
Percent SIRM
100
90
80
70
60
50
40
30
20
10
0
1
10
100
1000
Magnetic Field (mT)

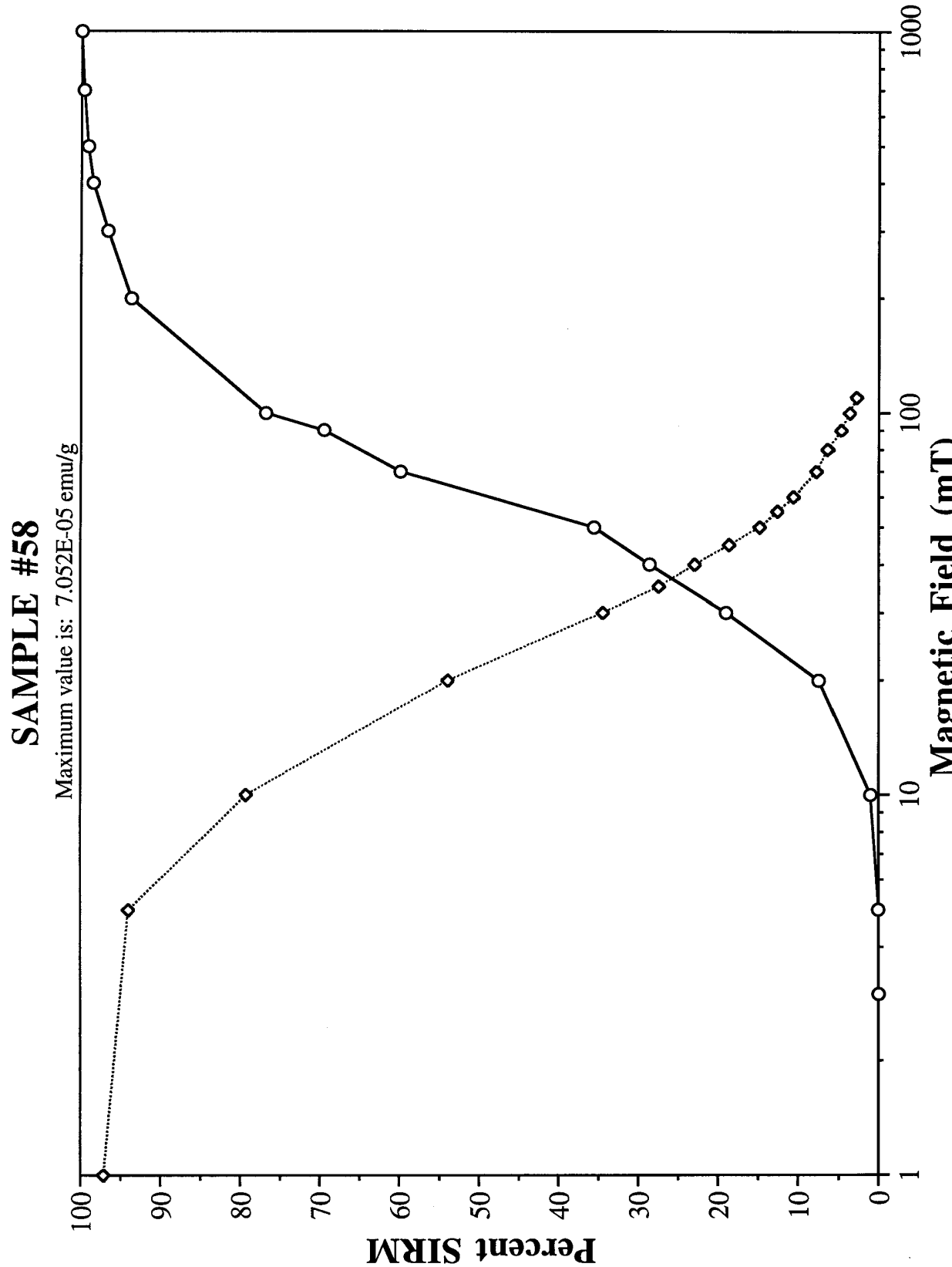
SAMPLE #58
Maximum value is: 7.052E-05 emu/g
Percent SIRM
100
90
80
70
60
50
40
30
20
10
0
1
10
100
1000
Magnetic Field (mT)

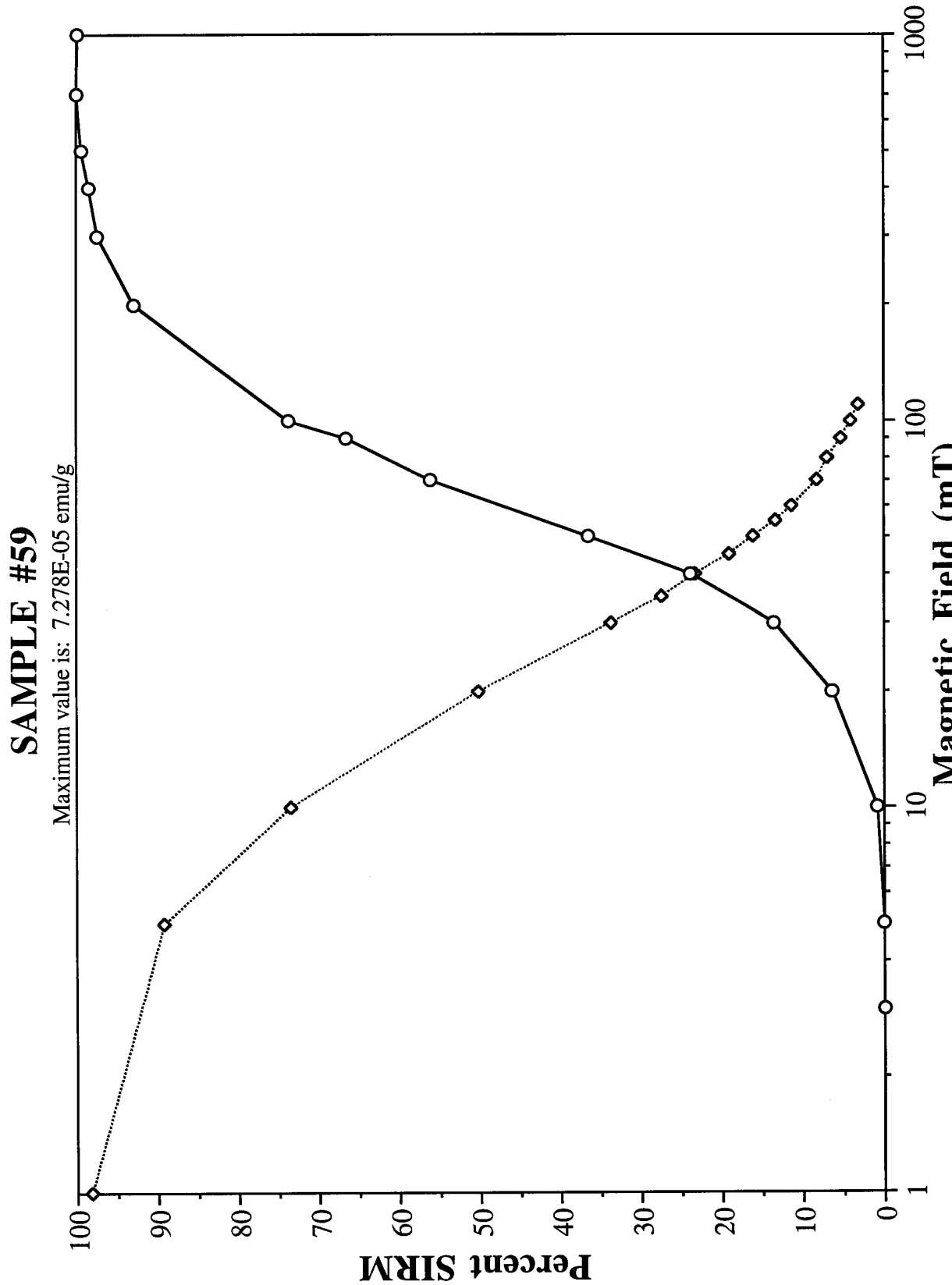
SAMPLE #59
Maximum value is: 7.278E-05 emu/g
Percent SIRM
100
90
80
70
60
50
40
30
20
10
0
1
10
100
1000
Magnetic Field (mT)

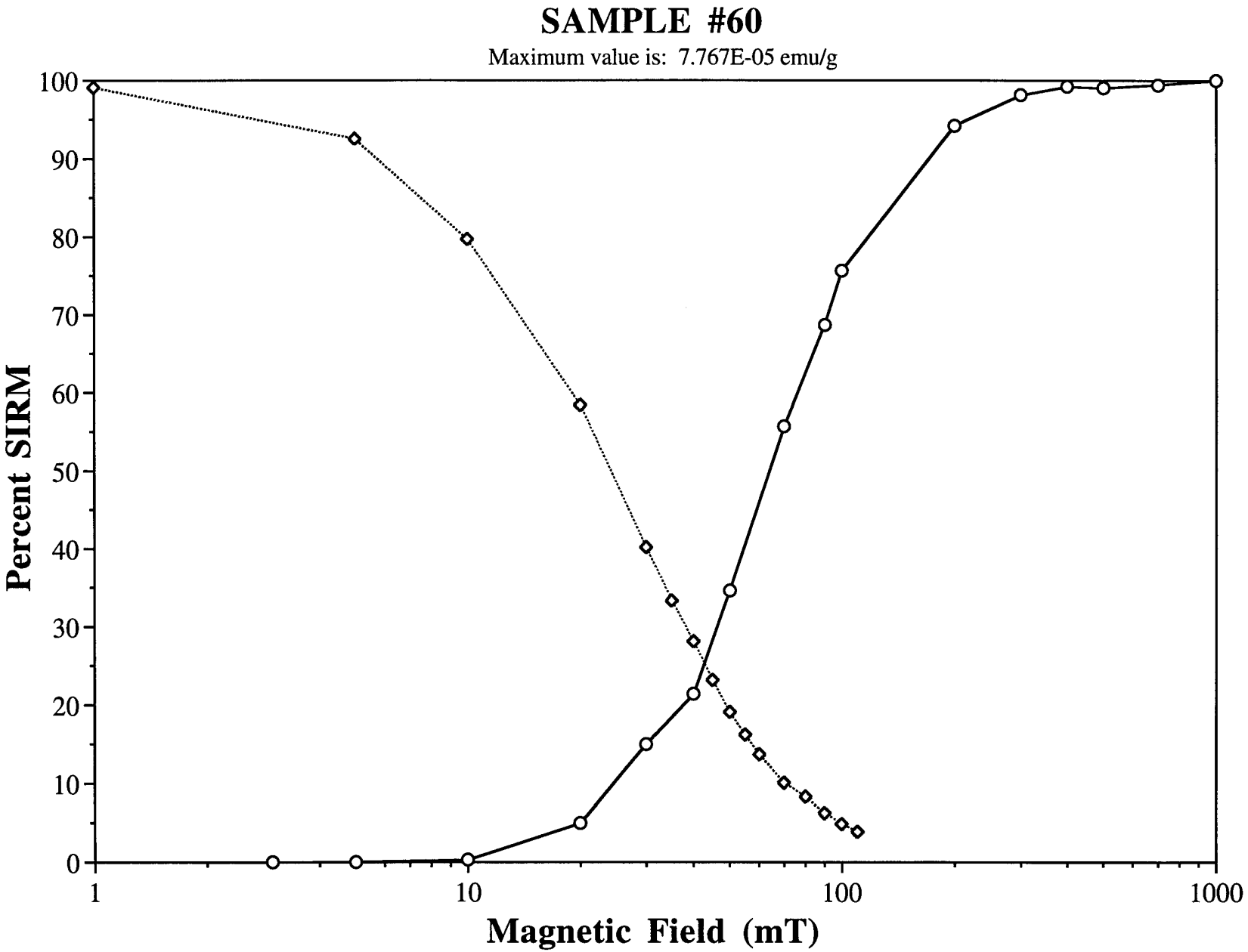
SAMPLE #60
Maximum value is: 7.767E-05 emu/g
Percent SIRM
100
90
80
70
60
50
40
30
20
10
0
1
10
100
1000
Magnetic Field (mT)

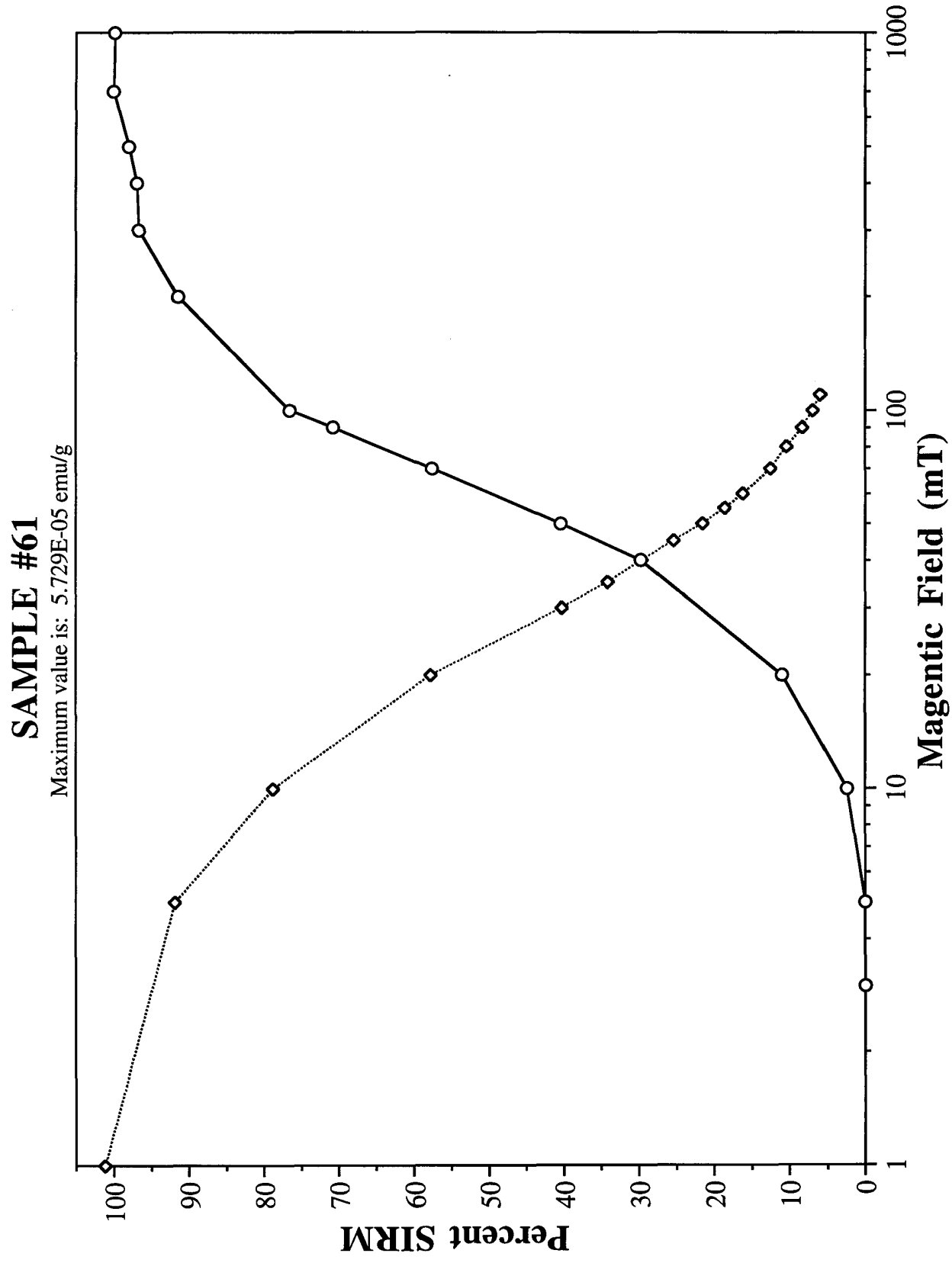
SAMPLE #61
Maximum value is: 5.729E-05 emu/g
Percent SIRM
100
90
80
70
60
50
40
30
20
10
0
1
10
100
1000
Magentic Field (mT)

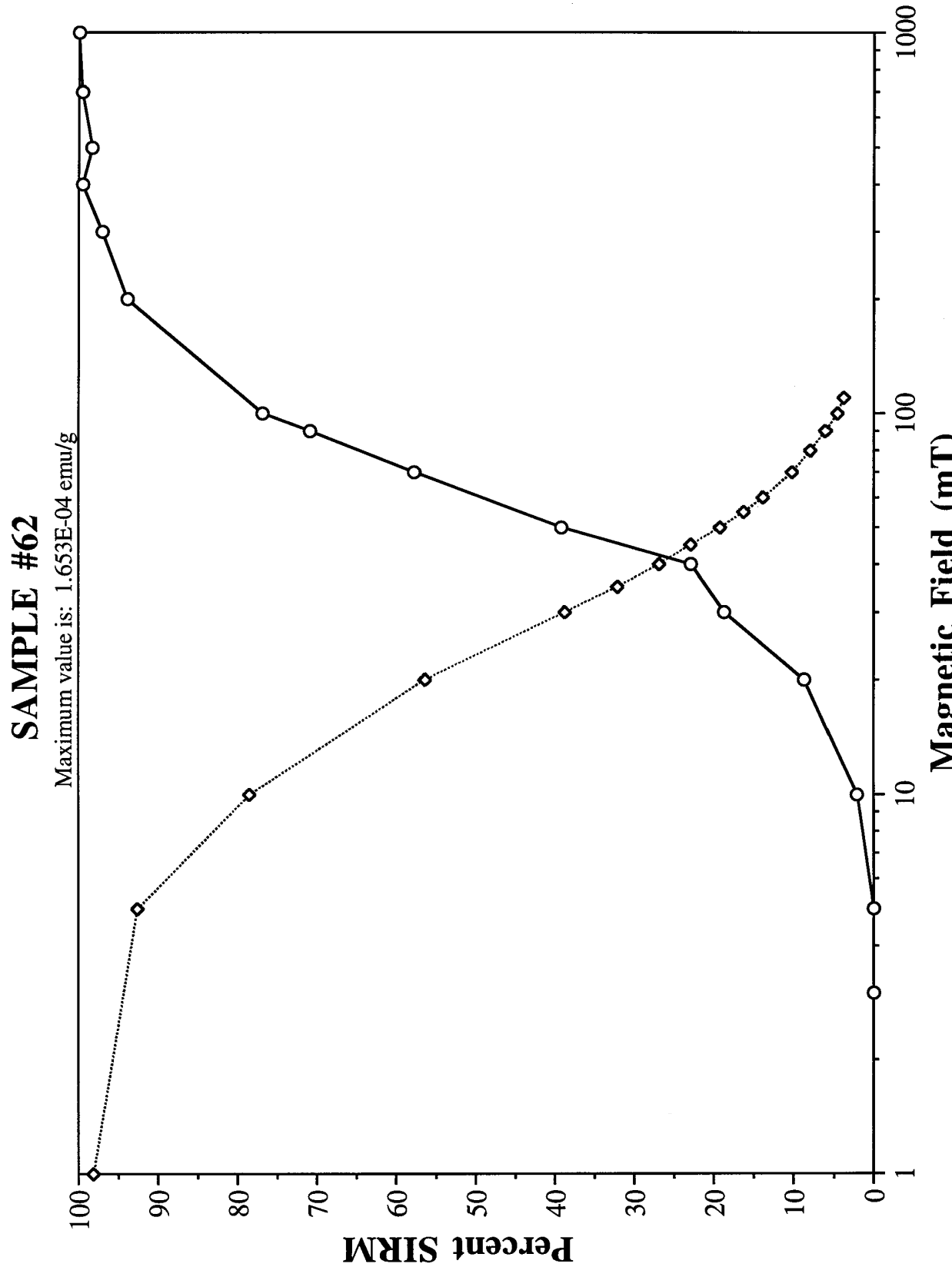
SAMPLE #62
Maximum value is: 1.653E-04 emu/g
Percent SIRM
100
90
80
70
60
50
40
30
20
10
0
1
10
100
1000
Magnetic Field (mT)

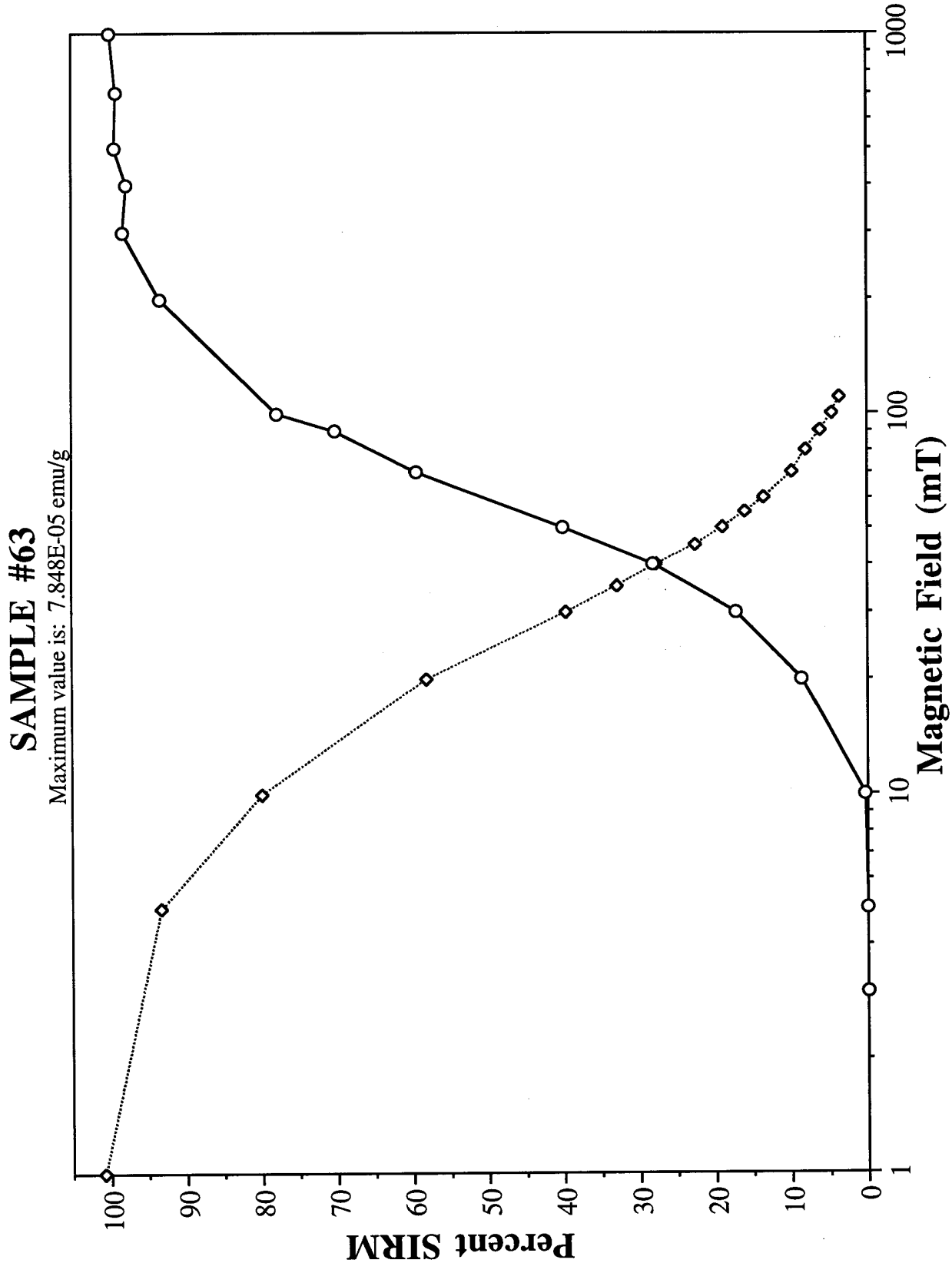
SAMPLE #63
Maximum value is: 7.848E-05 emu/g
Percent SIRM
100
90
80
70
60
50
40
30
20
10
0
1
10
100
1000
Magnetic Field (mT)

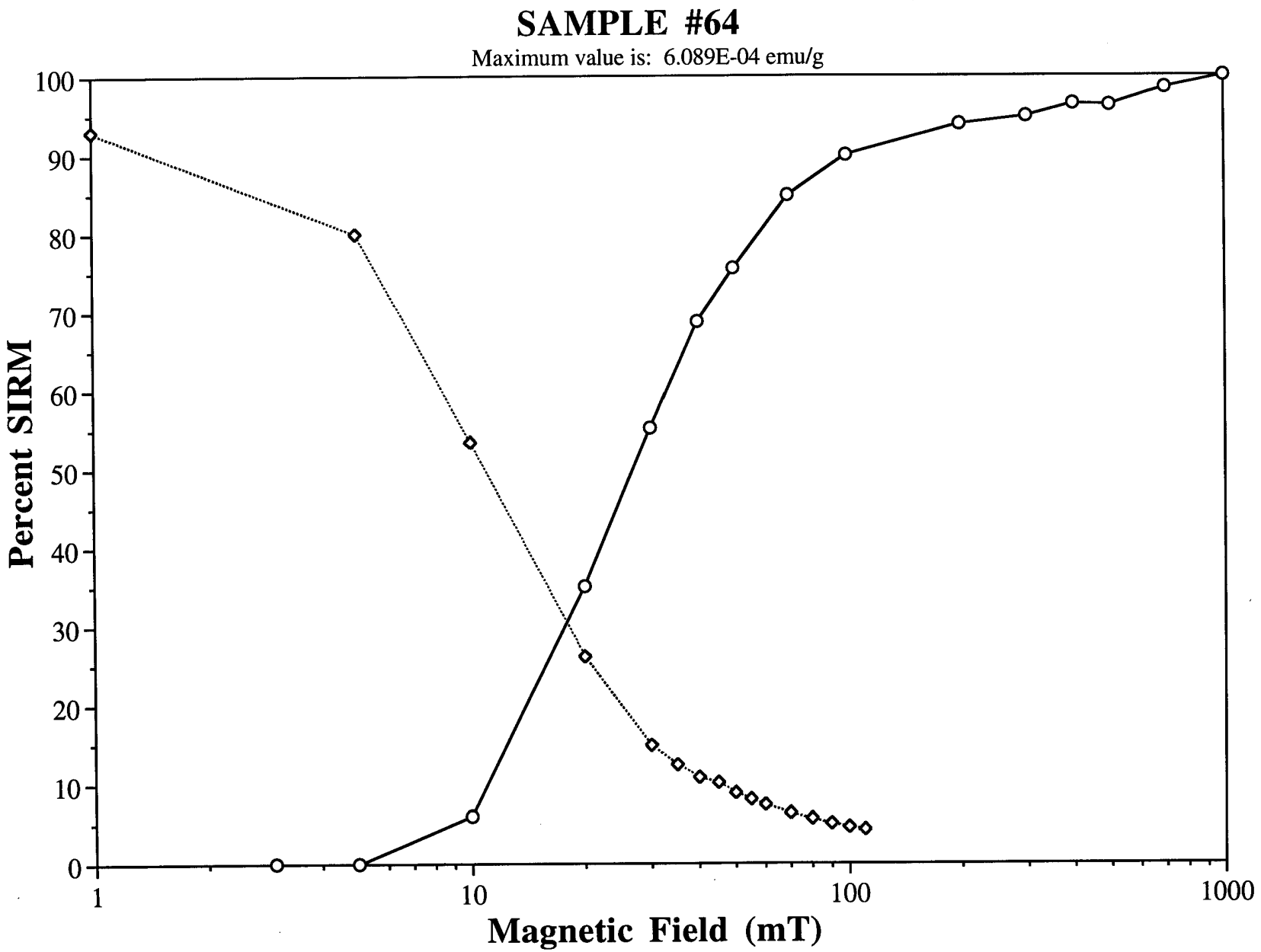
SAMPLE #64
Maximum value is: 6.089E-04 emu/g
Percent SIRM
100
90
80
70
60
50
40
30
20
10
0
1
10
100
1000
Magnetic Field (mT)